1994

High power UHF/microwave transmission line study

Thomas W. Jones
San Jose State University

HIGH POWER UHF/MICROWAVE TRANSMISSION LINE STUDY

A Thesis

Presented to

The Faculty of the Department of Mechanical Engineering

San Jose State University

In Partial Fulfillment

of the Requirements for the Degree

Master of Science

by

Thomas W. Jones

December, 1994

APPROVED FOR THE DEPARTMENT OF MECHANICAL ENGINEERING

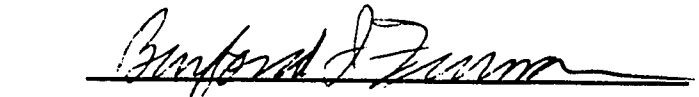

Dr. Buford Furman

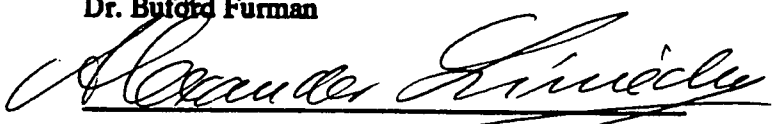

Dr. Alexander Liniecki

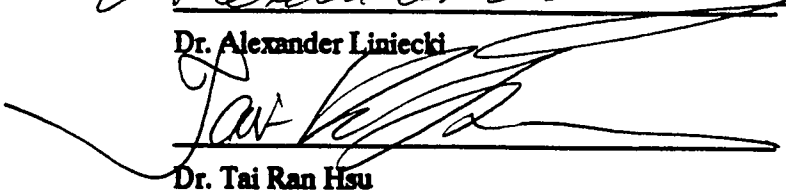

Dr. Tai Ran Hsu

APPROVED FOR THE UNIVERSITY

ABSTRACT

HIGH POWER UHF/MICROWAVE TRANSMISSION LINE STUDY

by Thomas W. Jones

Increased power aperture is one technique which can be employed to improve a radar system's low radar cross-section target detection. Such systems require high performance transmission lines which are capable of transmitting high average power.

This thesis studies the thermal effects associated with **high power transmission** at **UHF** and **L-Band** frequencies. In this study four **rigid air-cooled low-loss coaxial transmission lines** were fabricated and high power tested. **Fluoroptic Thermometry** was successfully used to measure the inner conductor temperatures.

FEA models were used to predict the steady state temperatures of the rigid air-cooled low-loss coaxial transmission lines. Empirically derived expressions were used for calculating the internal **convection coefficients.** Expressions are also derived for calculating the heating due to conductor losses. For the horizontally oriented line, favorable correlation was realized between test and model results.

ACKNOWLEDGMENTS

This project would not have been realized without the assistance of the following individuals and organizations to which I extend my sincerest appreciation.

I would like to acknowledge and thank Dr. Tai Hsu, Chairperson of the SJSU Mechanical Engineering Department. Dr. Hsu's guidance, support and patience throughout this project was greatly appreciated. I would also like to express my appreciation to the Mechanical Engineering Department and Lou Schallberger for his support and for the use of the Luxtron Fluoroptic Thermometer.

Also, I want to thank Jim Scherer, Ron Bungo and the rest of the management of Loral Randtron Systems for sponsoring this project. The cost of fabricating and testing of the specimens was very expensive and would not have been realized without Loral's financial support.

Finally, I would like to thank Jon Dunn and Pete Hochscheid for their assistance during high power testing. Jon is also credited for the writing of the data acquisition software, which was used during testing.

TABLE OF CONTENTS

TABLE OF CONTENTS

LIST OF FIGURES

LIST OF FIGURES

LIST OF TABLES

NOMENCLATURE

a	Outside diameter inner conductor, (in).
A	Cross sectional area, (in^2) or broadwall dimension rectangular waveguide (in) or constant.
b	Inside diameter outer conductor, (in).
B	Narrow wall dimension rectangular waveguide (in) or constant.
c_p	Specific heat of air, $\left(\frac{BTU}{lb_m - °F}\right)$.
d	Inside diameter of inner conductor, (in).
D	Outside diameter of outer conductor, (in).
$\%D_a$	Percent difference between T_a calculated and T_a measured.
$\%D_b$	Percent difference between T_b calculated and T_b measured.
F	Frequency, (GHz).
F_c	Cutoff frequency where $F_c = \frac{11.811}{\pi(b+a)}$, (GHz).
h_1	Convection coefficient at outside surface of inner conductor, $\left(\frac{BTU}{hr - in^2 - °F}\right)$.
h_2	Convection coefficient at inside surface of outer conductor, $\left(\frac{BTU}{hr - in^2 - °F}\right)$.
h_3	Convection coefficient at OD of outer conductor, $\left(\frac{BTU}{hr - in^2 - °F}\right)$.
g	Acceleration due to gravity, $32.2\frac{ft}{s^2}$.
k	Thermal conductivity, $\left(\frac{BTU}{hr - in - °F}\right)$ or $\left(\frac{BTU}{hr - ft - °F}\right)$.
K_1	Constant, $\left(\frac{\text{BTU}}{\text{in hr° F}}\right)$.
K_2	Constant, $\left(\frac{\text{BTU}}{\text{in hr° F}^2}\right)$.
N_{G_R}	Grashof number, dimensionless.
N_{P_R}	Prandtl number, dimensionless.

NOMENCLATURE

P	Power, (kW).
P_{in}	Power at input port of line, (kW).
P_{out}	Power at output port of line, (kW).
ΔP_a	Power dissipated within inner conductor, (kW).
ΔP_b	Power dissipated within outer conductor, (kW).
ΔP_T	Power dissipated within transmission line, (kW).
q	Heat flux, $\left(\frac{\text{BTU}}{\text{hr}}\right)$.
$\dot{q}_a$	Heat source of inner conductor, $\left(\frac{BTU}{hr - in^3}\right)$.
$\dot{q}_b$	Heat source of outer conductor, $\left(\frac{BTU}{hr - in^3}\right)$.
Q	Volumetric flow rate of air, (SCFH).
SCFH	Standard cubic feet per hour.
T	Temperature (°F).
T_{amb}	Ambient temperature (°F).
T_a	Temperature inner conductor (°F).
T_b	Temperature outer conductor (°F).
T_o	75°F, temperature at which ρ_o is defined.
ΔT	$T - T_{amb}$, (°F).
ΔT_a	$T_a - T_{amb}$, (°F).
ΔT_b	$T_b - T_{amb}$, (°F).
V	Velocity cooling air, $\left(\frac{in}{hr}\right)$.
VSWR	Voltage Standing Wave Ratio.
y	Position along length of coax line, (inch).
Z_o	Characteristic impedance of transmission line where $Z_o = \frac{138}{\sqrt{\varepsilon}}\log\left(\frac{b}{a}\right)$, (ohms).

NOMENCLATURE

α_a	Attenuation of inner conductor, $\left(\frac{dB}{100'}\right)$.
α_b	Attenuation of outer conductor, $\left(\frac{dB}{100'}\right)$.
α_C	Attenuation of line due conductor losses, $\left(\frac{dB}{100'}\right)$.
α_D	Attenuation of line due dielectric losses, $\left(\frac{dB}{100'}\right)$.
α_T	Attenuation of coaxial transmission line, $\left(\frac{dB}{100'}\right)$.
β	$\frac{d}{dT}, \left(\frac{1}{°C}\right)$.
δ	Skin depth, (inches).
ε	Dielectric constant, $\left(\varepsilon' - j\varepsilon''\right)$ or emissivity.
ε'	Real part of dielectric constant.
$\tan\delta$	Loss tangent of dielectric, $\left(\frac{\varepsilon'}{\varepsilon''}\right)$.
θ	Position of test specimen relative to the horizon, (Degrees).
λ	Wavelength, (inches).
μ	Permeability, $\left(\frac{Weber}{Amp-m}\right)$ or viscosity of air, $\left(\frac{lb_m}{sec-ft}\right)$.
ρ	Resistivity, (ohms-cm) or density of air, $\left(\frac{lb_m}{in^3}\right)$.
ρ_o	Resistivity at T_O, (ohms-cm).
σ	Stefan-Boltzmann constant, $1.19E-11\frac{BTU}{in^2 hr° R^4}$.
ϕ	Angular position around coax line, (°).

I. INTRODUCTION

Background

Over the years engineers and researchers from various disciplines have been making advancements in radar technology. One area of continual advancement is in the detection of low radar cross-section (LRCS) targets at increasing distances. Numerous techniques have been applied to improve LRCS target detection. Some of these techniques include upgrades to system software and hardware, which tend to reduce the effects associated with clutter and jamming. Another *brute force* approach is to increase the amount of power aperture. For certain applications this approach is attractive because it is relatively straight forward and because improvements to system software and hardware can lead to diminishing returns.

Some applications have requirements for many transmission lines which interface the radar transmitter(s) to the antenna. The routing of the transmission lines can present packaging problems to the design engineer. This problem is especially pertinent for UHF or L-Band radar systems, where routing of transmission lines can be unwieldy. For higher power systems the design engineer must also deal with the problems associated with line losses such as line heating and overall system losses.

This study investigates the thermal problems associated with high power transmission at UHF and L-Bands (0.3 GHz - 2.0 GHz), and it advances the state of the art of radar technology through the development and testing of small diameter air-cooled low-loss coaxial transmission lines.

Current Technology

The coaxial and waveguide are two general categories of transmission lines and are commonly used in the transmission of high frequency radio frequency (RF) and microwave energy. The coaxial conductor is a transmission line in which electromagnetic waves propagate (refer to references [5] or [6] for a detailed discussion of transmission line theory) through a dielectric medium bounded by concentric inner and outer conductors. A typical cross section of a coaxial transmission line is shown in Figure 1. Coaxial lines operate from DC up to the cutoff frequency, F_c.

Coaxial transmission lines are available in flexible, semi-rigid and rigid forms. In general the flexible coax can be bent to a minimum radii of 5 diameters, the semi-flexible to a minimum bend radii of 10 diameters while the rigid cannot be bent. Thus, routing of flexible and semi-rigid is much less constraining than routing of the rigid.

Typically, flexible and semi-rigid coax lines are constructed with a solid dielectric filler. Materials used for these fillers include Teflon (TFE), solid /foamed Polyethylene (PE) and solid/foamed Ethylene Propylene (EP). Rigid lines are almost always air filled and use dielectric support beads to hold the inner conductor in place.

Air has a dielectric value, ε, of 1 while solid dielectric fillers typically have values ranging between 1.4 - 3.5. Dielectric losses increase with increasing ε. The ratio of inner to outer conductor diameters increases with decreasing ε. This results in a larger inner conductor diameter which yields decreased inner conductor losses. Thus the increase in inner conductor diameter and lower dielectric losses explains why air filled coaxial transmission lines are typically used in higher power applications.

The outer conductors for the flexible lines are typically constructed of braided copper or aluminum wire. The outer conductors for semi-flexible lines are typically constructed of copper or aluminum tubing. Corrugated tubing is also a commonly used material. Rigid lines are typically constructed of precision copper or aluminum tubing. Inner conductors are typically constructed of copper or aluminum. For certain applications, lines have silver and/or gold plated conductor surfaces to keep line losses to a minimum. Flexible and semi-flexible lines are typically jacketed.

A number of different waveguide designs exist; including circular, elliptical and rectangular. Regan [6] gives a detailed discussion on the pros and cons for different waveguide designs. This study will address only the most commonly used waveguide, the rectangular which is shown in Figure 2. Unlike the coaxial transmission line, which can propagate from DC to f_c, the waveguide has a limited bandwidth of operation (refer to [6] for further discussion on Guided-Wave concept of propagation). Typically, a rectangular waveguide is constructed out of copper or aluminum tubing. Like rigid coax, routing of rectangular waveguide can be constraining. In comparison to coax lines, waveguides tend to be very low in loss which results in higher power capabilities. King [10] presents curves and expressions for calculating the continuous wave (CW) power rating of the rectangular waveguide. At UHF and L-Band frequencies air filled waveguides may be prohibitive in size. However, the size of the waveguide can be reduced by dielectrically loading the inner cavity.

Table 1 presents a comparison among a small sample of different types of commercially available transmission lines. From this table it can be noted that waveguides are physically quite large and would not be suitable for the applications of interest. A high dielectric (ε = 10 - 40) filler might be considered for reducing the waveguide size. However, the number

of suitable high dielectric materials is limited. Ceramics are the only commonly used high dielectric material, because they are low in loss and stable. The problem with ceramics is that they tend to be heavy, a poor thermal conductor, susceptible to thermal stress cracking and tend to be very brittle. Because of these problems, this study will not address waveguide transmission lines.

Macalpine [9] studied the steady state heating effects within a dielectrically loaded coax. He identifies that the power-handling capacity of a transmission line is established by: 1) the maximum voltage breakdown within the line and 2) by the maximum temperature rise that components can withstand before significant degradation. The phenomenon associated with voltage breakdown is more of a peak power issue and is beyond the scope of this study. Macalpine constructed a closed form solution for solving the thermal problem associated with the dielectrically loaded coaxial cable.

Nero [1] studied methods for improving the power capacity of the rigid air filled coaxial line. His first approach was to investigate the effects of using thermally conductive support beads. The idea behind this approach was to develop a thermally conductive path from the inner to the outer conductor. His first specimen incorporated Beryllium Oxide (BeO) support beads. These beads were incorporated into a 30-ohm 1/2" air filled coax line (CU - inner and AL - outer). The inner conductor temperature, T_a, was measured at 600°F when P = 2.4 kW at F = 0.9 GHz. The second specimen incorporated Fluoroloy-H support beads and were incorporated into a 50-ohm 1/2" air filled coax line (AL - inner and AL - outer). T_a and T_b were measured at 500°F and 200°F respectively when P = 2 kW at F = 0.76 GHz. Nero, noted that *the dominant mode of heat transfer from the inner to outer conductor was gaseous conduction.*

His second approach included the use of forced air which was blown between the inner and outer conductors. In this approach heat was removed from the inner conductor through both conduction and convection. A 75-ohm 1/2" air filled coaxial (SS w/ CU plating - inner and AL - outer) specimen was tested. During testing forced air was blown between inner and outer conductors. T_a and T_b were measured at 600°F and 290°F respectively, when P = 4 kW at F = 0.938 GHz.

A third approach included the use of forced liquid cooling through the inner conductor. This approach used water as a coolant, which has a high specific heat. The heat was primarily removed from the inner conductor through convection. A 50-ohm 1/2" air filled coaxial (AL - inner and AL - outer) specimen was tested. During testing, 68°F water was pumped through the inner conductor at a flow rate of 0.1 GPM. T_a and T_b were measured at 125°F and 225°F respectively, when P = 8 kW at F = 0.98 GHz.

The final approach included the use of forced liquid cooling through both the inner and around the outer conductors. This approach used water as a coolant and most of the heat was removed from both the inner and outer conductors through convection. A 48-Ohm 3/8" air filled coaxial (AL - inner and AL - outer) specimen was fabricated. During testing 71°F water was pumped through the inner conductor at a flow rate of 0.15 GPM. 81-96°F water was pumped through a cooling jacket, which encased the outer conductor at a flow rate of 0.1 GPM. T_a and T_b were measured at 119°F and 163°F respectively, when P = 9 kW at F = 0.944 GHz.

This study clearly showed that forced liquid cooling can dramatically increase the power capacity of the coaxial transmission line. There are several problems associated with implementing liquid cooling into a real system. Liquids are a poor medium for RF energy

propagation. If coolant were to leak into the RF circuit the results could be catastrophic, possibly resulting in damage to the radar system. To implement this approach would require the development of a new connector design, which would not only produce a good electrical connection but a perfect fluid connection. If liquid cooling were incorporated, it would complicate the servicing of lines. To achieve a reliable liquid cooling system design would require extensive testing and resources.

Nero's work showed promising results for the forced air design. If refined, this approach was thought to be a more workable solution to increasing the power capacity. Dry air is an inert fluid and does not effect the RF circuit. A second advantage to this approach is that new connector designs would not be required, because the current rigid line connectors form air tight connections. Servicing would not be any more difficult than on existing systems where lines are pressurized. It is thought that a refined forced air cooling line could easily be incorporated into a radar system and that incorporation would have a minimal impact on system cost.

Therefore, the rest of this study will focus on the further development of the air-cooled low-loss coaxial transmission line. Chapter II addresses the test methodology and results. Chapter III presents a complete discussion on the development of FEA models used to model various air-cooled coaxial lines. A discussion and comparison of test and calculated results is made in Chapter IV. Chapter V summarizes the findings and makes recommendations.

TABLE 1 — Comparison Commercial Transmission Lines

Type	Size	Construction	F (GHz)	α (dB/100')	P_{max} (kW)
Flexible 50Ω Coax RG-58B/U	a = 0.035" b = 0.116" D = 0.195"	In: 19/.0072" Out:Braided Tin/CU Filler: PE Jacket: Yes	DC - 1	10.0 (.4 GHz) 17.5 (1 GHz)	0.085 (.4 GHz) 0.05 (1 GHz)
Semi-Flexiable 50Ω Coax RG-259/U	a = 0.117" b = 0.314" D = 0.465"	In: AG Plated CU Out: AL Fill.: TFE Tubes Jacket: Yes	DC - +10	2.7 (.4 GHz) 4.4 (1 GHz)	1.3 (.4 GHz) 0.8 (1 GHz)
Semi-Flexiable 50Ω Coax RG-377/U	a = 0.168" b = 0.45" D = 0.63"	In: AG Plated CU Out: AL Fill.: TFE Tubes Jacket: Yes	DC - 8.5	1.9 (.4 GHz) 3.1 (1 GHz)	2.3 (.4 GHz) 1.4 (1 GHz)
Semi-Flexiable 50Ω Coax RG-256/U	a = 0.331" b = 0.833" D = 1.093"	In: AG Plated CU Out: AL Fill.: TFE Tubes Jacket: Yes	DC - 4.5	3.1 (.4 GHz) 1.7 (1 GHz)	5.4 (.4 GHz) 3.2 (1 GHz)
Rigid 50Ω Coax EIA 7/8"	a = 0.125" b = 0.785" D = 0.875"	In: CU Out: CU Filler: Air Jacket: No	DC - 4.2	0.9 (.45 GHz) 1.2 (.8 GHz)	2.0 (.45 GHz) 1.5 (.8 GHz)
Rigid 50Ω Coax EIA 1-5/8"	a = 0.341" b = 1.527" D = 1.625"	In: CU Out: CU Filler: Air Jacket: No	DC - 2.8	0.41 (.45 GHz) 0.54 (.8 GHz)	6.8 (.45 GHz) 5.0 (.8 GHz)
Rigid 50Ω Coax EIA 3-1/8"	a = 0.664" b = 3.027" D = 3.125"	In: CU Out: CU Filler: Air Jacket: No	DC - 1.35	0.2 (.45 GHz) 0.27 (.8 GHz)	22.5 (.45 GHz) 16.5 (.8 GHz)
Rectangular Waveguide WR 1800	A = 18.0" B = 9.0"	W/G: CU Filler: Air	0.41 - 0.625	0.056 - 0.038	3,000 - 5,000 [10]
Rectangular Waveguide WR 975	A = 9.75" B = 4.875"	W/G: CU Filler: Air	0.75 - 1.12	0.137 - 0.095	800 - 1,300 [10]

FIGURE 1 — Typical Coaxial Transmission Line

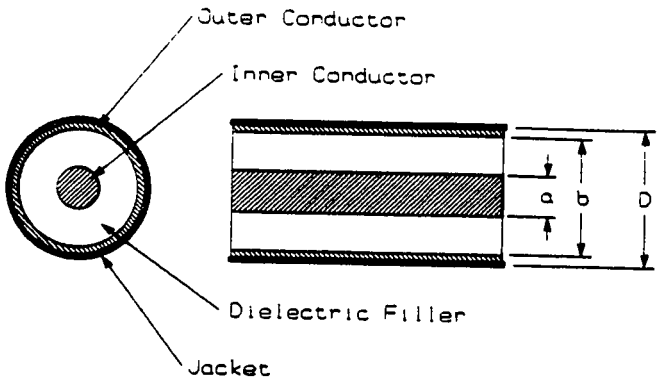

FIGURE 2 — Typical Rectangular Waveguide

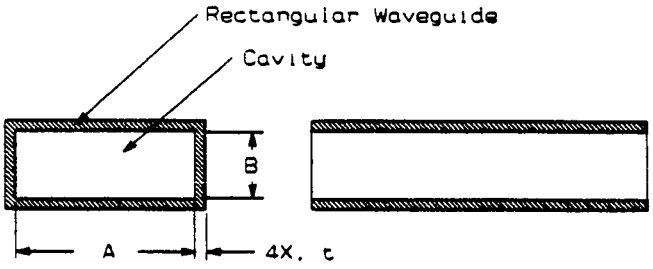

Objectives/Approach

The primary objective of this study is to develop an air-cooled low-loss coaxial transmission line which could be incorporated into high power UHF or L-Band radar systems. A real application was identified in which the outside diameter of the coaxial line could not exceed 1/2". A power capacity of 8 kW CW (continuous wave, i.e. non pulsed wave form) at 0.45 GHz was also established as a design goal.

The internal forced air cooling approach, where the conductors are cooled by free air convection, was identified as the most suitable approach. From Heat Transfer theory it is commonly known that a heated rod which is cooled by free air convection will assume different temperature gradients with change in orientation. Therefore, it was thought that this effects should be investigated. Moreno, [5], suggested that 33-ohm coax line is the optimum impedance for power-carrying capacity. The 50-ohm line is an industrial standard commonly used in radar applications. Therefore, it was determined that both 33 and 50-ohm specimens should be evaluated. Finally, it is known that inner conductor material selection will have a significant effect on line attenuation. Aluminum and copper inner conductors were evaluated in this study. Test specimens were fabricated and high power tested. Measurements were taken at steady state conditions.

The second objective was to develop a model which could be used by the design engineer to predict steady state operating temperatures. A computer model using commercially available FEA software, [3], was used in this study. Several FEA models were constructed. Equations were derived for calculating heat sources and convection coefficients. From the measured temperature data, expressions for calculating the internal convection coefficients were empirically derived.

The final objective was to find an accurate method for measuring inner conductor temperature. Accurate T_b measurement data is needed if the other two objectives were to be realized.

II. HIGH POWER TESTS

Introduction

This chapter describes the setup, procedures and results of evaluating four rigid coaxial transmission lines (specimens) which were tested to steady state at high RF power. The purpose of this test was to measure the steady state temperatures of the specimens' inner and outer conductors. As shown in Figure 3 a forced air transmission line cooling system was designed. The first test objective was to evaluate the effectiveness of this cooling system. The second objective was to measure the changes in operating temperature for specimens with different inner conductors. Finally, the third objective was to collect data which could be used to further develop the model described in Chapter III.

Test Specimens

Four, 1/2" diameter by 60" long rigid air coaxial transmission lines were constructed for this test. All specimens used a common, 6061 aluminum, outer conductor assembly. 6061 aluminum is commonly used for rigid transmission lines because it has: low resistivity, is easy to machine, is dip brazeable and good mechanical properties. Inner conductor assemblies for specimens #1 and #3 were machined from copper alloy 101, while specimens #2 and #4 were machined from 6061 aluminum. Copper alloy 101 was chosen for an inner conductor material because of its low resistivity and is readily available. Specimens #1 and #2 had a center section (approximately 26" in length) with a characteristic impedance, Z_o, of 33-ohms. Two step transformers located on both sides of the 33-ohm section provided a transformation to 50-ohms. Z_o was a constant 50-ohms for specimens #3 and #4. Teflon beads were used to support the inner conductors concentrically within the outer conductor assembly. All specimens were designed such that

forced air could be passed between the inner and outer conductors. Figure 3 defines the configuration of the four test specimens.

FIGURE 3 — Configuration of Test Specimens

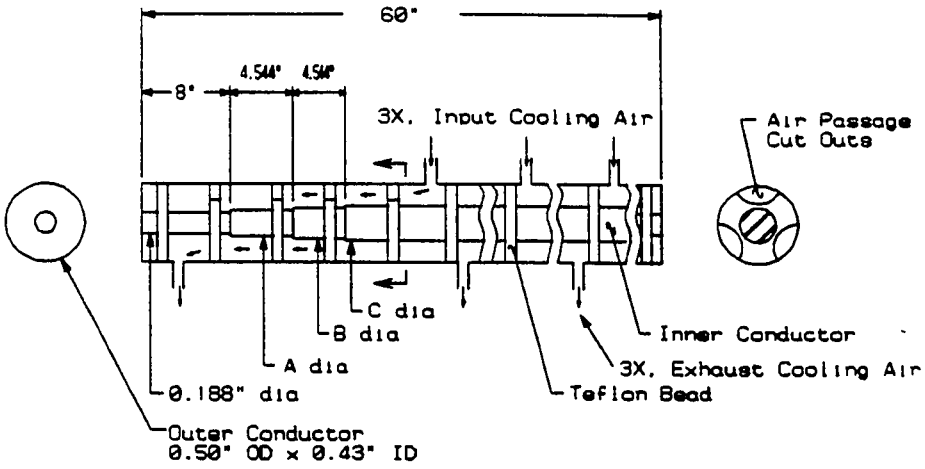

Specimen	Z_0	Mat'l Outer	Mat'l Inner	A dia	B dia	C dia
#1	33 Ω	6061 AL	CU Alloy 101	0.210"	0.229"	0.248"
#2	33 Ω	6061 AL	6061 AL	0.210"	0.229"	0.248"
#3	50 Ω	6061 AL	CU Alloy 101	0.188"	0.188"	0.188"
#4	50 Ω	6061 AL	6061 AL	0.188"	0.188"	0.188"

Test Setup

Figure 4 shows a picture of the Aydin Model 1518A2 klystron power amplifier used for this test. Figure 5 shows a block diagram of the test setup. Figures 6 and 7 show pictures of the setup configured for specimen evaluation in the horizontal and vertical positions (θ = 0° and 90°).

One objective of this test was to establish an accurate technique of measuring the inner conductor temperature. Nero [1] had used self-adhesive temperature sensing labels to measure the inner conductor temperature, T_a. These labels change color with temperature giving a permanent record of only the maximum temperature, during the temperature excursion. Accuracy of the measurement is dependent upon the user's ability to correctly interpret the change in color. Other types of sensors such as thermocouples and RTDs have electrical leads and are of a metallic construction. Consequently, these devices tend to disrupt the electrical fields within the transmission line and can ultimately cause electrical breakdown. These devices tend to couple with the strong electrical fields, within the transmission line, resulting in sensor noise and feigned heating of the sensor. Wickersheim and Sun [2] discuss various applications suited for fluoroptic thermometry. One application discussed is temperature measurement within the presence of strong microwave fields. The non metallic construction of the fluoroptic probe gives accurate temperature measurements, which are non intrusive to the electrical fields.

A 4-channel, Luxtron Model 755 Fluoroptic Thermometer was used to measure the real time temperature of the specimens' inner conductors. This instrument was classified by Wickersheim and Sun [2] as *Second Generation* and the principle of operation is as follows. A Xenon flash lamp sends a pulsed light excitation (λ of 350 - 500 nm) down a fiber optic cable. The end of the cable is either coated or in close proximity to some

phosphor sensing material (magnesium fluorogermanate). This excitation will cause the material to fluorescence; the emitted light is red in color (λ of 620 - 700 nm). The decay time of the red light varies with temperature. Therefore, the temperature of the sensing material is determined by measuring the decay time of the emitted red light.

Figures 8 and 9 show the Luxtron MSA contacting and Luxtron PDA remote sensing probes used in this test. The tip of the MSA contacting probe should make intimate contact to the surface under test to insure accurate measurement. Accurate measurements can be made with the tip of the PDA remote sensor placed as far 0.25" away from a treated surface. Bosses were incorporated onto the outer conductor assembly. The bosses permitted the Fluoroptic probes to pass through the outer conductor wall. Compression gaskets were used to secure the probes in place during testing and formed an air tight seal around the probe.

Type T thermocouples were used to monitor the outer conductor, ambient air and cooling air temperatures. Thermocouples could be used for these measurements since the strong electrical fields were contained within the transmission line. Thermocouples were secured to the outer conductor with aluminum tape. Figure 10 shows a typical sensor installation. Figure 11 and Table 2 identifies where sensors were positioned on the specimen.

The specimens were designed so that air could be passed between the inner and outer conductors. The specimen was divided into three 20" long sections. Solid Teflon support beads were used to isolate air flow between sections. Teflon beads with air passage cutouts were installed within each section. A cooling system control panel was used to control the air flow and line pressure in each of the three sections. Figure 12 shows a block diagram of the cooling system. The cooling system control panel is pictured in

Figure 6. The cooling system was calibrated to operate at 15 psig and with volumetric flow rate of cooling air, Q, of 0, 10 and 20 standard cubic feet per hour (SCFH). The line pressure and flow rates were set by adjusting the needle valves at both the input and output of each section. For all tests, each of the three sections was adjusted to equal flow states. Bottled dry air was used during the first day of testing and oil-free shop air was used on subsequent days.

TABLE 2 — Sensor Identification

Pos	Instrument	Ch	Sensor	Location
1	Luxtron	1	MSA	Contacting Inner Conductor, y = 2.0"
2	Luxtron	2	MSA	Contacting Inner Conductor, y = 21.9"
3	Luxtron	3	PDA	Remote Inner Conductor, y = 30.9"; #1 @ 0°
			MSA	Contacting Inner Conductor, y = 30.9"; #1 @ 90°, #2, #3 & #4
4	Luxtron	4	MSA	Contacting Inner Conductor, y = 58.0"
5	Beckman	1	Type T	Boundary Layer, y ≈ 2.0" & ≈ 0.5" away from OD
6	Beckman	2	Type T	Boundary Layer, y ≈ 2.0" & ≈ 0.06" away from OD
7	Beckman	3	Type T	Contacting Outer Conductor, y = 2.0"
8	Beckman	4	Type T	Contacting Outer Conductor, y = 21.9"
9	Beckman	5	Type T	Contacting Outer Conductor, y = 30.9"
10	Beckman	6	Type T	Contacting Outer Conductor, y = 58.0"
11	Beckman	7	Type T	Boundary Layer, y ≈ 58.0" & ≈ 0.06" away from OD
12	Beckman	8	Type T	Boundary Layer, y ≈ 58.0" & ≈ 0.5" away from OD
13	Beckman	9	Type T	Input Air to Cooling System
14	Beckman	10	Type T	Ambient Temperature
15	Beckman	10	Type T	Exhaust Air, Section 1
16	Beckman	10	Type T	Exhaust Air, Section 2
17	Beckman	10	Type T	Exhaust Air, Section 3

FIGURE 4 — Aydin Model 1518A2 Klystron Power Amplifier

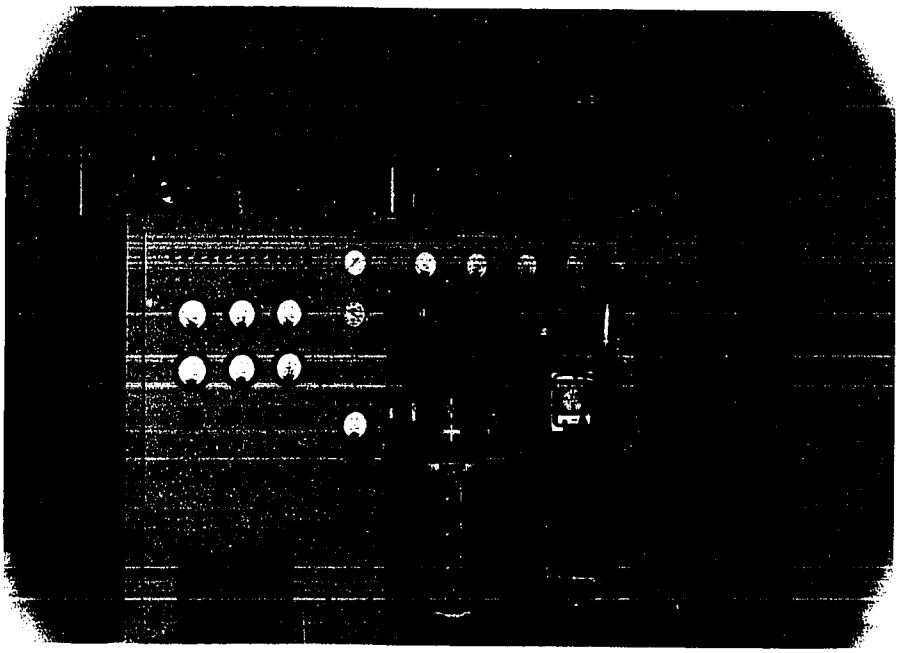

FIGURE 5 — Block Diagram of Test Setup

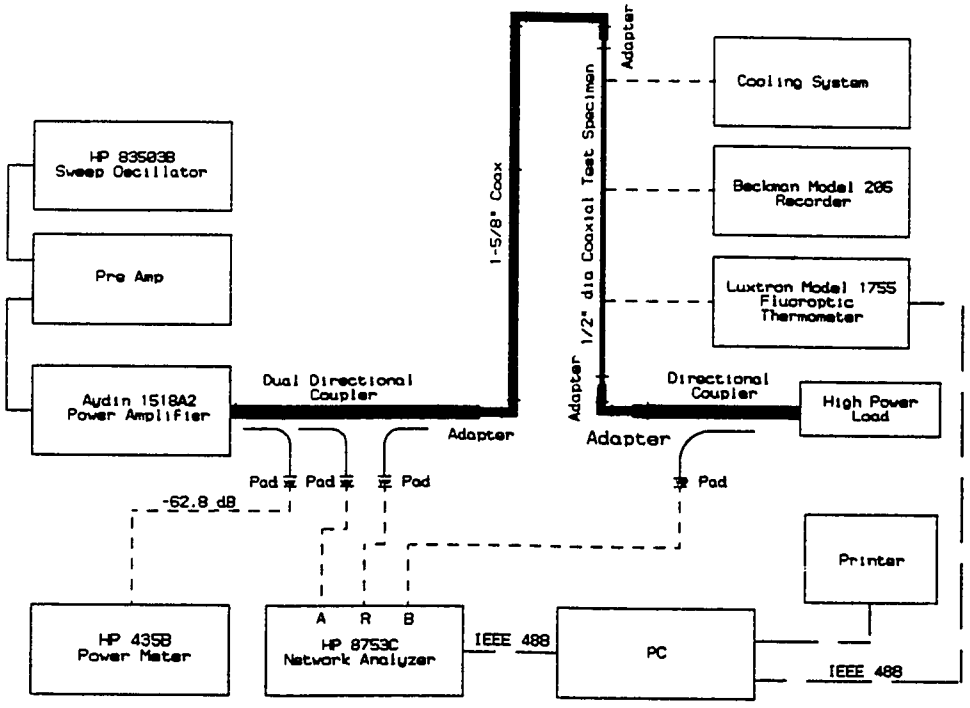

FIGURE 6 — Test Setup in $\theta = 0°$ Configuration

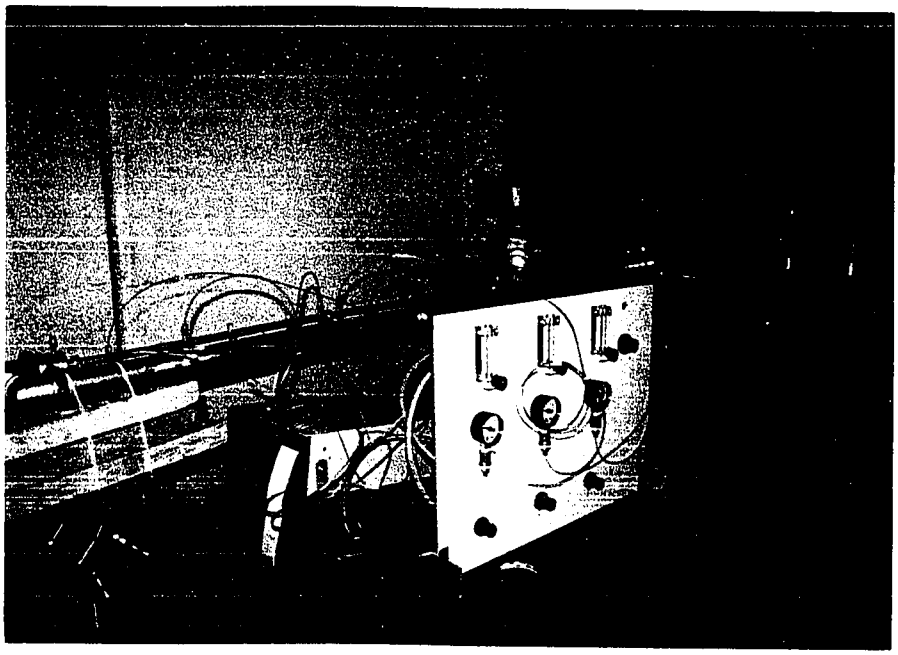

FIGURE 7 — Test Setup in $\theta = 90°$ Configuration

FIGURE 8 — Luxtron MSA Contacting Probes

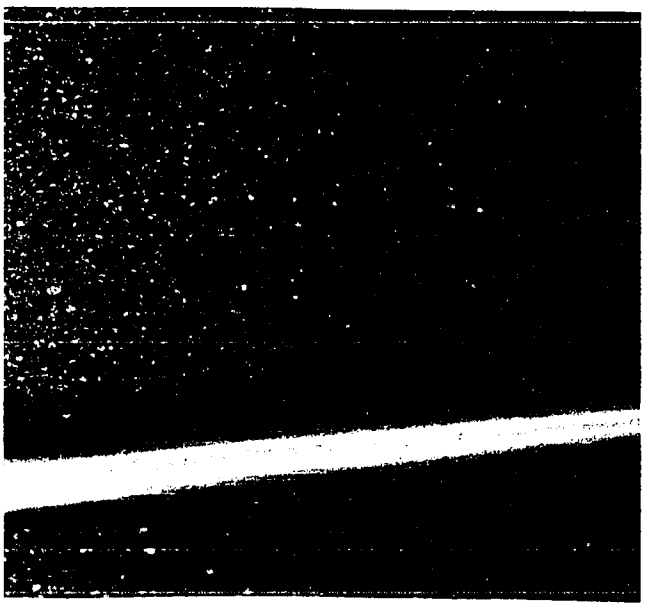

FIGURE 9 — Luxtron PDA Remote Sensing Probe
Note: Sensing Material on Inner Conductor.

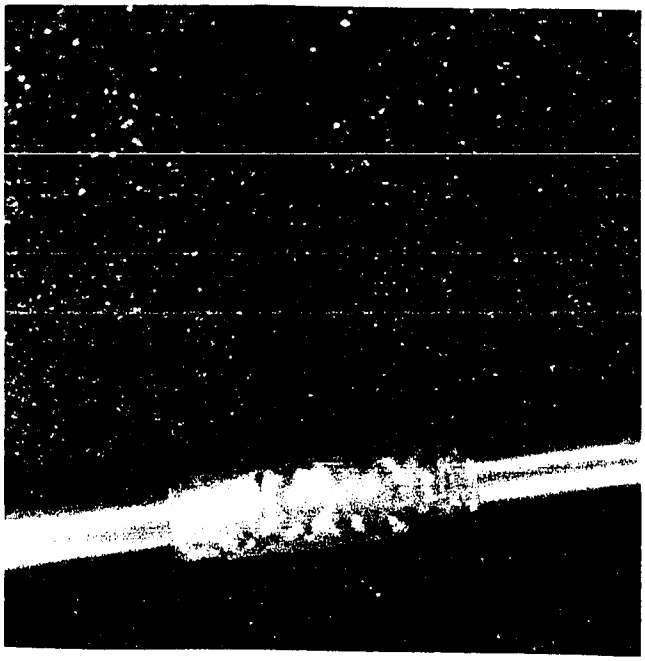

FIGURE 10 — Typical Sensor Installation

**Luxtron probe can be seen passing through the center of the Boss.
A Type T thermocouple is taped to the right side of the Outer Conductor.
The other two Type T thermocouple measured the external air stream.**

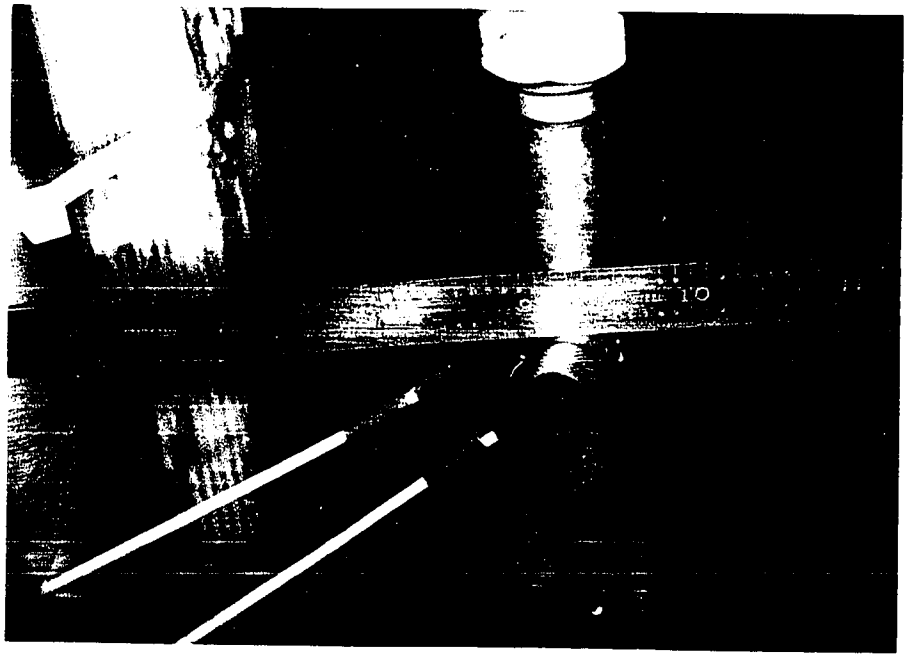

FIGURE 11 — Sensor Placement

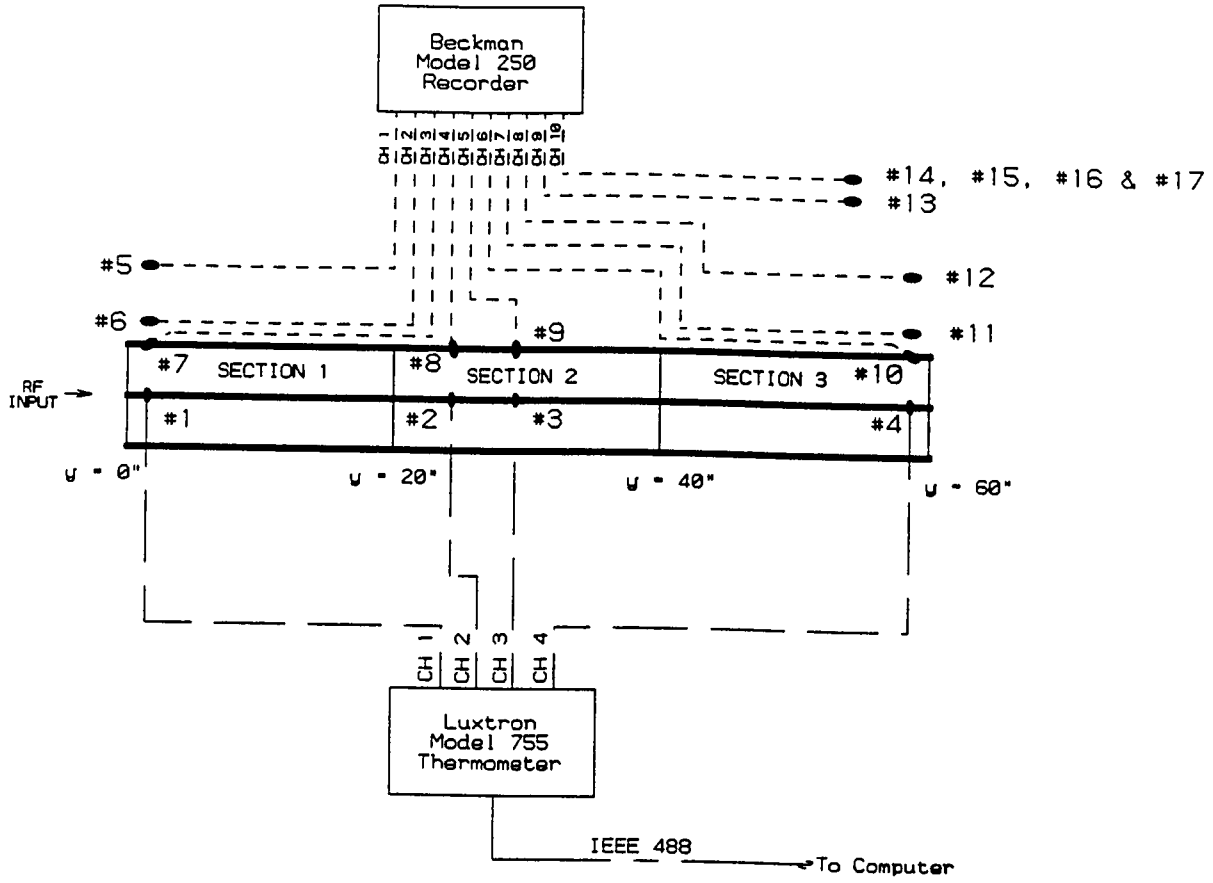

FIGURE 12 — Diagram Cooling System

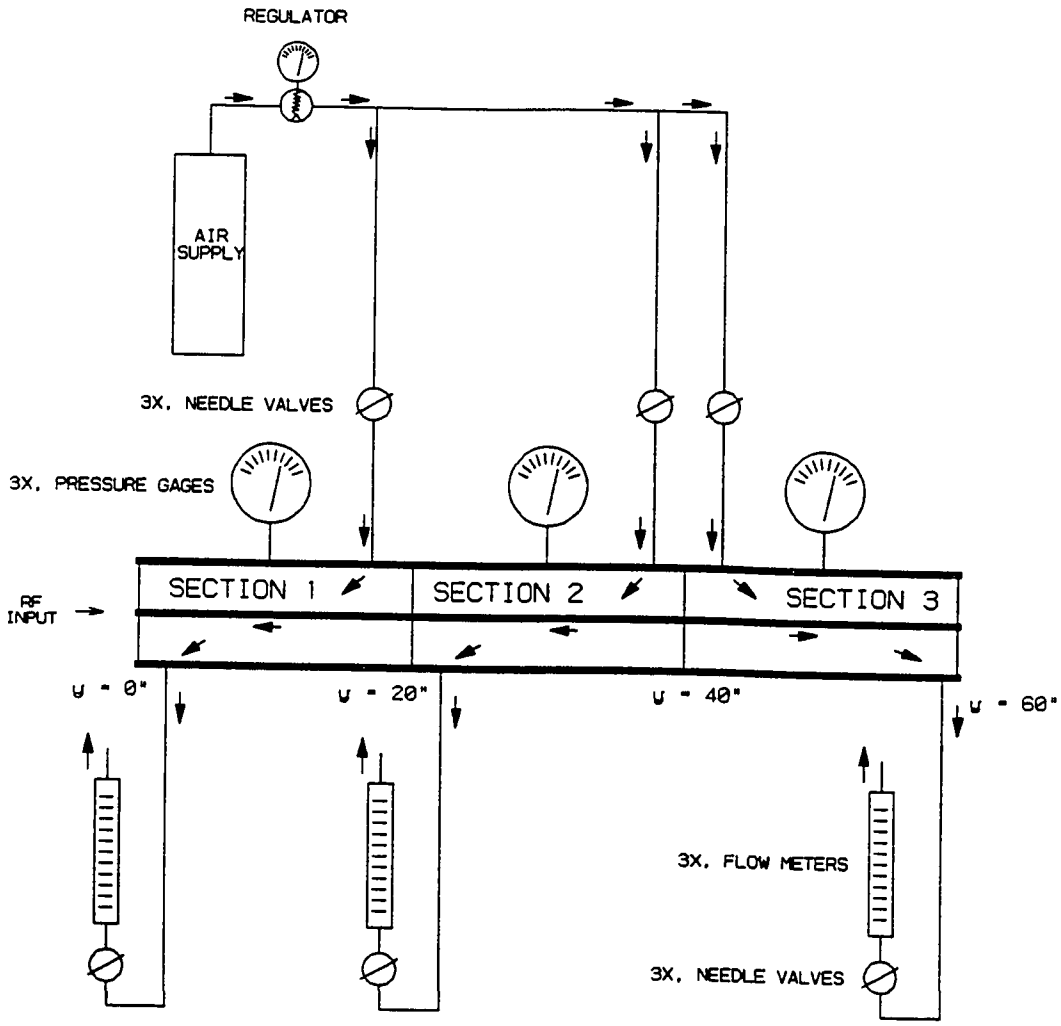

Test Plan

The general test procedure was to apply RF power and monitor test conditions using the specimens and the setup as described above. A L-Band high power CW source was locally available. Since a limited amount of time was available for testing it was decided to conduct all testing at a fixed frequency, F. Therefore, all testing was conducted at an arbitrarily chosen F of 0.8 GHz. Testing at each state was conducted at a fixed power level. The setup was assumed to have reached steady state conditions when the temperature readings had stabilized. Data was recorded at the steady state conditions. Recorded data included: date of test; time at which data was recorded; specimen configuration; power output from high power source; relative insertion loss (Insertion loss is a measure of line loss, commonly expressed in dB.) and VSWR (Were voltage standing wave ratio, is a measure of how well the line is matched. As VSWR increases so does the amount of reflected incident energy.), temperature sensor readings; line pressure; cooling air flow rate; and any comments or observations. Data collection software was written to automate the process of collecting data from the Luxtron thermometer and the HP 8753C network analyzer. The Beckman recorder was setup to printout temperature readings. After data was recorded the setup was taken to a new state by either incrementally increasing the amplifier power or by incrementally changing Q. Q was incrementally increased from 0 to 10 SCFH or from 10 to 20 SCFH, while maintaining a constant 15 psig line pressure. Testing was terminated when any of the sensors measured ≥400°F and Q was 20 SCFH.

Test Results

Specimens were tested as listed in Table 3. On average ΔT_a and ΔT_b decreased by 25% when Q was increased from 0 to 10 and from 10 to 20 SCFH. Incorporation of the copper

inner conductor further reduced ΔT_a by 20% and ΔT_b by 9%. On average ΔT_a measured higher 6% and ΔT_b measured higher 35% for the 33-ohm specimens.

Tabular results listing measured temperatures and calculated ΔTs have been included in Appendices A and B. Data listed in Appendix A is the data as recorded during testing. Data listed in Appendix B presents calculated change in temperature relative to T_{amb} (sensor #14).

Appendix C includes plots of ΔT at y = 21.9" versus P. This position was chosen: 1) as it is a worst case position since the cooling air is exhausted at y = 20" and 2) because there should be minimal sinking influences caused by the test adapters.

Delta temperature distribution for both inner and outer conductors is presented in Appendices D and E respectively. As would be expected, for the cases where Q = 0 SCFH the temperature distribution is such that the maximum temperature occurs at approximately y = 30". But for the other cases, where $Q \neq 0$, the temperature at y = 31" is notably lower than at y = 22". This occurs because in section 2, the cooling air was injected in at y = 40" and exhausted at y = 20". This results in the heating of the cooling air as it flows from y = 31" to y = 22".

In general the testing progressed smoothly, but some observations were noted during testing which might have influenced the results. No calibration kits were available to calibrate the HP 8753C; so only relative measurements for insertion loss and VSWR could be taken during high power testing. However, an adapter substitution technique was used

to measure the relative insertion loss and VSWR of the specimens; results are presented in Table 4.

During the testing of specimen #1 ($\theta = 0°$) the temperatures measured from sensor #3, the Luxtron PDA remote sensing probe, were questionable. For example, at 2 kW and 0 SCFH a 70°F-plus difference between this and the adjacent probes was recorded. During test setup there was some difficulty in getting this probe to work properly. The suspected cause for erroneous reading might be attributed to the poor application of the sensing material. The MDA probes appeared to be non intrusive and did not cause any breakdown problems; therefore, it was decided not to use the PDA probe on any subsequent testing and instead use a MDA probe.

The high power amplifier used for this test was designed for commercial use and designed to operate continually at 10 kW. This test required relatively low power output levels for this amplifier; hence, fluctuations in power output of ±0.2 dB were observed. At a nominal 5 kW output a ±0.2 dB fluctuation equals ±235 watts. During testing the power level was constantly monitored and adjusted as required.

It was intended that all testing be conducted in still air, so that free air convection cooling could be realized at the outer surface of the specimens. Testing was conducted in back of the high power amplifier where exhaust air from the amplifier's blower was vented. Large sheets of foam were used to divert this air flow.

Lifting of some of the aluminum tape, used to attach the thermocouples, had been observed after some of the runs. Also, the adapters located at each end of the specimen were large and massive relative to the specimens. These adapters tended to act as sinks during high

power testing; thus, a larger then anticipated temperature gradient, along the length of the specimen, was measured.

The test setup was evaluated for repeatability. These checks were made during the testing of specimens #1 ($\theta = 0°$) and #2 ($\theta = 0°$). Repeatability of the Luxtron thermometer was $\leq 3\%$ if the results from specimen #1/probe #3 are disregarded (erroneous results due to remote sensor) and specimen #2/probes #1 and #4 are disregarded (boundary condition effects due to adapters). Repeatability of the type T thermocouples was $\leq 4\%$ if the sensors at the ends of the specimens are disregarded (boundary condition effects due to adapters).

The rise in cooling air temperature was measured with sensors #14, #15, #16 and #17. Thermocouple #14 measured the ambient air temperature while thermocouple #15, #16 and #17 measured the exhaust temperatures from sections 1, 2 and 3 respectively. The test setup for these measurements was clumsy, as thermocouples #14, #15 and #16 where manually positioned in the exhaust stream at the time of measurement. Thus measurement accuracy was dependent upon the operator's measurement technique. Figure 13 presents a plot of average measured temperature rise for the 50 Ohm specimens at various test conditions. However, upon further review, based upon further testing, it is believed that the measured exhaust stream temperatures are in error. The calculated heat, resulting from the transfer of heat to the air stream is only 0.6 to 2.5 $\frac{BTU}{hr}$; which accounts for less than 2.2% of the total calculated heat resulting from conductor losses.

TABLE 3 — Test Sequence

Date	Specimen	θ	P (kW)	Q (SCFH)
2/25/93	#1	0°	0.25	0
			0.50	0
			1.00	0
			0.50	0
			1.00	0
			2.00	0
			2.00	10
			2.00	20
			3.00	10
			4.00	20
			4.50	20
			5.00	20
			5.00	20*
			6.00	20*
2/26/93	#1	90°	0.50	0
			1.00	0
			2.00	0
			3.00	0
			3.00	10
			4.00	10
			5.00	20
			5.50	20
			5.50	20*
			7.00	20*
2/26/93	#4	90°	1.00	0
			3.00	0
			3.00	10
			4.00	10
			4.00	20
			4.50	20
3/4/93	#2	90°	1.00	0
			3.00	0
			3.00	10
			4.00	10
			4.00	20
			4.50	20
3/4/93	#2	0°	1.00	0
			3.00	0
			3.00	10
			4.00	10
			4.00	20
			4.78	20
			1.00	0
			4.78	20
3/5/93	#3	0°	1.00	0
			3.00	0
			3.00	10
			4.50	10
			4.50	20
			6.50	20
3/5/93	#3	90°	3.00	0
			3.00	10
			4.50	10
			4.50	20
			6.50	20

* External cooling with fan plus internal cooling with Q = 20 SCFH.

TABLE 4 — Measured Insertion Loss & VSWR

Specimen	Measured I-Loss Pre Test	Measured I-Loss Post Test	Measured VSWR Pre Test	Measured VSWR Post Test
#1	0.140 dB	0.150 dB	1.040	1.047
#2	0.160 dB	0.150 dB	1.066	1.100
#3	-	0.104 dB	-	1.069
#4	0.150 dB	-	1.026	-

FIGURE 13 — Measured Temperature Rise of Cooling Air
(Results are questionable, see page 27)

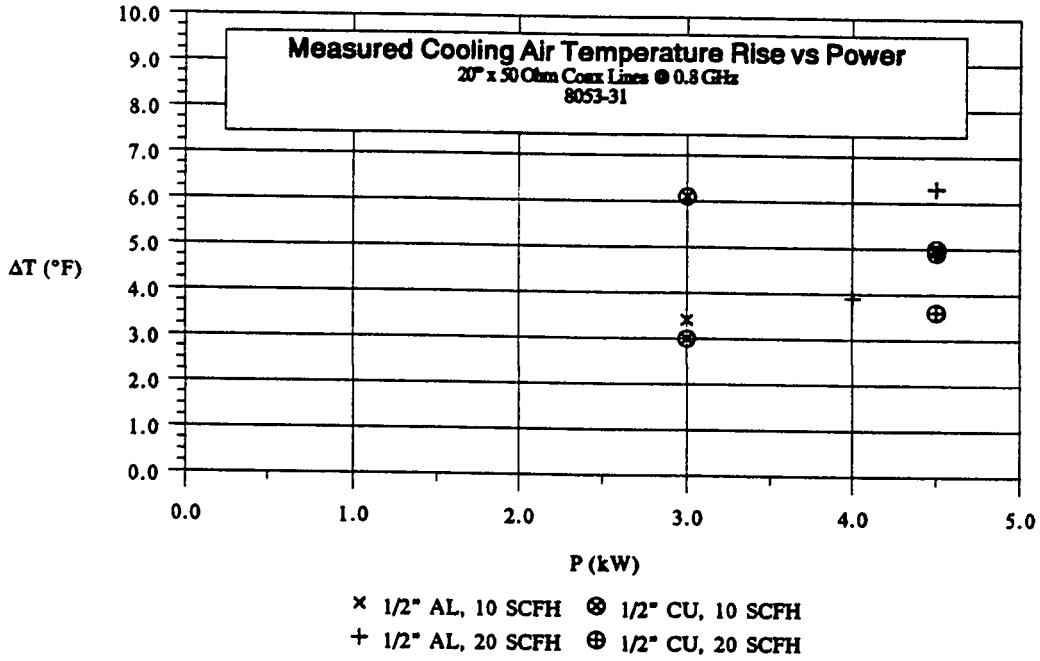

III. THERMAL ANALYSIS

Introduction

This chapter describes the development of two FEA models which were used to analyze the coaxial transmission lines. An order of magnitude analysis showed the significant modes of heat transfer for this problem.

The following analysis calculates and compares the heat flux due to conduction, convection and radiation for a 1" section of 50-ohm 1/2" diameter line operating at 1 kW, 0.8 GHz and Q = 0 SCFH. The following values were measured during high power testing:

$$\Delta T_a = 75^\circ F$$

$$\Delta T_b = 31.6^\circ F.$$

Heat flux from convection can be determined from Newton's Cooling Law.

$$q_c = h_1 A_a \Delta T_a + h_2 A_b \Delta T_b. \qquad (2\text{-}1)$$

Convection values for Q = 0 SCFH were empirically established:

$$h_1 = h_2 = 0.007 \frac{BTU}{in^2 hr^\circ F}.$$

Inner and outer conductor surface areas are expressed as:

$$A_a = \pi(0.188")(1") = 0.591 in^2$$

$$A_b = \pi(0.430")(1") = 1.351 in^2.$$

Thus solving (2-1) yields:

$$q_c = 0.610 \frac{BTU}{hr}.$$

Heat flux due to radial conduction can be determined from Fourier's Law of Heat Conduction.

$$q_k = kA\frac{dT}{dx} \qquad (2\text{-}2)$$

Where for air

$$k = 1.108E-3\frac{BTU}{inhr^\circ F}$$

$$A = \pi\left(\frac{0.188" + 0.430"}{2}\right)(1") = 0.971in^2$$

$$\frac{dT}{dx} = \frac{75.0^\circ F - 31.6^\circ F}{0.121"} = 358.7\frac{^\circ F}{in}$$

thus solving (2-2)

$$q_k = 0.386\frac{BTU}{hr}.$$

Heat flux due to radiation can be determined from the following expression.

$$q_r = \sigma A_a \varepsilon (T_{in}^4 - T_{out}^4) \qquad (2\text{-}3)$$

where

$$\sigma = 1.19E-11\frac{BTU}{in^2hr^\circ R^4}$$

$$A_a = \pi(0.188")(1") = 0.591in^2$$

$$\varepsilon = 0.2 \text{ (assumed)}$$

$$T_{in} = 75^\circ F = 535^\circ R$$

$$T_{out} = 31.6^\circ F = 491.6^\circ R$$

thus solving (2-3)

$$q_r = 0.0331\frac{BTU}{hr}$$

From this analysis it can be seen that both convection and conduction play significant roles in the cooling of the line; while the effects due to radiation do not. Effects of radiation could have more a significant influence at higher line temperatures. Also, the effects of radiation could have a significant influence if the inner and outer conductors surfaces could be finished so that an emissivity approaching 1 could be realized.

During model development good correlation between FEA model COAX1 and results from Nero [1] were obtained. This occurred when both convection and conduction modes of heat transfer were assumed between the inner and outer conductors. Therefore, the models which are presented take into account only the effects of convection and conduction.

Model Development

Two FEA models were constructed to predict the steady state temperatures of the four specimens defined in Chapter II. IMAGES-Thermal [3] was the FEA program used during this study. The first model constructed was of a 50-ohm coaxial transmission line and had a file name of COAX7. The second model was of a 33-ohm coaxial transmission line and had a file name of COAX8.

Figure 14 shows COAX7, which consisted of 84 nodes and 60 elements. To simplify the model, axisymmetric solid elements were used. The model geometry is as follows: a 60" long by 0.188" diameter rod that is concentrically centered within a 60" long by 0.50" OD by 0.035" thick tube. Material properties of aluminum were used to model the 0.50" OD tube. Material properties of both copper and aluminum were used to model the 0.188" diameter rod. A hard copy output of COAX7 has been included in appendix F.

Figure 15 shows COAX8, which consisted of 132 nodes and 96 elements. To simplify the model, axisymmetric solid elements were used. The model geometry is as follows: a 60" long by four step (0.188" to 0.205" to 0.229" to 0.248" dia.) rod that is concentrically centered within a 60" long by 0.50" OD by 0.035" thick tube. Material properties of aluminum were used to model the 0.50" OD tube. Material properties of both copper and aluminum were used to model the stepped rod. A hard copy output of COAX8 has been included in appendix G.

It should be noted that details such as the bosses, for the Luxtron probes and air fittings, and line connections have been ignored in both of these models. A model, COAX5, of a 50-ohm coax line which included these details was constructed. Results from this model showed that these details yielded minor (≤2%), localized variations in the calculated results. Therefore, these details were not modeled within COAX7 and COAX8.

The cross section of the line forms an annular channel. In this channel air flow can be simulated by adjusting the values of the convection coefficients, h_1 and h_2. At the outer surface of the tube free air convection was simulated by the convection coefficient h_3.

FIGURE 14 — Model of 50-ohm Coax Line

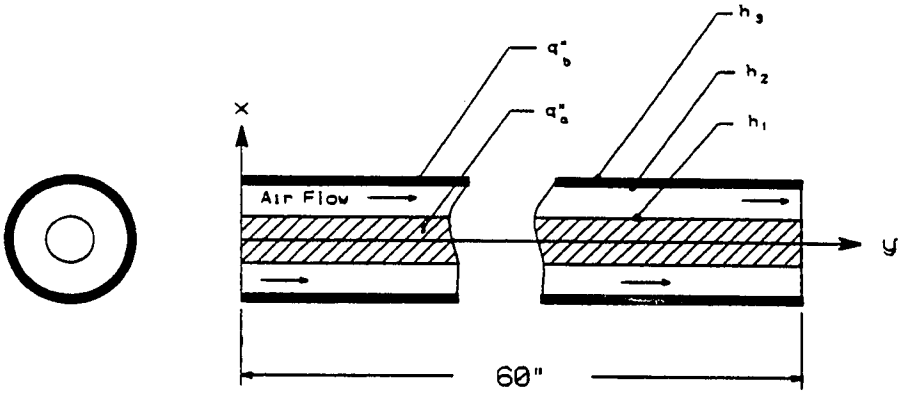

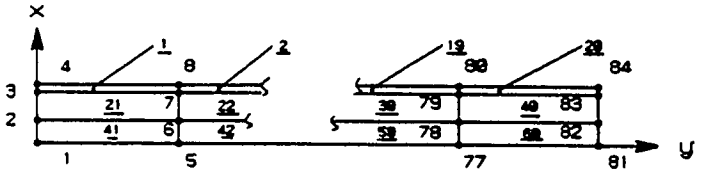

Element Definition:

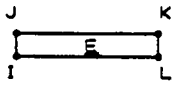

Convection Coefficents

Coeff.	Elements	Face
h_1	41 - 60	J - K
h_2	1 - 20	I - L
h_3	1 - 20	J - K

Heat Sources

	Elements
q''_a	41 - 60
q''_b	1 - 20

FIGURE 15 — Model of 33-ohm Coax Line

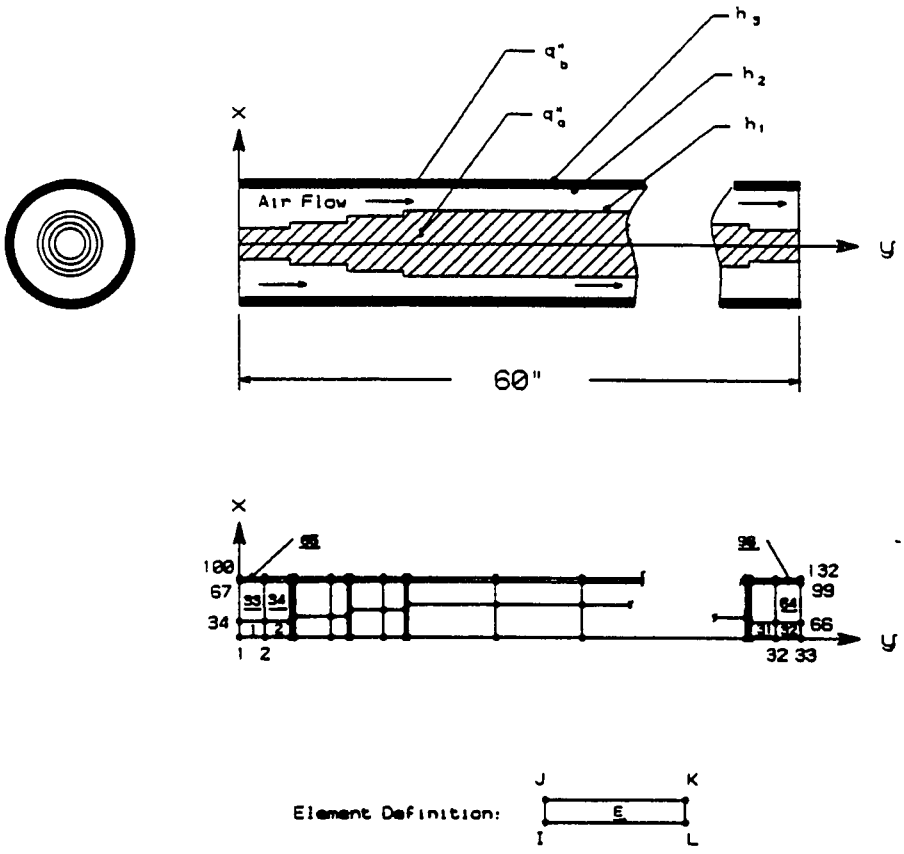

Element Definition:

Convection Coefficients

Coeff.	Elements	Face
h_1	1 - 32	J - K
h_2	65 - 96	I - L
h_3	65 - 96	J - K

Heat Sources

	Elements
q''_a	1 - 32
q''_b	65 - 96

Thermal Conductivity

Thermal conductivity, k, for aluminum, copper and air was expressed as a linear function:

$$k = K_1 + K_2T. \qquad (2\text{-}4)$$

The values for the constants K_1 and K_2 were determined by linearization of tabular data from Kreith [4]. Values of K_1 and K_2 are listed in Table 5.

TABLE 5 — Values Thermal Conductivity

Material	K_1 $\left(\frac{BTU}{in\ hr°\ F}\right)$	K_2 $\left(\frac{BTU}{in\ hr°\ F^2}\right)$
Aluminum	8.333	3.922E-3
Copper	18.616	-1.574E-3
Air	1.108E-3	1.55E-6

Heat Sources

Both the inner and outer conductors generate heat as a result of transmission line losses, α_T. The heating due to the inner and outer conductor losses are defined by q_a^* and q_b^*. This section derives these heating source terms.

Moreno [5] stated that UHF/microwave transmission line losses could be caused by the following: hysteresis losses, radiation leakage losses, mismatch losses, resistive losses and dielectric losses. Since the coaxial lines in this study are not constructed out of ferromagnetic materials, losses due to hysteresis need not be considered. Losses due to radiation leakage are not considered because coaxial lines tend to be shielded very well;

therefore, losses due to leakage are inconsequential. The lines in this study were very well matched (i.e. low VSWR). The specimens had a measured VSWR ≤ 1.10; thus, ≤ 0.23% of the incident power was reflected. Since the amount of reflected power was so low, this analysis ignored mismatch losses. Resistive losses, α_C, and dielectric losses, α_D, are considered in this model. The sum of these two losses yields the total loss of the transmission line, α_T.

$$\alpha_T = \alpha_C + \alpha_D \tag{2-5}$$

Moreno [5] defines α_C and α_D as:

$$\alpha_C = \frac{27.2}{\lambda}\left(\frac{\delta_a \mu_a}{a} + \frac{\delta_b \mu_b}{b}\right)\frac{\sqrt{\varepsilon_1}}{\ln\frac{b}{a}} \tag{2-6}$$

$$\alpha_D = 27.3\frac{\sqrt{\varepsilon_1'}}{\lambda}\tan\delta \tag{2-7}$$

Where α_C and α_D are in dB/unit length. The value for permeability, μ, is assumed equal to unity for non-ferromagnetic materials. The dielectric constant for the air, ε, is also equal to unity. Wavelength, λ, can be expressed in inches as a function of F, in GHz.

$$\lambda = \frac{11.811}{F} \tag{2-8}$$

From transmission line theory [5, 6] conductor currents, at the frequencies of interest, are concentrated at the surface where current density is a maximum at the surface and decreases exponentially with depth. Skin depth, δ, is defined as the depth into the skin where the value of the current density is e^{-1} that of the surface.

$$\delta = 0.06266\sqrt{\frac{\rho}{F\mu}} = 0.06266\sqrt{\frac{\rho}{F}}. \qquad (2\text{-}9)$$

Resistivity, ρ, can be expressed as a function of T.

$$\rho = \rho_o\left[1+\beta(T-T_o)\right] \qquad (2\text{-}10)$$

Table 6 lists values for ρ_o and β for various conductor materials.

TABLE 6 — ρ_o and β

Material	ρ_o (ohms-cm)	β (1/°F)
Aluminum	2.830E-6	2.17E-3
Copper	1.720E-6	2.17E-3
Silver	1.629E-6	2.11E-3
Gold	2.440E-6	1.89E-3

Equation (2-6) can be rewritten, by substituting results from (2-8), (2-9) and (2-10) and by setting μ and ε_1 to 1. Where α_C is expressed in dB per 100' of line and T_o is 75°F.

$$\alpha_C = \frac{173.16\sqrt{F}}{\ln\frac{b}{a}}\left(\frac{\sqrt{\rho_{o_a}\left[1+\beta_a(T-T_o)\right]}}{a}+\frac{\sqrt{\rho_{o_b}\left[1+\beta_b(T-T_o)\right]}}{b}\right) \qquad (2\text{-}11)$$

Figures 16 and 17 show plots of α_C versus F and α_C versus T for the four specimens. From these graphs, it should be noted that the 33-ohm lines (specimens #1 & #2) have higher losses than the 50-ohm lines (specimens #3 & #4). Also, specimens #1 and #3 with the copper inner conductors have lower losses than specimens #2 and #4 with the aluminum inner conductors.

Equation (2-7) can be simplified through substitution of (2-8), ε' and $\tan\delta$. For Teflon, the material used to fabricate the support beads, $\varepsilon' = 2.08$ and $\tan\delta = 0.0005$. α_D is expressed in dB per 100' of line.

$$\alpha_D = 27.3\frac{F\sqrt{\varepsilon_1'}}{11.811}\tan\delta = 27.3\frac{F\sqrt{2.08}}{11.811}0.0005 = 0.001667F \qquad (2\text{-}12)$$

The specimens, which were tested, had 13 - 0.125" thick Teflon support beads. Thus, the total buildup of beads accounted for 2.7% of the specimens' overall length. Therefore, equation (2-12) was factored by 2.7% which yielded:

$$\alpha_D = 0.000045F. \qquad (2\text{-}13)$$

At 0.8 GHz, α_D = 3.6E-5 dB per 100'. Dielectric losses, α_D accounts for <0.002% of α_T; therefore, losses due to α_D will be assumed negligible. However, dielectric losses can be significant in other applications where the transmission line is filled with a higher dielectric.

The definition of α_T, in terms of power is:

$$-\alpha_T = 10\log\left(\frac{P_{out}}{P_{in}}\right). \qquad (2\text{-}14)$$

The power loss within a 100' line is defined as:

$$\Delta P_T = P_{in} - P_{out} = P_{in}\left[1-\left(\frac{P_{out}}{P_{in}}\right)\right] = P_{in}\left[1-10^{\frac{-\alpha_T}{10}}\right], \qquad (2\text{-}15)$$

where $P_{in} = P$. Power loss due to the inner and outer conductors, ΔP_a and ΔP_b, can be expressed in terms of $\frac{\alpha_a}{\alpha_T}$.

$$\Delta P_a = \left(\frac{\alpha_a}{\alpha_T}\right) P\left[1 - 10^{\frac{-\alpha_T}{10}}\right] \qquad (2\text{-}16)$$

$$\Delta P_b = \left(1 - \frac{\alpha_a}{\alpha_T}\right) P\left[1 - 10^{\frac{-\alpha_T}{10}}\right] \qquad (2\text{-}17)$$

Equation (2-11) defines the total conductor losses where the two terms within the bracket represent the losses of the inner and outer conductors respectively. From the bracketed terms within (2-11) the following expression was derived.

$$\frac{\alpha_a}{\alpha_T} = \frac{b\sqrt{\rho_a}}{b\sqrt{\rho_a} + a\sqrt{\rho_b}} = \frac{b\sqrt{\rho_{o_a}\left[1+\beta_a(T-T_o)\right]}}{b\sqrt{\rho_{o_a}\left[1+\beta_a(T-T_o)\right]} + a\sqrt{\rho_{o_b}\left[1+\beta_b(T-T_o)\right]}} \qquad (2\text{-}18)$$

The source of heating caused by transmission line losses within the inner and outer conductors, $q_a^{\cdot}$ and $q_b^{\cdot}$, can be approximated by the following expressions:

$$q_a^{\cdot} = 2.843\frac{\Delta P_a}{A_a} \qquad (2\text{-}19)$$

$$q_b^{\cdot} = 2.843\frac{\Delta P_b}{A_b} \qquad (2\text{-}20)$$

where heating was assumed uniformly distributed throughout the cross section of the coax line.

In reality the heating will be maximum at the conductors' skin and will decrease with skin depth. A FEA model (COAX1) was constructed and two cases were run. The first case assumed uniform heating throughout the cross section, and the second case assumed heating only at the conductors' skin surface. There was good agreement between the results of these two cases with only a 1% difference. A_a and A_b are cross sectional areas of the inner and outer conductors, in square inches.

$$A_a = \frac{\pi}{4}a^2 \tag{2-21}$$

$$A_b = \frac{\pi}{4}\left(D^2 - b^2\right) \tag{2-22}$$

By substitution of results from (2-11), (2-16), (2-17), (2-18), (2-21) and (2-22) into (2-19) and (2-20) the inner and outer conductor source of heating definition is expressed as:

$$q_a^{\cdot} = 3.62\left(\frac{b\sqrt{\rho_{o_a}\left[1+\beta_a(T-T_o)\right]}}{b\sqrt{\rho_{o_a}\left[1+\beta_a(T-T_o)\right]}+a\sqrt{\rho_{o_b}\left[1+\beta_b(T-T_o)\right]}}\right)\frac{P}{a^2}\left(1-10^{-\frac{17.316\sqrt{F}}{\ln\frac{b}{a}}\left(\frac{\sqrt{\rho_{o_a}\left[1+\beta_a(T-T_o)\right]}}{a}+\frac{\sqrt{\rho_{o_b}\left[1+\beta_b(T-T_o)\right]}}{b}\right)}\right) \tag{2-23}$$

$$q_b^{\cdot} = 3.62\left(1-\frac{b\sqrt{\rho_{o_a}\left[1+\beta_a(T-T_o)\right]}}{b\sqrt{\rho_{o_a}\left[1+\beta_a(T-T_o)\right]}+a\sqrt{\rho_{o_b}\left[1+\beta_b(T-T_o)\right]}}\right)\frac{P}{D^2-b^2}\left(1-10^{-\frac{17.316\sqrt{F}}{\ln\frac{b}{a}}\left(\frac{\sqrt{\rho_{o_a}\left[1+\beta_a(T-T_o)\right]}}{a}+\frac{\sqrt{\rho_{o_b}\left[1+\beta_b(T-T_o)\right]}}{b}\right)}\right) \tag{2-24}$$

Figures 18 and 19 show plots of $q_a^{\bullet}$ and $q_b^{\bullet}$ versus temperature for the case where P is 1 kW and F is 0.8 GHz. It is interesting to note that the inner conductor heating is less for the 33-ohm lines while the outer conductor heating is less for the 50-ohm lines. Heating of the inner conductor is less while heating of the outer conductor is greater for specimens with copper inner conductors. Equations (2-23) and (2-24) were used to calculate the heating values for inner and outer conductors. The results from these calculations were used in the FEA models.

FIGURE 16 — α_C versus F

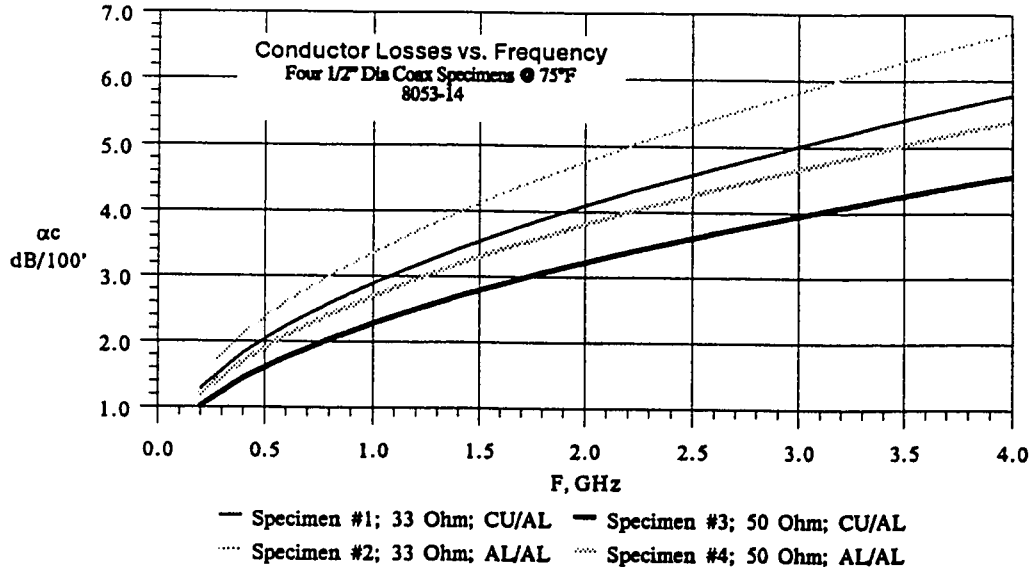

FIGURE 17 — α_C versus T

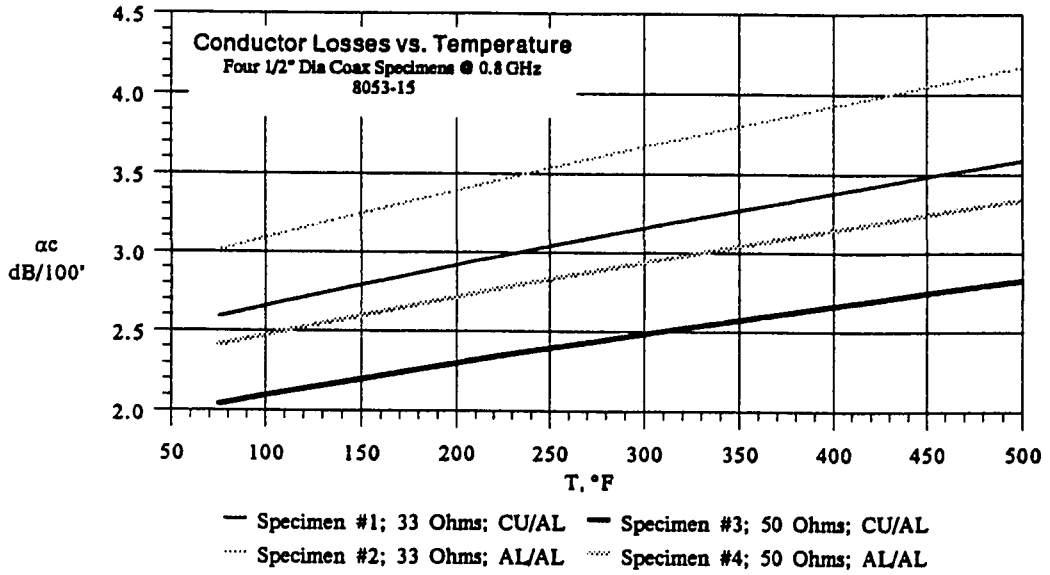

FIGURE 18 — $q_a^{\bullet}$ versus T

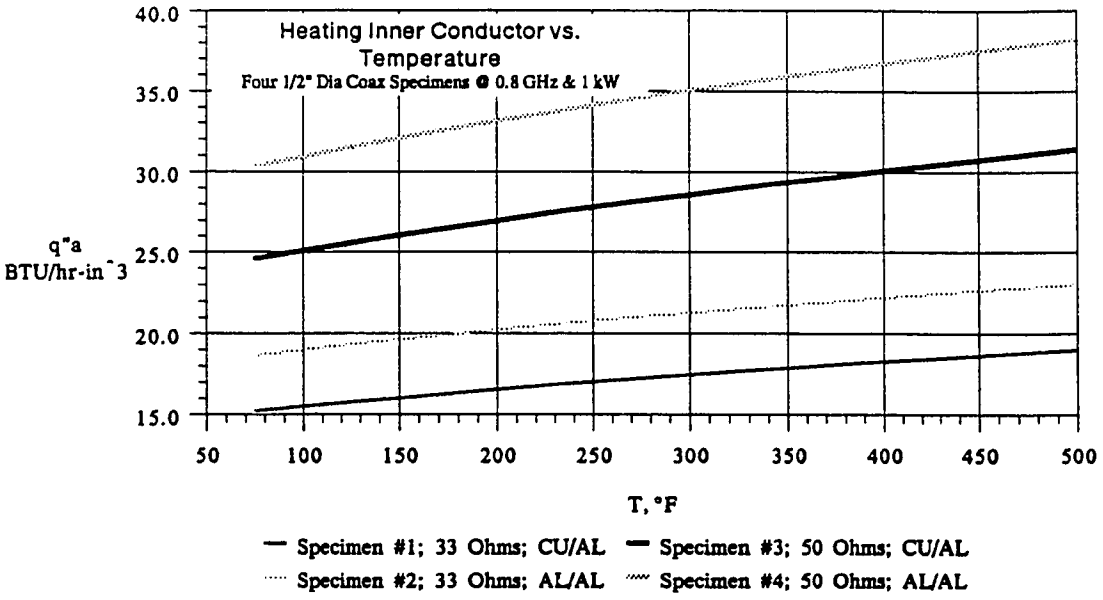

FIGURE 19 — $q_b^{\bullet}$ versus T

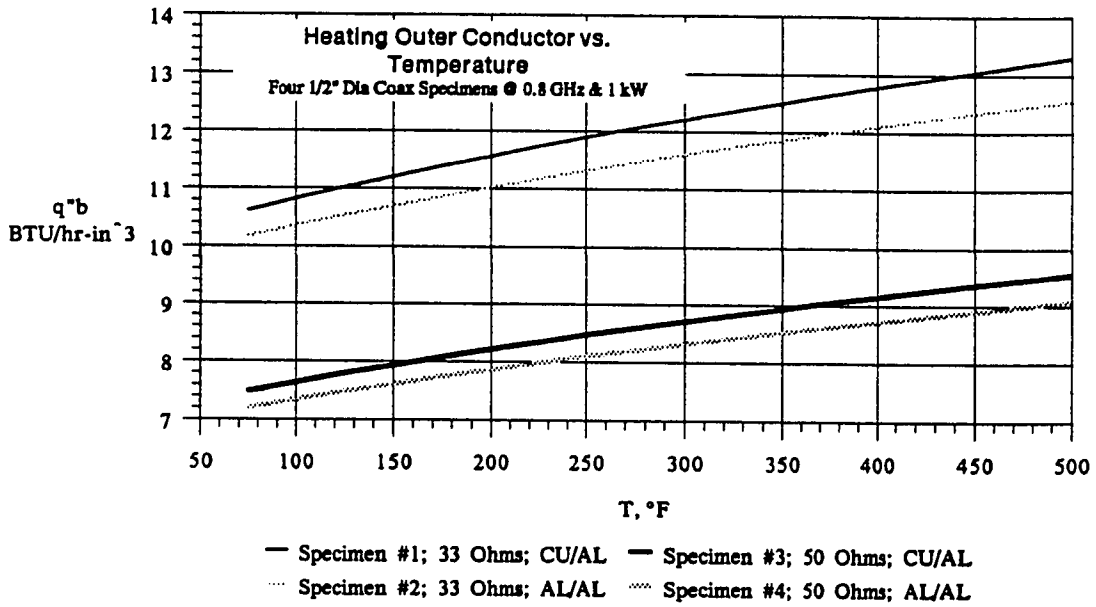

Convection Coefficients

The average natural convection coefficient at the outer surface of the outer conductor, h_3, is determined for two cases. The two cases are for the horizontal and vertical line orientations. Local values for natural convection coefficient versus ϕ, angular position around outer conductor, were not calculated in these cases. From earlier analysis, using FEA model COAX5, it was calculated that the maximum temperature variant, as a function of ϕ, was < 0.4% for a 1/2" - 50-ohm transmission line operating at 1 kW.

For the case of the horizontal line McAdams [7] presents a simplified equation for determining the average value for h_c at the outer surface of a heated horizontal cylinder. Results from this equation are expressed as h_3, in units of $\left(\frac{BTU}{hr-in^2-°F}\right)$ and is valid when the product of the Grashof and Prandtl numbers is $10^3 < N_{G_{z_D}} N_{P_R} < 10^9$.

$$h_3 = 0.00349\left(\frac{\Delta T}{D}\right)^{0.25} \qquad (2\text{-}25)$$

$$N_{G_{R_D}} N_{P_R} = \left[\frac{\rho^2 g \beta \Delta T D^3}{20736\mu^2}\right]\left[\frac{c_p \mu}{k}\right] \qquad (2\text{-}26)$$

Where ΔT is the temperature difference in °F between the outer conductor skin and ambient air. D is the outside diameter in inches, and k is the thermal conductivity of the ambient air in $\frac{BTU}{hr-in-°F}$. Figure 20 presents a graph of h_3 versus ΔT for standard line sizes. Figure 21 presents a plot of $N_{G_{R_D}} N_{P_R}$ versus ΔT for standard line sizes.

Frank [4] defines the local value of h_{c_y} at the outer surface of a heated vertical cylinder in standard air as:

$$h_{c_y} = 59.04\frac{k}{y}\left(N_{G_{R_y}} N_{P_R}\right)^{0.25}. \qquad (2\text{-}27)$$

Where k, thermal conductivity of the air, is in $\frac{BTU}{hr - in - ^\circ F}$ and y is, position along length of line, expressed in inches. The average value for h_c, or h_3, can be expressed as:

$$h_3 = \frac{1}{L}\int_0^L h_{c_y}\, dy = 78.72\frac{k}{L}\left(N_{G_{R_y}} N_{P_R}\right)^{0.25} \qquad (2\text{-}28)$$

$$N_{G_{R_y}} N_{P_R} = \left[\frac{\rho^2 g\beta\Delta T y^3}{20736\mu^2}\right]\left[\frac{c_p\mu}{k}\right] \qquad (2\text{-}29)$$

(2-28) is valid for $10^3 < N_{G_{R_y}} N_{P_R} < 10^9$. Figure 22 presents a graph of h_3 versus ΔT for various lengths of coaxial lines. Figure 23 shows $N_{G_{R_y}} N_{P_R}$ versus ΔT for at various values of y.

Values for convection coefficients, h_1 and h_2 were determined empirically. Values for h_1 and h_2 were assumed and input in FEA models COAX7 and COAX8. Results from these calculations were compared to the test results and iterated until good correlation was achieved. Table 7 lists these empirically derived values for h_1 and h_2.

TABLE 7 — Empirical Values of h_1 & h_2

Q (SCFH)	h_1 & h_2 $\left(\frac{BTU}{hr - in^2 - ^\circ F}\right)$
0	0.007
10	0.012
20	0.017

From Table 7 it should be noted that the convection coefficient increases linearly with flow rate. Frank [4] suggests that the method of *Determination of Dimensionless Groups* can be used in the correlation of experimental convection heat-transfer data. Applying this method, assuming that $h_1 = h_2$, and assuming that the convection coefficients are approximately proportional to Q, the following expression was derived.

$$h_1 = h_2 = A\frac{k}{b} + B\rho c_p V \qquad (2\text{-}30)$$

where A and B are constants and the expression for V, air velocity, is:

$$V = \frac{Q}{A_b - A_a} \qquad (2\text{-}31)$$

Constant A was calculated by assuming V = 0 and using the empirically derived convection coefficient value for Q = 0. The calculated value for A is 2.037. Constant B is then calculated to be 0.004144, by using results from runs where Q = 10 and 20 SCFH. Determination of these constant results in the following expression for h_1 and h_2.

$$h_1 = h_2 = 2.037\frac{k}{b} + 0.004144\rho c_p V \qquad (2\text{-}32)$$

Figures 24, 25, 26 and 27 presents curves of h_1 and h_2 versus T for 1/2" - 50-ohm, 1/2" - 33-ohm, 7/8" - 50-ohm and 1-5/8" - 50-ohm coax lines for conditions where Q is 0, 10 and 20 SCFH.

FIGURE 20 — h_3 versus ΔT for Horizontal Coax Lines

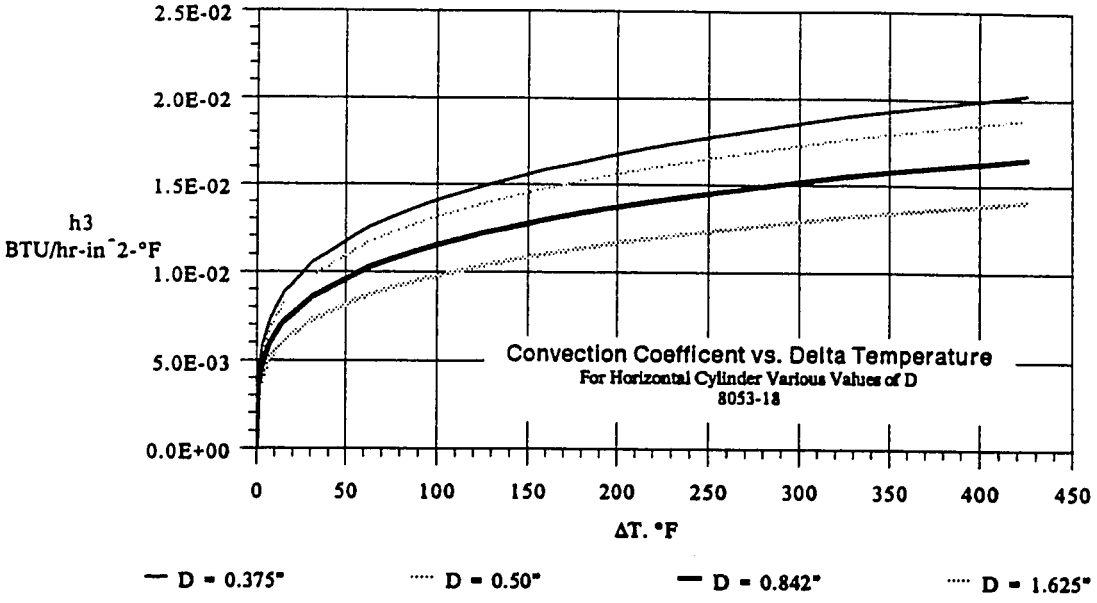

FIGURE 21 — $N_{G_{RD}} N_{P_R}$ versus ΔT

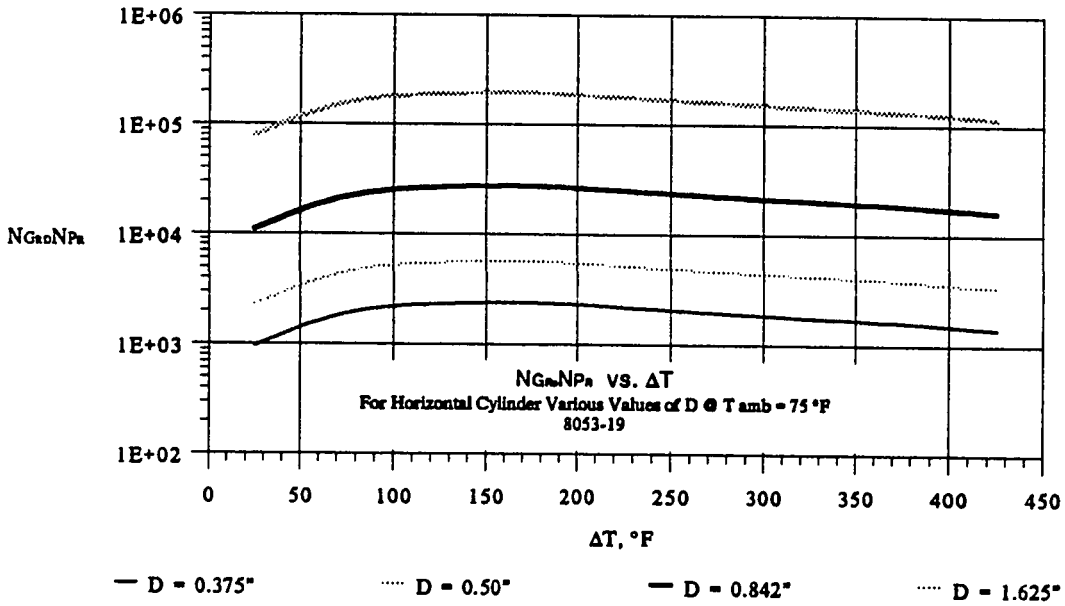

FIGURE 22 — h_3 versus ΔT for Vertical Coax Line

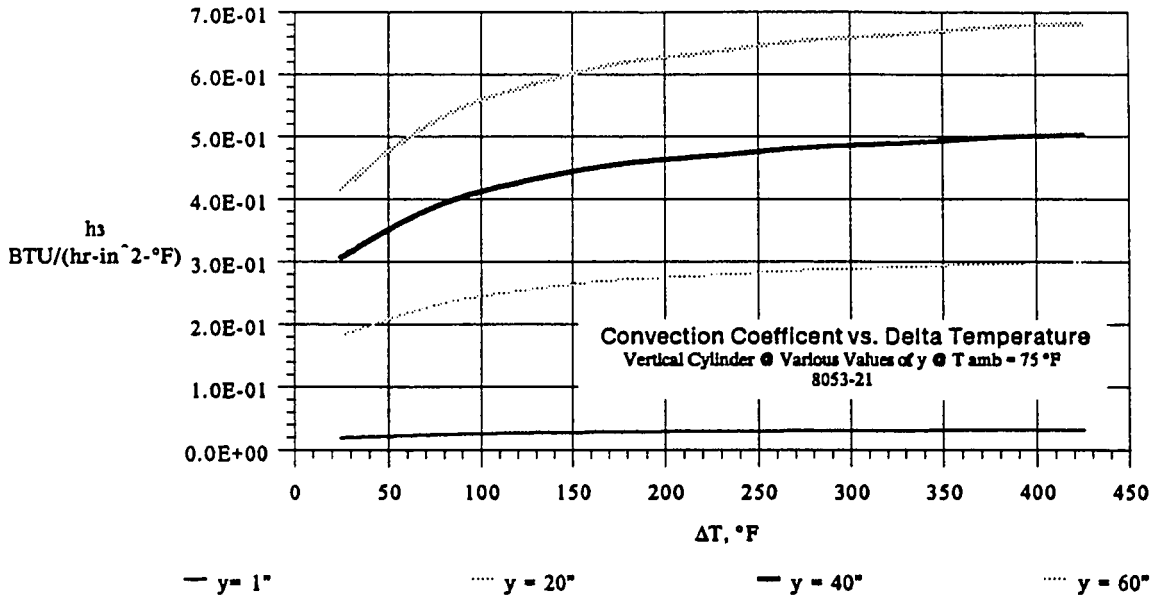

FIGURE 23 — $N_{G_R} N_{P_R}$ versus ΔT

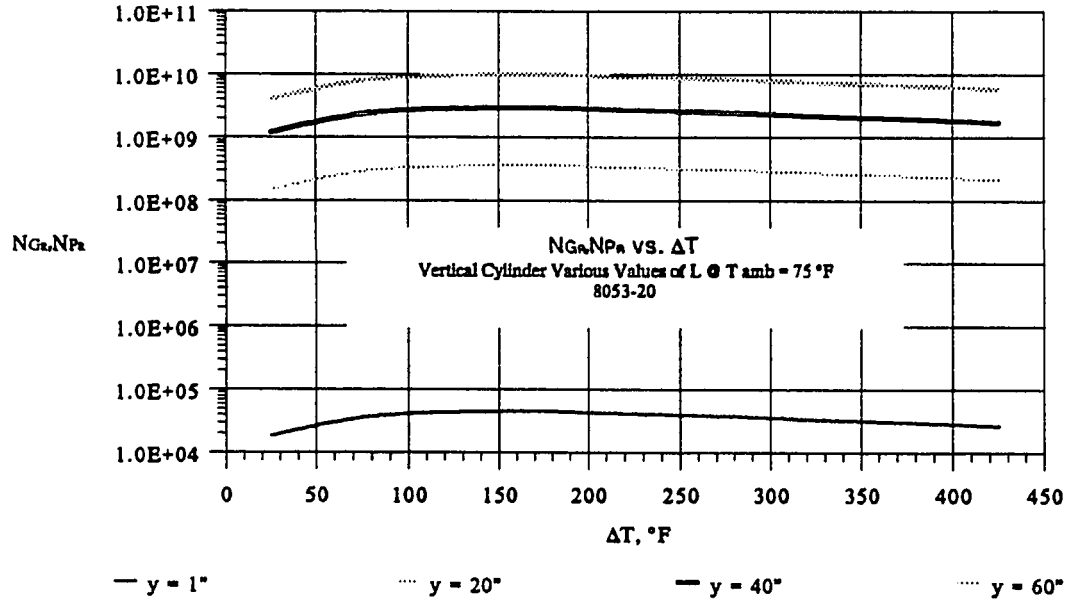

FIGURE 24 — h_1 and h_2 versus T for 1/2" - 50-ohm Coax Line

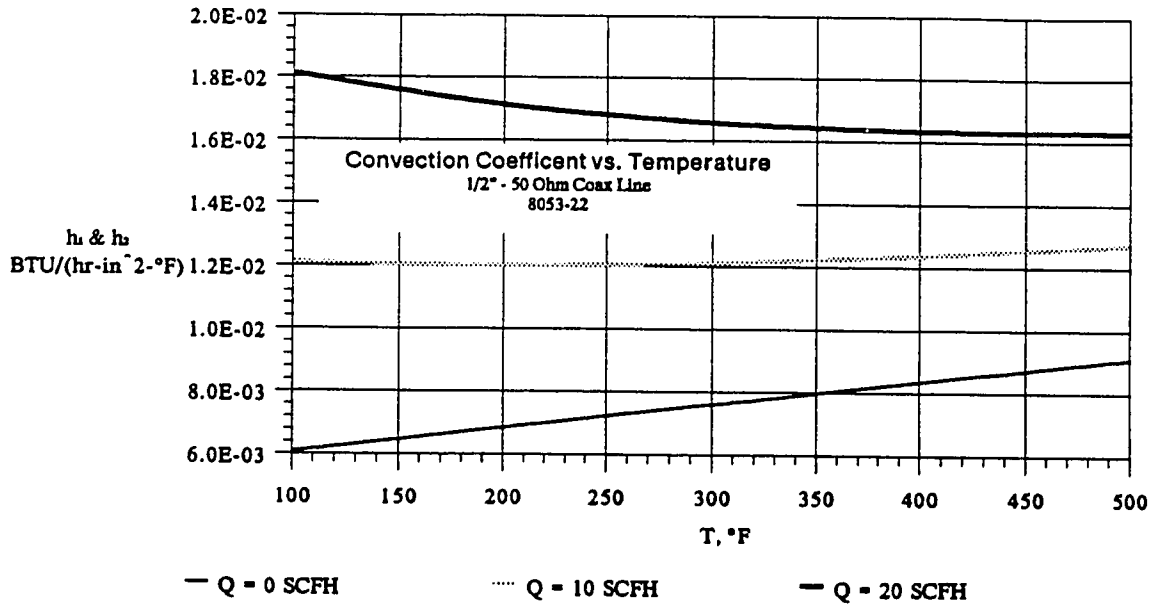

FIGURE 25 — h_1 and h_2 versus T for 1/2" - 33-ohm Coax Line

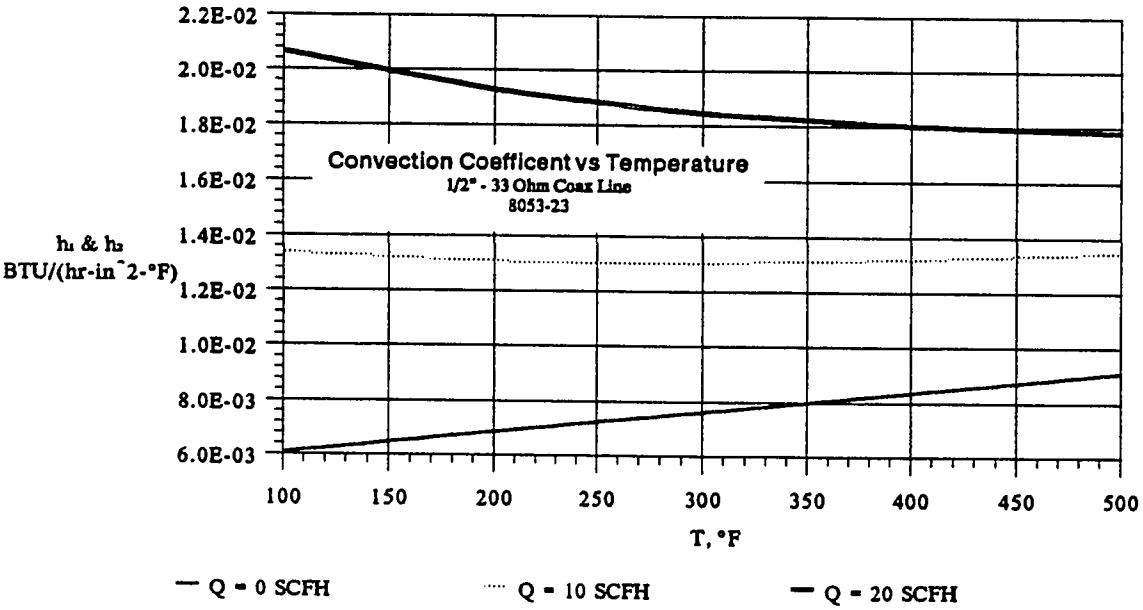

FIGURE 26 — h_1 and h_2 versus T for 7/8" - 50-ohm Coax Line

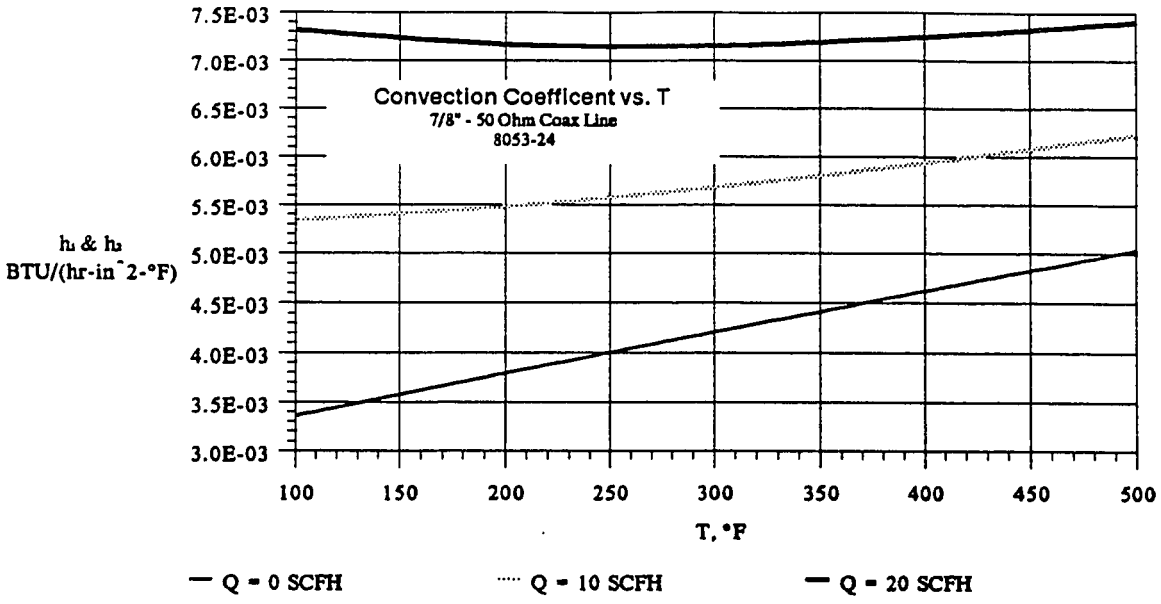

FIGURE 27 — h_1 and h_2 versus T for 1-5/8" - 50-ohm Coax Line

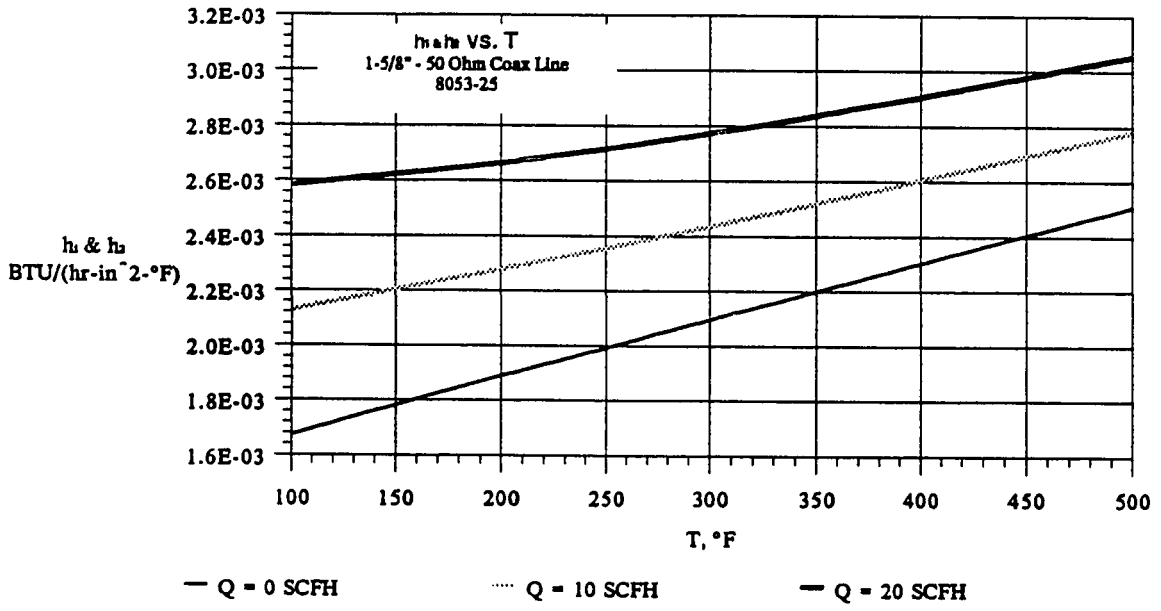

Results — FEA Models

A nine step approach to modeling the coaxial transmission lines is outlined in this section. This approach uses FEA models COAX7 and COAX8 and the expressions previously developed. Four configurations of transmission lines are modeled: 1) 1/2" - 50-ohm Transmission Line at $\theta = 0°$; 2) 1/2" - 50-ohm Transmission Line at $\theta = 90°$; 3) 1/2" - 33-ohm Transmission Line at $\theta = 0°$; 4) 1/2" - 33-ohm Transmission Line at $\theta = 0°$. For each model type runs were made for transmission lines with both the aluminum and copper inner conductors. For all runs it was assumed that the outer conductor was constructed of aluminum and that the frequency of operation was at a fixed frequency of 0.8 GHz. In the next chapter a comparison will be made between these calculated and the measured test results.

Systematic Approach to Modeling — 1/2" - 50-ohm Transmission Line @ $\theta = 0°$

Step 1 Values for thermal conductivity from Table 5 were used in COAX7. The outer conductor (Elements 1-20) was assumed to be fabricated from aluminum. The inner conductor (Elements 41-60), was assumed to be fabricated from either aluminum or copper. Air was assumed to occupy the annular passage (Elements 21-40).

Step 2 A value for T_{amb} was assumed.

Step 3 Values for T_a and T_b were assumed.

Step 4 Using either (2-32) or Figure 24, h_1 was calculated at T_a, and this result was assigned to Elements 41-60 (Face J-K). This value was also used for h_2 and assigned to Elements 1-20 (Face I-L).

Step 5 Using either (2-25) or Figure 20, h_3 was calculated at T_b, and this result was assigned to Elements 1-20 (Face J-K).

Step 6 Using either (2-23) or Figure 18, $q_a^{\cdot}$ was calculated at T_a, and this result was assigned to Elements 41-60.

Step 7 Using either (2-24) or Figure 19, $q_b^{\cdot}$ was calculated at T_a, and this result was assigned to Elements 1-20.

Step 8 Values for T_a and T_b were calculated using COAX7..

Step 9 Repeat Steps 4-8 using calculated values of T_a and T_b. Repeat until assumed and calculated temperatures are in close agreement.

Results from this model, for seven cases, are summarized in Table 8. Graphs of these results are shown in Figures 28 - 36.

Systematic Approach to Modeling — 1/2" - 50-ohm Transmission Line $\theta = 90°$

Step 1 Values for thermal conductivity from Table 5 were used in COAX7. The outer conductor (Elements 1-20) was assumed to be fabricated from aluminum. The inner conductor (Elements 41-60), was assumed to be fabricated from either aluminum or copper. Air was assumed to occupy the annular passage (Elements 21-40).

Step 2 A value for T_{amb} was assumed.

Step 3 Values for T_a and T_b were assumed.

Step 4 Using either (2-32) or Figure 24, h_1 was calculated at T_a, and this result was assigned to Elements 41-60 (Face J-K). This value was also used for h_2 and assigned to Elements 1-20 (Face I-L).

Step 5 Using either (2-28) or Figure 22, h_3 was calculated at T_b, for various discrete positions, y. For this study the line was broken up into four sections consisting of:

1) Elements 1-4 (0"≤y≤12")
2) Elements 5-10 (12"≤y≤30")
3) Elements 11-16 (30"≤y≤48")
4) Elements 17-20 (48"≤y≤60").

Step 6 Using either (2-23) or Figure 18, $q_a^{\cdot}$ was calculated at T_a, and this result was assigned to Elements 41-60.

Step 7 Using either (2-24) or Figure 19, $q_b^{\cdot}$ was calculated at T_a, and this result was assigned to Elements 1-20.

Step 8 Values for T_a and T_b were calculated using COAX7..

Step 9 Repeat Steps 4-8 using calculated values of T_a and T_b. Repeat until assumed and calculated temperatures are in close agreement.

Results from this model, for three cases, are summarized in Table 9. Graphs of these results are shown in Figures 39 - 41.

Systematic Approach to Modeling — 1/2" - 33-ohm Transmission Line @ $\theta = 0°$

Step 1 Values for thermal conductivity from Table 5 were used in COAX8. The outer conductor (Elements 65-96) was assumed to be fabricated from aluminum. The inner conductor (Elements 1-32), was assumed to be fabricated from either aluminum or copper. Air was assumed to occupy the annular passage (Elements 33-64).

Step 2 A value for T_{amb} was assumed.

Step 3 Values for T_a and T_b were assumed.

Step 4 Using either (2-32) or Figure 24, h_1 was calculated at T_a, and this result was assigned to Elements 1-32 (Face J-K). This value was also used for h_2 and assigned to Elements 65-96 (Face I-L).

Step 5 Using either (2-25) or Figure 20, h_3 was calculated at T_b, and this result was assigned to Elements 65-96 (Face J-K).

Step 6 Using either (2-23) or Figure 18, $q_a^{\cdot}$ was calculated at T_a, for various sections of line. For this study the line was broken up into the seven different sections consisting of:

1) Elements 1-4
2) Elements 5-8
3) Elements 9-11

4) Elements 12-21
5) Elements 22-24
6) Elements 25-28
7) Elements 29-32.

Step 7 Using either (2-24) or Figure 19, $q_b^{\bullet}$ was calculated at T_a, and this result was assigned to Elements 65-96.

Step 8 Values for T_a and T_b were calculated using COAX8.

Step 9 Repeat Steps 4-8 using calculated values of T_a and T_b. Repeat until assumed and calculated temperatures are in close agreement.

Results from this model, for four cases, are summarized in Table 10. Graphs of these results are shown in Figures 44 - 47.

Systematic Approach to Modeling — 1/2" - 33-ohm Transmission Line @ $\theta = 90°$

Step 1 Values for thermal conductivity from Table 5 were used in COAX8. The outer conductor (Elements 65-96) was assumed to be fabricated from aluminum. The inner conductor (Elements 1-32), was assumed to be fabricated from either aluminum or copper. Air was assumed to occupy the annular passage (Elements 33-64).

Step 2 A value for T_{amb} was assumed.

Step 3 Values for T_a and T_b were assumed.

Step 4 Using either (2-32) or Figure 24, h_1 was calculated at T_a, and this result was assigned to Elements 1-32 (Face J-K). This value was also used for h_2 and assigned to Elements 65-96 (Face I-L).

Step 5 Using either (2-28) or Figure 22, h_3 was calculated at T_b, for various discrete positions, y. For this study the line was broken up into four discrete sections consisting of:

1) Elements 65-69 (0"≤y≤9")
2) Elements 70-80 (9"≤y≤30")
3) Elements 81-91 (30"≤y≤51")

4) Elements 92-96 (51"≤y≤60").

Step 6 Using either (2-23) or Figure 18, $q_a^{\bullet}$ was calculated at T_a, for various sections of line. For this study the line was broken up into the seven different sections consisting of:

1) Elements 1-4;
2) Elements 5-8
3) Elements 9-11
4) Elements 12-21
5) Elements 22-24
6) Elements 25-28
7) Elements 29-32.

Step 7 Using either (2-24) or Figure 19, $q_b^{\bullet}$ was calculated at T_a, and this result was assigned to Elements 65-96.

Step 8 Values for T_a and T_b were calculated using COAX8.

Step 9 Repeat Steps 4-8 using calculated values of T_a and T_b. Repeat until assumed and calculated temperatures are in close agreement.

Results from this model, for two cases, are listed in Table 11. Figure 50 includes a plot of these results for specimen #2 at 4.5 kW.

TABLE 8 - Summary Results 1/2" - 50-ohm Transmission Line @ $\theta = 0°$

P, (kW)	1	3	3	4.5	4.5	6.5	1	3	4.5
Q, (SCFH)	0	0	10	10	20	20	0	10	20
Mat'l Inner	CU	CU	CU	CU	CU	CU	AL	AL	AL
T_{amb}, (°F)	75	75	75	80	80	80	75	75	75
h_1, $\left(\frac{BTU}{hr-in^2-°F}\right)$ Element 41-60, Face J-K (2-32) or Fig. 22	0.0062	0.0078	0.0120	0.0123	0.0168	0.0164	0.0068	0.0122	0.0163
h_2, $\left(\frac{BTU}{hr-in^2-°F}\right)$ Elements 1-20, Face I-L (2-32) or Fig. 22	0.0062	0.0078	0.012	0.0123	0.0168	0.0164	0.0068	0.0122	0.0163
h_3, $\left(\frac{BTU}{hr-in^2-°F}\right)$ Elements 1-20, Face J-K (2-25) or Fig. 18	0.0135	0.0158	0.0150	0.0170	0.0136	0.144	0.0132	0.0168	0.0168
$\dot{q}_a$, $\left(\frac{BTU}{hr-in^3}\right)$ Elements 41-60 (2-23) or Fig. 16	26	87	84	130.5	126	194	33	108	162
$\dot{q}_b$, $\left(\frac{BTU}{hr-in^3}\right)$ Elements 1-20 (2-24) or Fig. 17	7.9	26.4	25.5	44.8	38.7	59.1	7.7	25.5	38.2
T_a, (°F)	147.7	281.8	240.7	328.0	285.0	391.4	161.3	277.0	330.5
T_b, (°F)	104.0	154.5	136.9	174.9	158.1	200.4	107.2	141.4	157.4

TABLE 9 - Summary Results 1/2" - 50-ohm Transmission Line @ $\theta = 90°$

P, (kW)		3	4.5	6.5
Q, (SCFH)		0	10	20
Mat'l Inner		CU	CU	CU
T_{amb}, (°F)		80	80	80
$h_1, \left(\frac{BTU}{hr-in^2-°F}\right)$	Element 41-60, Face J-K (2-32) or Fig. 22	0.0072	0.0122	0.0162
$h_2, \left(\frac{BTU}{hr-in^2-°F}\right)$	Elements 1-20, Face I-L (2-32) or Fig. 22	0.0062	0.0078	0.0163
$h_3, \left(\frac{BTU}{hr-in^2-°F}\right)$	Elements 1-4, Face J-K (2-28) or Fig. 20	0.030	0.030	0.035
$h_3, \left(\frac{BTU}{hr-in^2-°F}\right)$	Elements 5-10, Face J-K (2-28) or Fig. 20	0.250	0.260	0.270
$h_3, \left(\frac{BTU}{hr-in^2-°F}\right)$	Element 11-16, Face J-K (2-28) or Fig. 20	0.420	0.430	0.445
$h_3, \left(\frac{BTU}{hr-in^2-°F}\right)$	Element 17-20, Face J-K (2-28) or Fig. 20	0.570	0.580	0.600
$q_a^{"}, \left(\frac{BTU}{hr-in^3}\right)$	Elements 41-60 (2-23) or Fig. 16	84.0	130.5	195.0
$q_b^{"}, \left(\frac{BTU}{hr-in^3}\right)$	Elements 1-20 (2-24) or Fig. 17	26.1	40.5	58.5
T_a / T_b, (°F)	y = 0"	261.5 / 128.9	307.2 / 141.4	368.3 / 152.1
T_a / T_b, (°F)	y = 6"	258.7 / 126.3	304.2 / 139.0	365.4 / 149.5
T_a / T_b, (°F)	y = 12"	250.2 / 97.7	294.7 / 102.9	355.5 / 108.5
T_a / T_b, (°F)	y = 18"	243.6 / 87.5	287.5 / 90.1	348.1 / 93.3
T_a / T_b, (°F)	y = 24"	241.1 / 87.4	285.1 / 90.0	345.7 / 93.2
T_a / T_b, (°F)	y = 30"	239.7 / 85.7	283.7 / 87.7	344.3 / 90.2
T_a / T_b, (°F)	y = 36"	238.8 / 84.5	282.8 / 86.2	343.4 / 88.2
T_a / T_b, (°F)	y = 42"	238.4 / 84.5	282.5 / 86.1	343.0 / 88.2
T_a / T_b, (°F)	y = 48"	238.1 / 83.8	282.1 / 85.3	342.7 / 87.0
T_a / T_b, (°F)	y = 54"	237.9 / 83.3	281.8 / 84.6	342.3 / 86.1
T_a / T_b, (°F)	y = 60"	237.8 /83.3	281.8 / 84.6	342.2 / 86.1

TABLE 10 - Summary Results 1/2" - 33-ohm Transmission Line @ θ = 0°

P	(kW)		1	3	4.5	4.78
Q	(SCFH)		0	10	20	20
Mat'l Inner			CU	CU	CU	AL
T_{amb}	(°F)		75	75	80	80
h_1	$\left(\frac{BTU}{hr-in^2-°F}\right)$	Element 1-32, Face J-K (2-32) or Fig. 23	0.0066	0.0132	0.0186	0.0180
h_2	$\left(\frac{BTU}{hr-in^2-°F}\right)$	Element 65-96 Face I-L (2-32) or Fig. 23	0.0066	0.0132	0.0186	0.0180
h_3	$\left(\frac{BTU}{hr-in^2-°F}\right)$	Element 65-96 Face J-K (2-25) or Fig. 18	0.009	0.014	0.014	0.0148
$q_a^{"}$	$\left(\frac{BTU}{hr-in^3}\right)$	Elements 1-4	26.0	84.0	128.3	176.9
		Elements 5-8	23.0	72.0	111.8	153.8
		Element 9-11	19.0	62.0	95.3	129.5
		Elements 12-21 (2-23) or Fig. 16	16.0	51.0	78.8	105.2
		Elements 22-24	19.0	62.0	95.3	129.5
		Elements 25-28	23.0	72.0	111.8	153.8
		Elements 29-32	26.0	84.0	128.3	176.9
$q_b^{"}$	$\left(\frac{BTU}{hr-in^3}\right)$	Elements 65-96 (2-24) or Fig. 17	11.3	36.0	39.4	58.3
T_a / T_b	(°F)	y = 0" & 60"	151.3 / 116.3	237.1 / 146.6	273.0 / 152.1	350.4 / 184.7
		y = 3" & 57"	151.2 / 116.4	236.6 / 146.6	272.5 / 152.1	349.7 / 184.7
		y = 6" & 54"	151.2 / 116.6	234.9 / 146.8	270.5 / 152.3	347.1 / 184.9
		y = 9" & 51"	151.1 / 117.2	231.8 / 147.5	266.9 / 153.2	341.3 / 186.0
		y = 12" & 48"	150.3 / 117.7	228.1 / 148.0	262.1 / 153.9	333.1 / 186.5
		y = 15" & 45"	149.0 / 118.2	224.0 / 148.5	256.5 / 154.5	322.8 / 186.7
		y = 18" & 42"	147.7 / 118.5	219.8 / 149.0	250.8 / 155.1	311.7 / 186.9
		y = 21" & 39"	146.9 / 118.7	217.1 / 148.9	247.3 / 155.0	305.7 / 186.3
		y = 24" & 36"	146.5 / 118.6	215.6 / 148.9	245.4 / 154.7	302.9 / 185.7
		y = 27" & 33"	146.2 / 118.6	214.8 / 148.6	244.4 / 154.5	301.7 / 185.3
		y = 30"	146.2 /118.6	214.6 / 148.4	244.1 / 154.4	301.4 / 181.1

TABLE 11 - Summary Results 1/2" - 33-ohm Transmission Line @ $\theta = 90°$

P_t	(kW)		4.5	4.5
Q	(SCFH)		20	20
Mat'l Inner			AL	CU
T_{amb}	(°F)		80	75
h_1	$\left(\frac{BTU}{hr-in^2-°F}\right)$	Element 1-32, Face J-K (2-32) or Fig. 23	0.0181	0.0181
h_2	$\left(\frac{BTU}{hr-in^2-°F}\right)$	Elements 65-96, Face I-L (2-32) or Fig. 23	0.0181	0.0181
h_3	$\left(\frac{BTU}{hr-in^2-°F}\right)$	Elements 65-69, Face J-K	0.030	0.030
		Elements 70-80, Face J-K (2-28) or Fig. 20	0.260	0.260
		Elements 81-91, Face J-K	0.440	0.430
		Elements 92-96, Face J-K	0.590	0.580
q_a''	$\left(\frac{BTU}{hr-in^3}\right)$	Elements 1-4	164	160
		Elements 5-8	141	140
		Element 9-11	120	120
		Elements 12-21 (2-23) or Fig. 16	99	99
		Elements 22-24	120	120
		Elements 25-28	141	140
		Elements 29-32	164	160
q_b''	$\left(\frac{BTU}{hr-in^3}\right)$	Elements 65-96 (2-24) or Fig. 17	53.6	69.3
T_a / T_b,	(°F)	y = 0"	312.6 / 143.8	302.6 / 147.5
		y = 6"	303.6 / 134.0	294.1 / 136.6
		y = 12"	278.3 / 91.1	273.1 / 87.7
		y = 18"	256.0 / 92.3	254.4 / 89.2
		y = 24"	247.6 / 92.1	245.9 / 88.9
		y = 30"	245.4 / 89.2	243.2 / 85.8
		y = 36"	245.8 / 87.4	243.9 / 83.7
		y = 42"	253.3 / 87.5	250.8 / 83.8
		y = 48"	272.5 / 87.3	265.6 / 83.6
		y = 54"	286.6 / 85.2	276.4 / 81.0
		y = 60"	290.3 / 85.3	279.6 / 81.1

IV. DISCUSSION AND COMPARISON OF RESULTS

Introduction

This chapter makes a comparison between the FEA model results, which are described in Chapter III, and the test results, which are described in Chapter II. A discussion of some observed discrepancies between these results is also made within this chapter. Comparisons are made on four line configurations: 1) 1/2" - 50-ohm, $\theta = 0°$; 2) 1/2" - 50-ohm, $\theta = 90°$; 3) 1/2" - 33-ohm, $\theta = 0°$; and 4) 1/2" - 33-ohm, $\theta = 90°$.

1/2" - 50-ohm @ $\theta = 0°$

Figures 28 - 36 show graphical comparisons of both test and calculated results for 1/2" - 50-ohm coaxial lines oriented at $\theta = 0°$. Figures 28 - 33 present the results for specimen #3. Figures 34 - 36 present results for specimen #4.

Calculated results were made with COAX7. Simplified boundary conditions where used. This resulted in 1-dimensional heat flow, which occurred in an outward radial direction. For these cases T_a and T_b did not vary with position, y.

A temperature contour was noted from the test data. From Figures 28, 29 and 34, where Q = 0, it is observed that the measured temperature distribution had a convex contour. It is believed that the cause of this temperature distribution can be attributed to the adapters, which were used during testing. These adapters were relatively massive in comparisons to the test specimens and tended to act as sinks.

From the measured data it was also observed that the contour changes with changes in operating conditions. For the case where $Q \neq 0$ an unexpected negative contour was noted between y = 22" to 31". An explanation for this unexpected distribution might be attributed to the cooling system. Air is injected into section 2 (20"≤y≤40") at y = 20" and is exhausted at y = 40". The cooling air increases in temperature as it flows through the line. This increase in cooling air temperature results in a higher specimen temperature. The measured temperature contour of T_a was observed to be concave when $P \geq 4.5$ kW and where Q = 20 SCFH (Figures 32, 33 & 36). It is thought that the cause for this contour is: 1) heating caused by high losses in the adapters' inner conductor; or 2) sinking caused by a cooler center conductor of the air-cooled transmission line.

Figures 37 and 38 show plots of average $\%D_a$ and $\%D_b$ between the calculated and measured results. Where $\%D_a$ and $\%D_b$ is defined as:

$$\%D_a = \frac{\sum_{y=2",22",31",58"} \left(T_{a_{Calculated}} - T_{a_{Measured}}\right)}{4} \qquad (4\text{-}1)$$

$$\%D_b = \frac{\sum_{y=2",22",31",58"} \left(T_{b_{Calculated}} - T_{b_{Measured}}\right)}{4} \qquad (4\text{-}2)$$

For these cases, the range of difference is $-18.8\% \leq \%D_a \leq +6\%$ and $-17.2\% \leq \%D_b \leq +2.2\%$. *In summary there was good correlation between the calculated and measured results.* The difference associated with T_a is fairly well distributed about the 0% line. However, the difference associated with T_b seems to be weighted slightly below the 0% line. It is thought that a smaller difference might be realized if some refinements were made to (2-25) the expression used in calculating h_3. This would be realized through a slight reduction in h_3.

FIGURE 28 — Comparison Results, Specimen #3 @ 1 kW & 0 SCFH

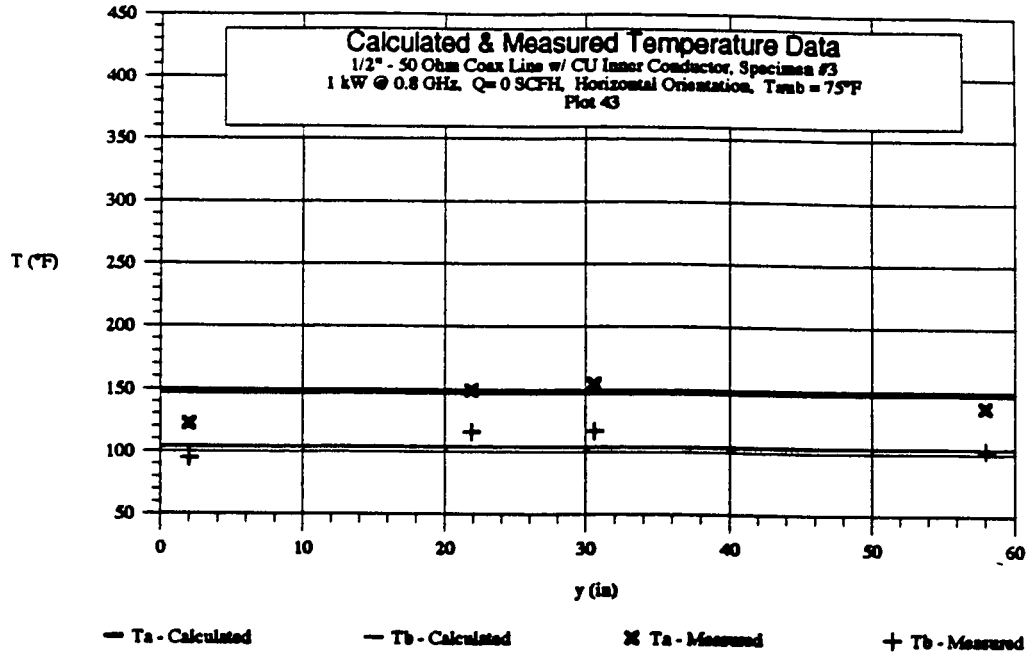

FIGURE 29 — Comparison Results, Specimen #3 @ 3 kW & 0 SCFH

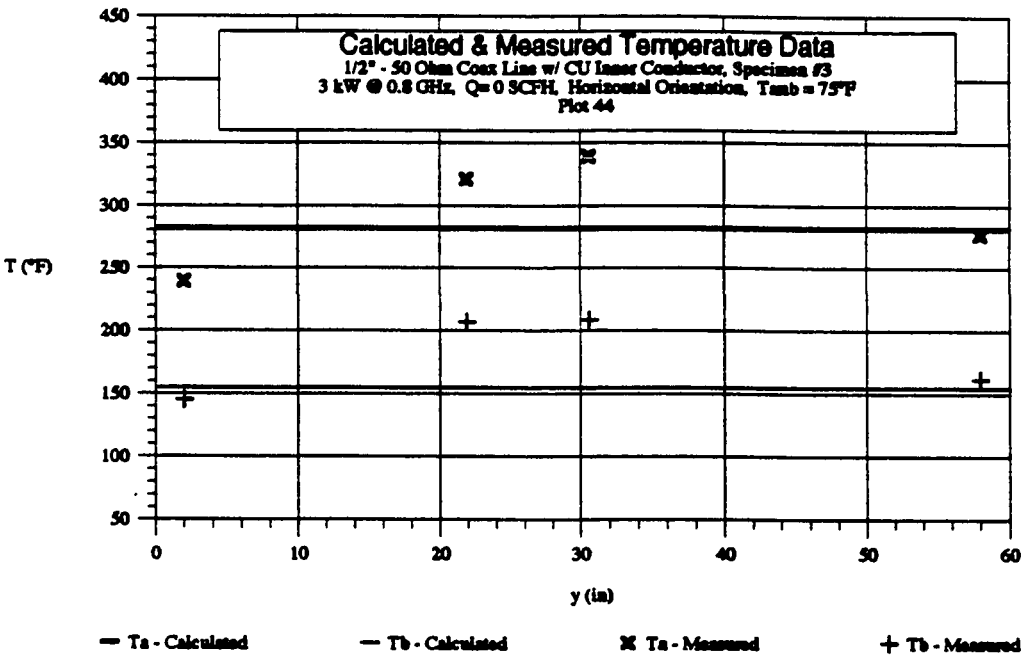

FIGURE 30 — Comparison Results, Specimen #3 @ 3 kW & 10 SCFH

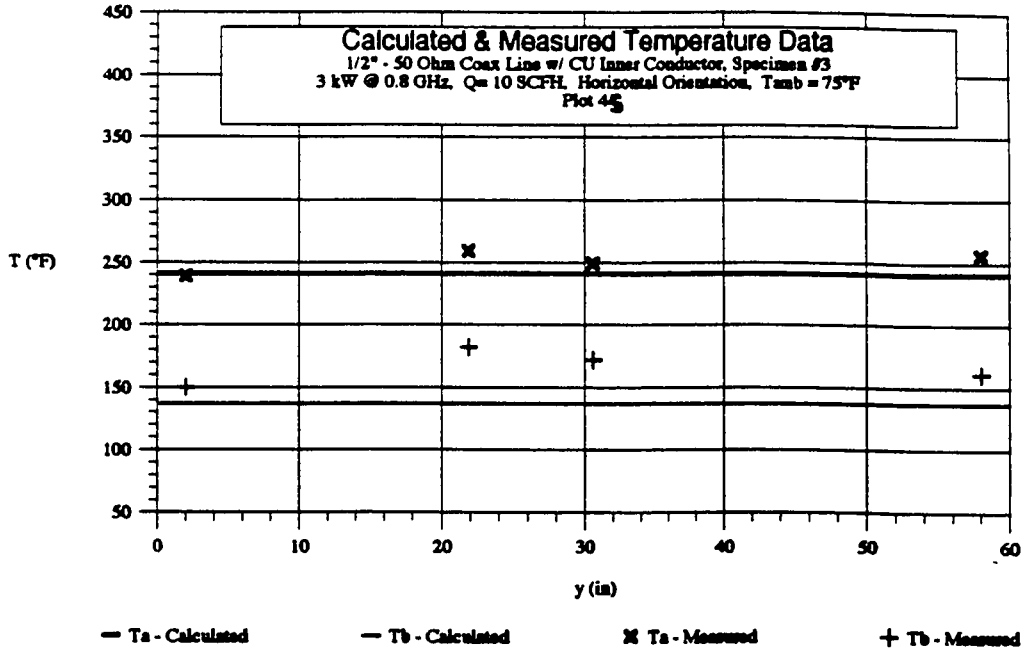

FIGURE 31 — Comparison Results, Specimen #3 @ 4.5 kW & 10 SCFH

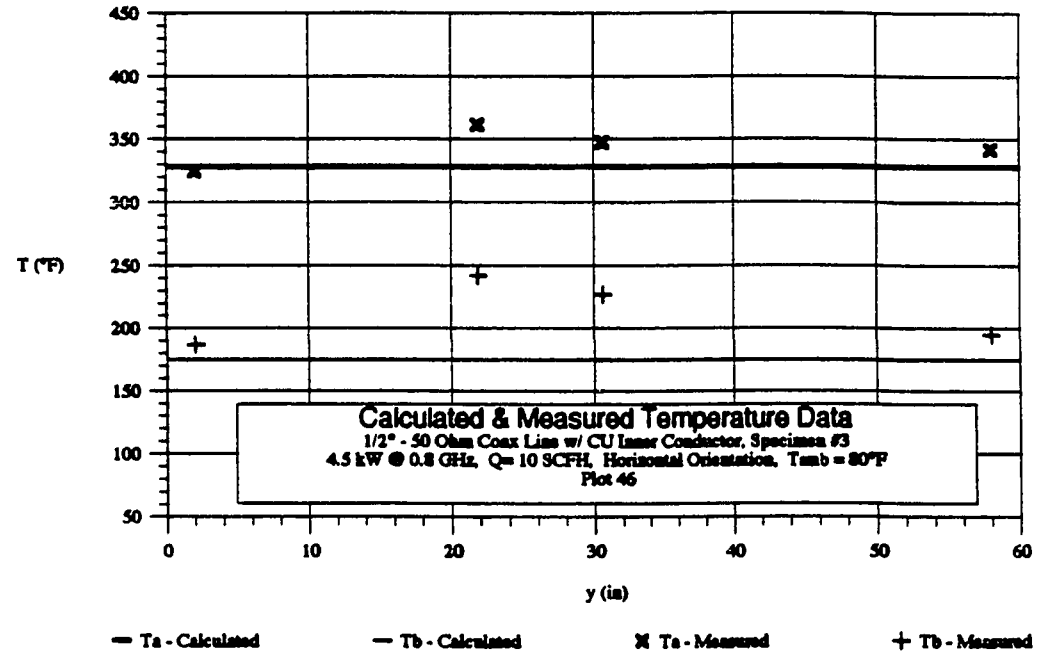

FIGURE 32 — Comparison Results, Specimen #3 @ 4.5 kW & 20 SCFH

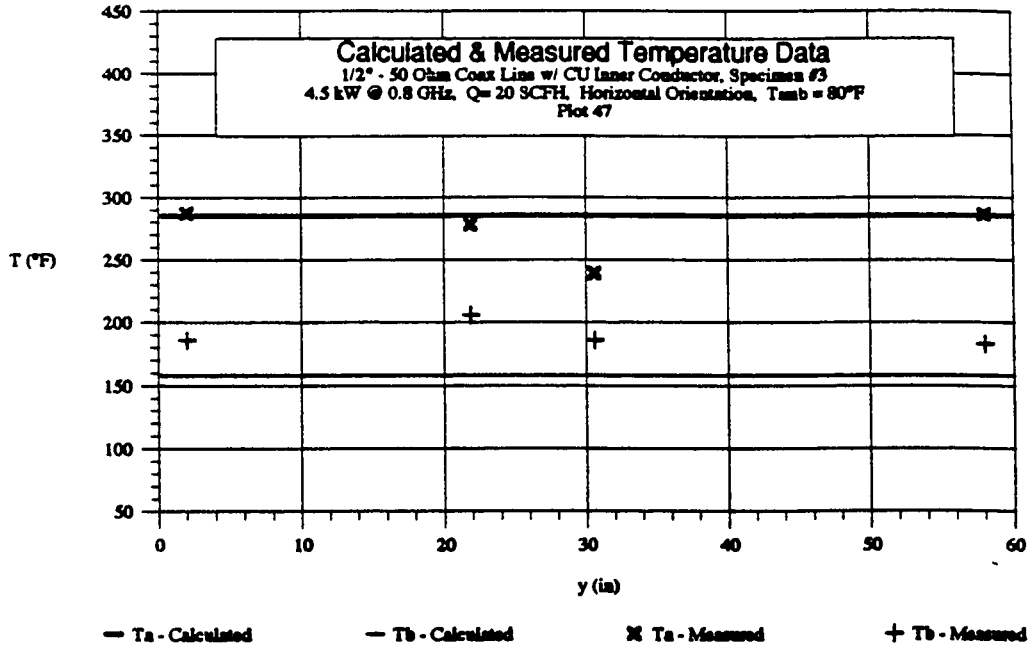

FIGURE 33 — Comparison Results, Specimen #3 @ 6.5 kW & 20 SCFH

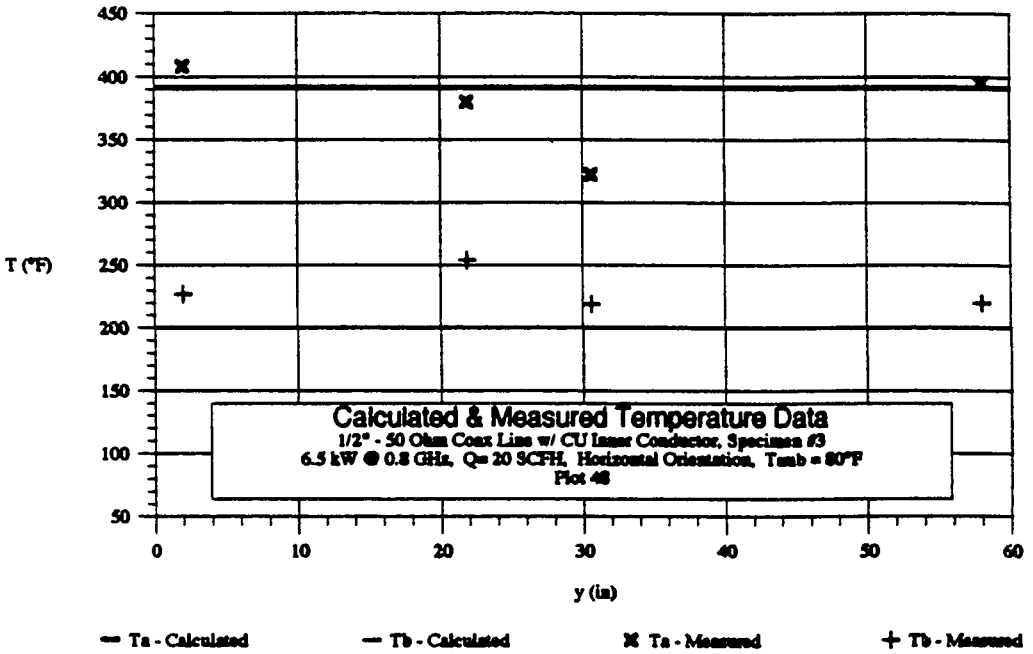

FIGURE 34 — Comparison Results, Specimen #4 @ 1 kW & 0 SCFH

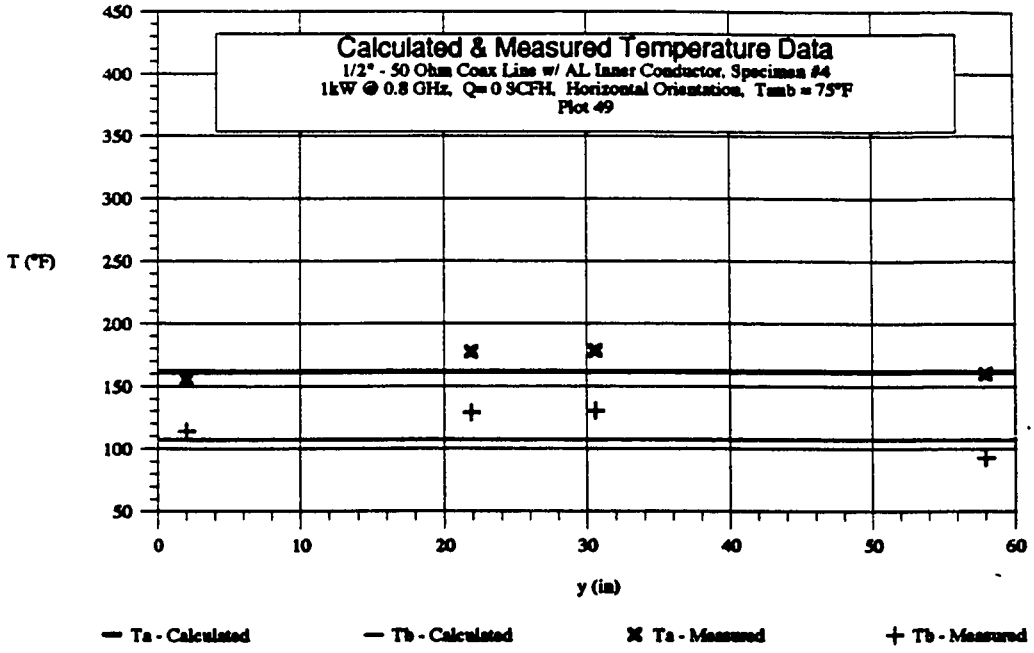

FIGURE 35 — Comparison Results, Specimen #4 @ 3 kW & 10 SCFH

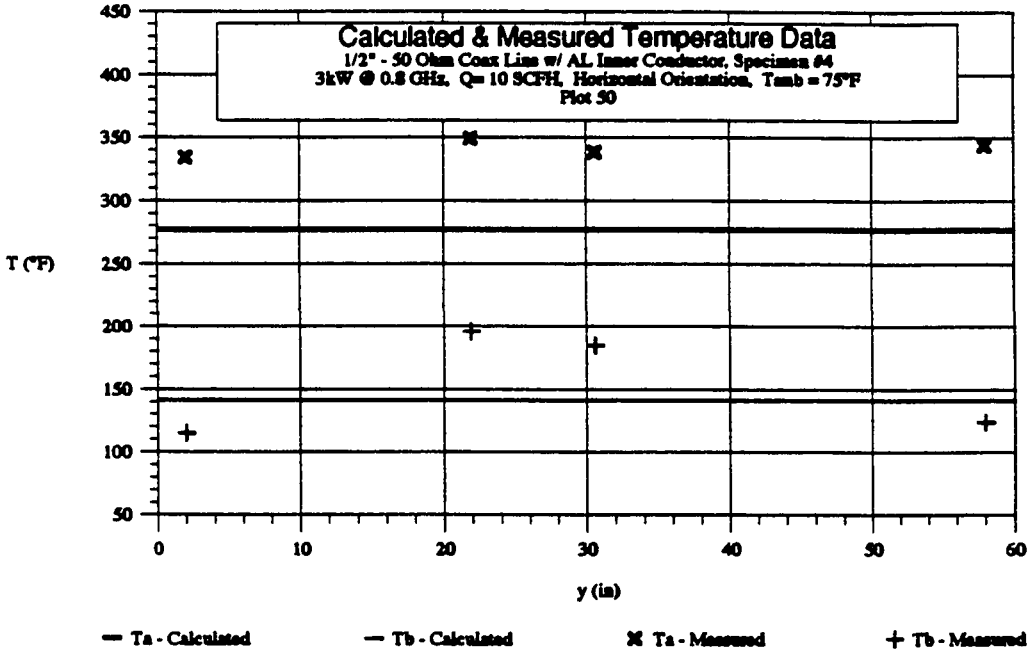

FIGURE 36 — Comparison Results, Specimen #4 @ 4.5 kW & 20 SCFH

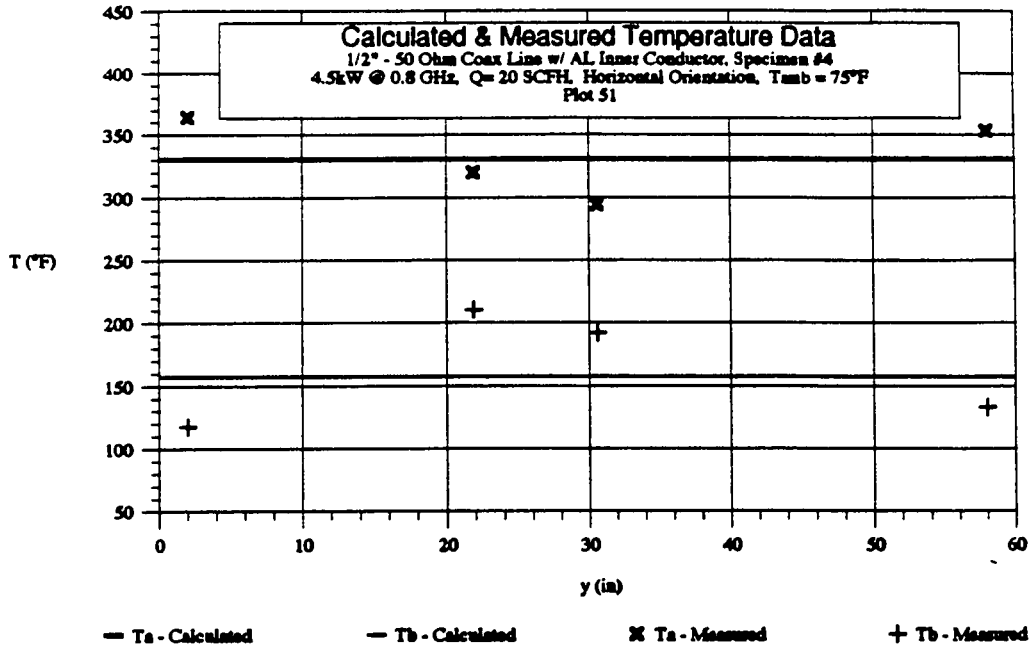

FIGURE 37 — $\%D_a$, 50-ohm Coax Line @ $\theta = 0°$

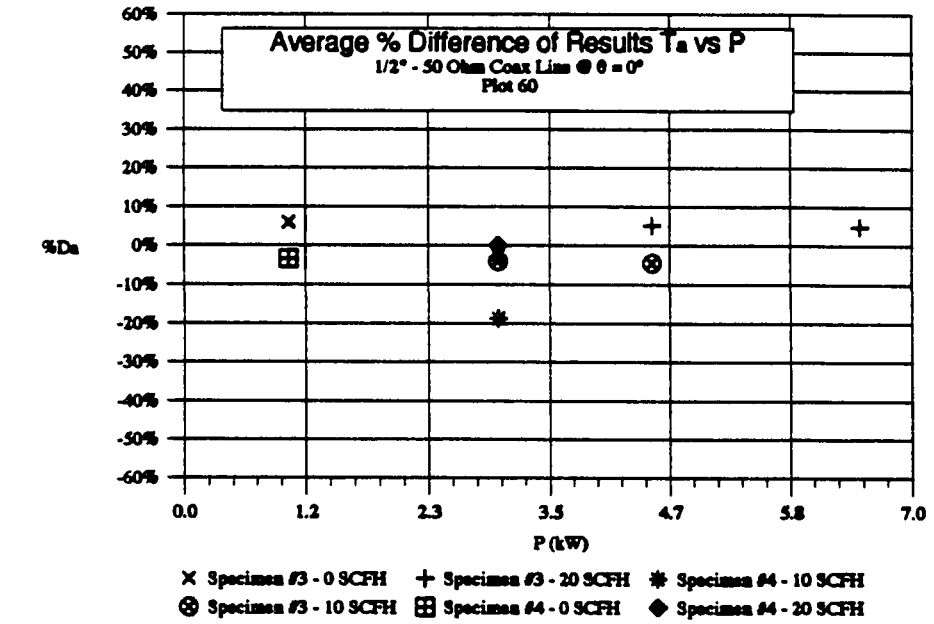

FIGURE 38 — $\%\Delta D_b$, 50-ohm Coax Line @ $\theta = 0°$

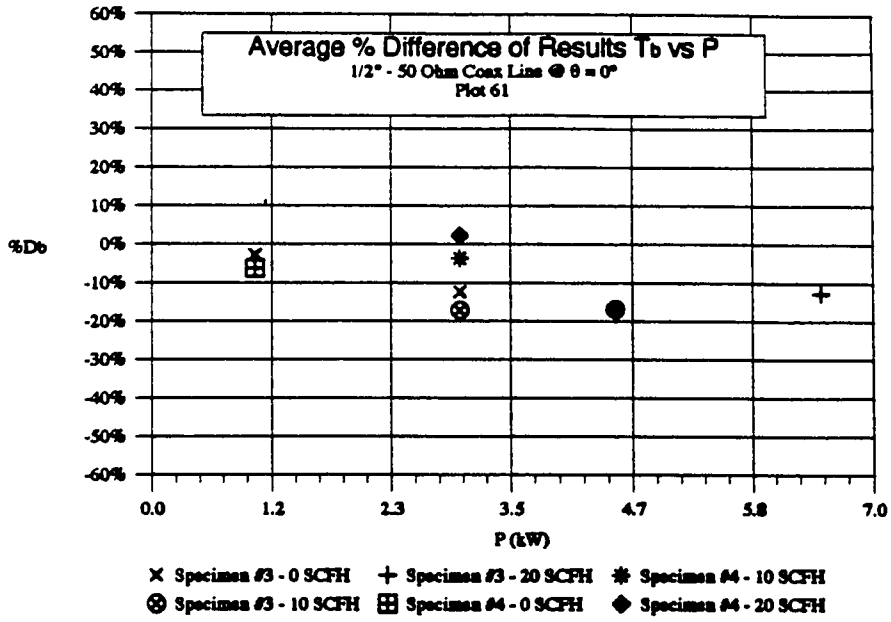

1/2" - 50-ohm @ $\theta = 90°$

Figures 39 - 41 show graphical comparisons of both test and calculated results for 1/2" - 50-ohm coaxial lines oriented at $\theta = 90°$. These figures present results for specimen #3, which had a copper inner conductor. No testing was done on specimen #4 in the vertical position.

Calculated results were made with COAX7. Boundary conditions used resulted in a 2-dimensional heat flow in both an outward radial and longitudinal directions. The longitudinal distribution produced decreasing temperatures with increasing y. The most notable change in temperature occurred within the localized region of $6" \leq y \leq 18"$. This

notable change is attributed to the large change in the convection coefficient, h_3, within this localized region.

A temperature contour was noted from the test data. In general the measured temperature distributions and magnitudes for these runs were similar to the previous runs at $\theta = 0°$. The adapters appeared to act as sinks, although the end temperatures tended to be slightly higher for these runs than was observed in the previous runs.

Figures 40 and 41 show plots of average $\%D_a$ and $\%D_b$ between the calculated and measured results. For these cases the range of difference is $-6.1\% \leq \%D_a \leq +17.4\%$ and $-45.7\% \leq \%D_b \leq -53.0\%$. *In summary there was good correlation for T_a, but there was poor correlation for T_b.* The difference associated with T_a is slightly weighted below the 0% line. However, the difference associated with T_b seems to be heavily weighted below 0% line. The effects due to line orientation tend to be secondary (and less then expected) and it is believed that a smaller difference could be realized if the previous model (1/2" - 50-ohm @ $\theta = 0°$) were applied. It is thought that the major cause for this large difference can be attributed to expression (2-28), used to calculate h_3. It should also be pointed out for values of $N_{G_R} N_{P_R}$ for y > 30" exceed, Frank's [4], recommended limit of 10^9. *In conclusion, further work needs to be done in developing any improved expression for calculating h_3 at $\theta = 90°$.*

FIGURE 39 — Comparison Results, Specimen #3 @ 3 kW & 0 SCFH

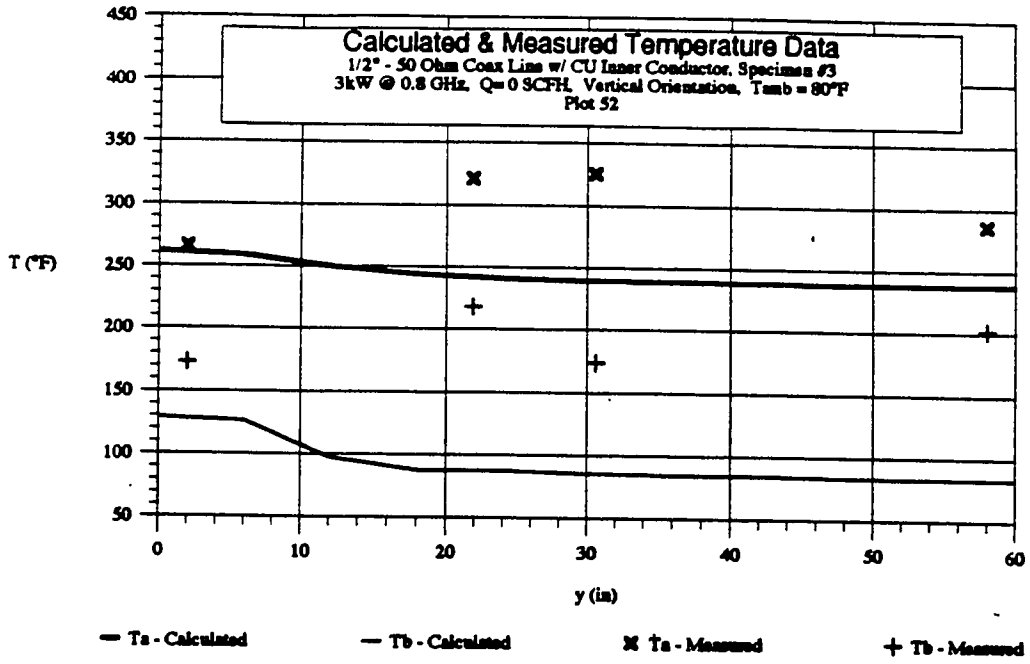

FIGURE 40 — Comparison Results, Specimen #3 @ 4.5 kW & 10 SCFH

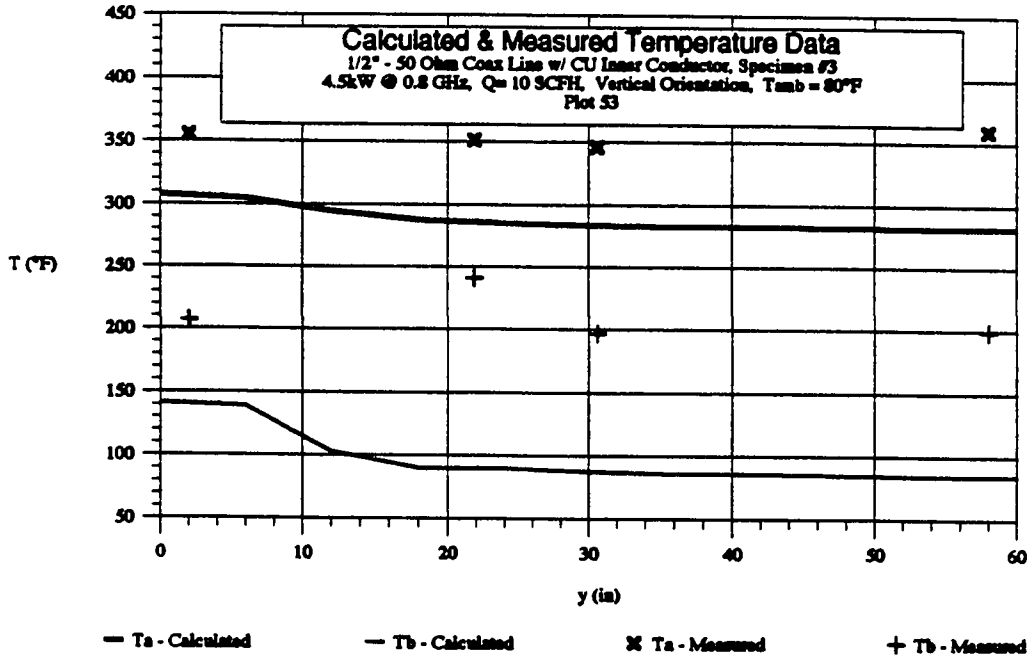

FIGURE 41 — Comparison Results, Specimen #3 @ 6 kW & 20 SCFH

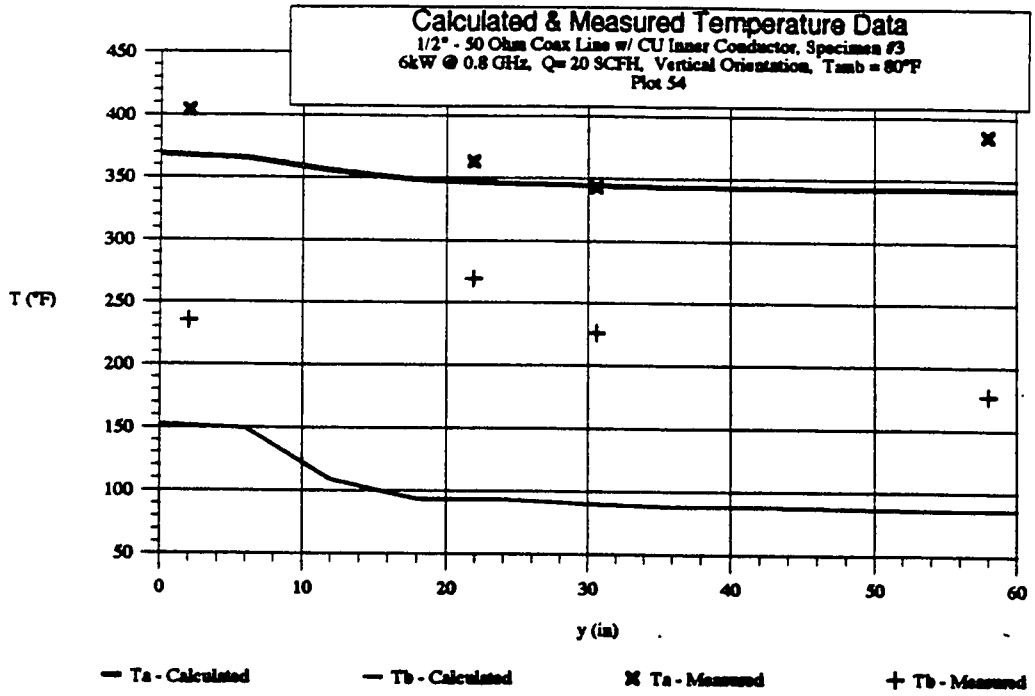

FIGURE 42 — $\%D_a$, 50-ohm Coax Line @ $\theta = 90°$

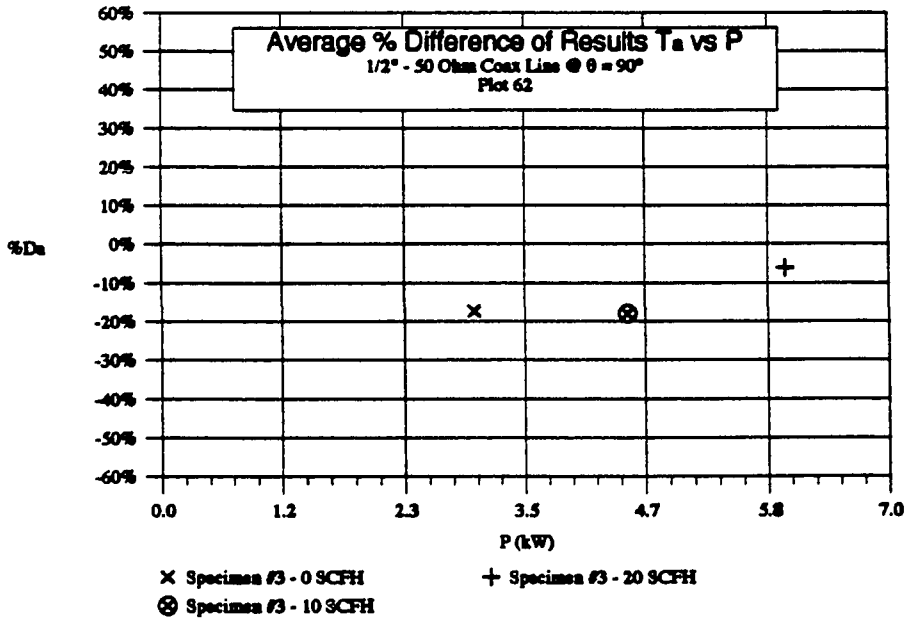

FIGURE 43 — $\%D_b$, 50-ohm Coax Line @ $\theta = 90°$

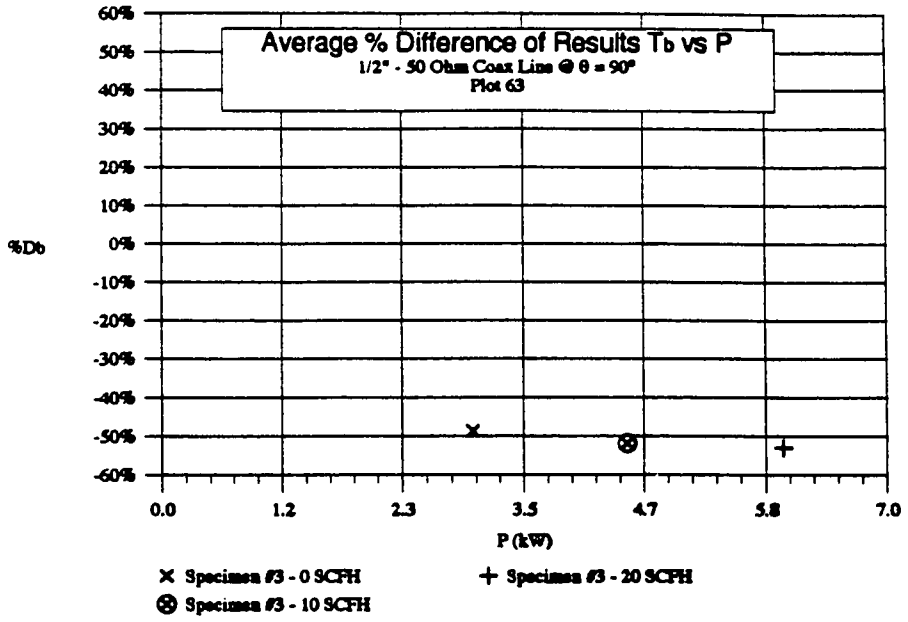

1/2" - 33-ohm @ $\theta = 0°$

Figures 44 - 47 show graphical comparisons of both test and calculated results for 1/2" - 33-ohm coaxial lines oriented at $\theta = 0°$. Figures 44 - 46 present the results for specimen #1. Figure 47 presents results for specimen #2.

Calculated results were made with COAX8. Boundary conditions used resulted in a 2-dimensional heat flow in both outward radial and longitudinal directions. The resulting longitudinal distribution for T_a is concave in shape and is symmetrical about the center of the line, y = 30". A slightly convex symmetrical distribution with a slight dip at y = 30" is calculated for T_b. These distributions are attributed to the change in $q_a^{"}$ with position, y. Each section of line was assigned a value of $q_a^{"}$ which was unique for each change in impedance.

A temperature contour was noted from the test data. The measured temperature distributions for T_a was: 1) concave for the case of P = 1 kW and Q = 0 SCFH (Figure 44); 2) flat distribution for the case of P = 3 kW and Q = 10 SCFH (Figure 45); 3) convex distribution was for the cases where P = 4.5 & 4.78 kW and Q = 20 SCFH (Figures 46 & 47). The temperature distribution of T_b for all cases (Figures 44 - 47) was convex. It is believed that the test adapters reduced both Ta and Tb.

Figures 48 and 49 show plots of average values for $\%D_a$ and $\%D_b$ between the calculated and measured results. For these cases the range of difference is $-18.3\% \leq \%D_a \leq +4.5\%$ and $-25.4\% \leq \%D_b \leq +0.7\%$. ***In summary there was good correlation between the calculated and measured results.*** The difference associated with T_a and T_b is weighted slightly below the 0% line. It is thought that a smaller difference might be realized if some refinements were made to (2-25), the expression used in calculating h_3. This would be realized if calculated values of h_3 were slightly reduced.

FIGURE 44 — Comparison Results, Specimen #1 @ 1 kW & 0 SCFH

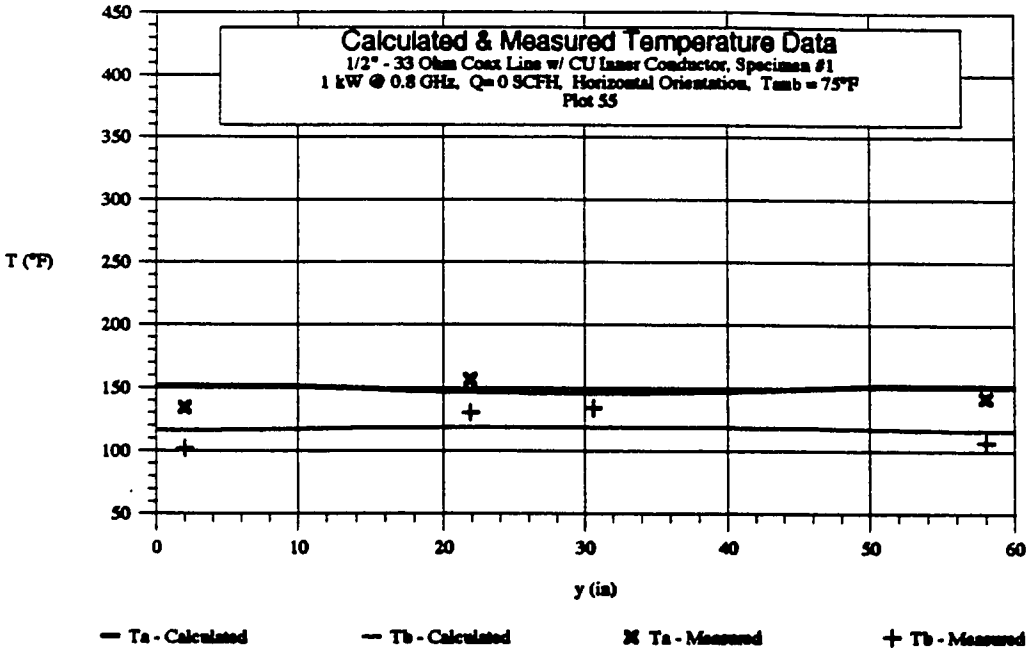

FIGURE 45 — Comparison Results, Specimen #1 @ 3 kW & 0 SCFH

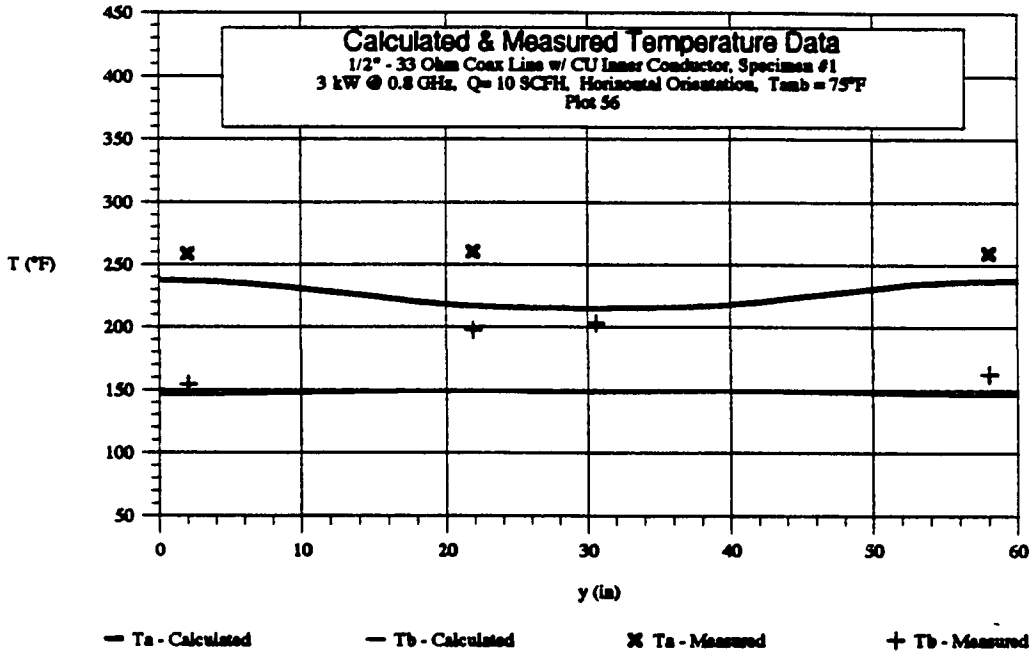

FIGURE 46 — Comparison Results, Specimen #1 @ 4.5 kW & 20 SCFH

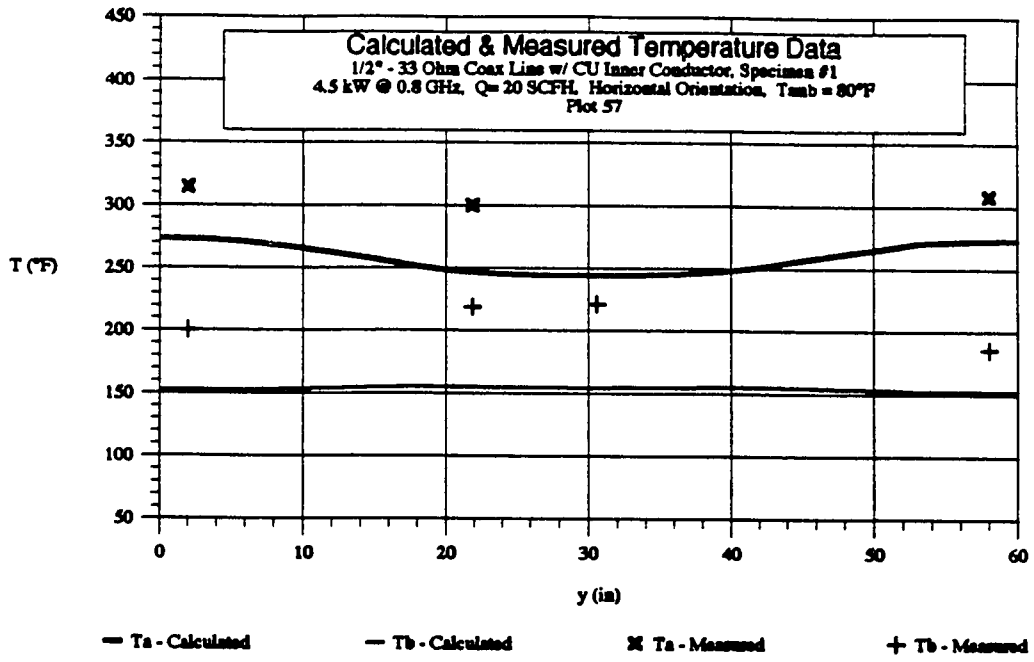

FIGURE 47 — Comparison Results, Specimen #2 @ 4.78 kW & 20 SCFH

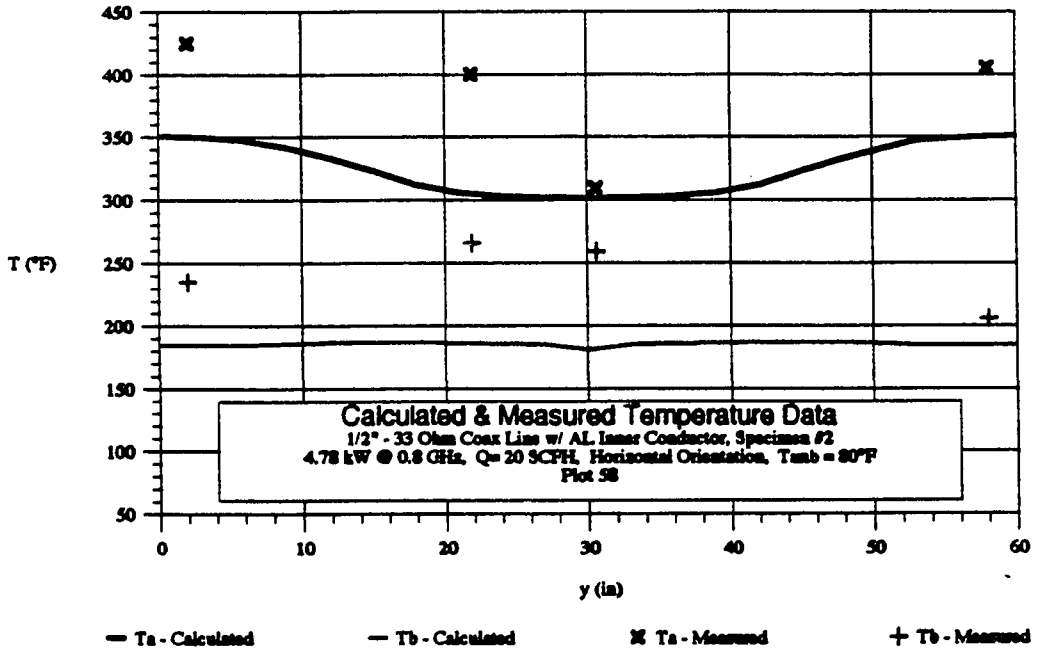

FIGURE 48 — $\%D_a$, 33-ohm Coax Line @ $\theta = 0°$

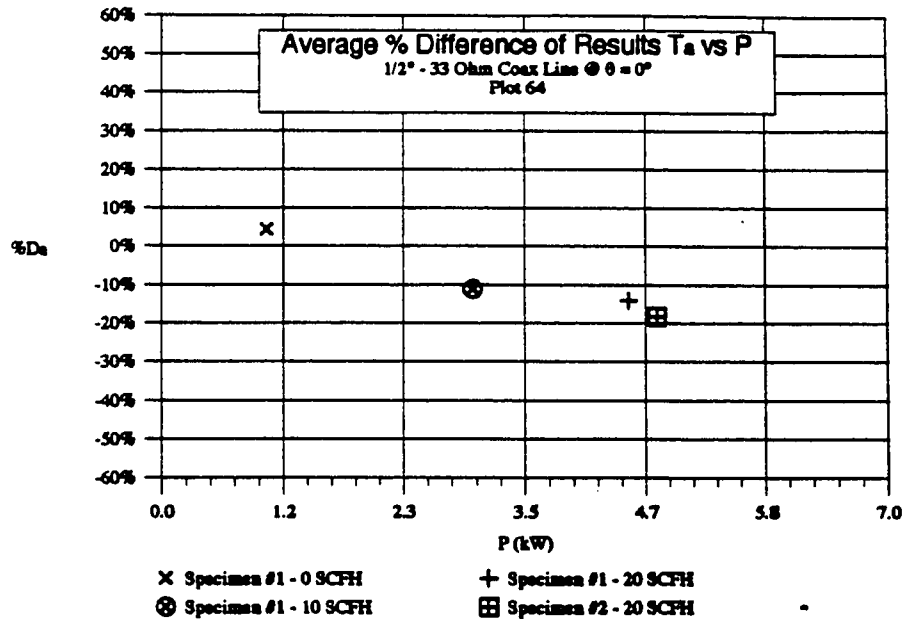

FIGURE 49 — $\%D_b$, 33-ohm Coax Line @ $\theta = 0°$

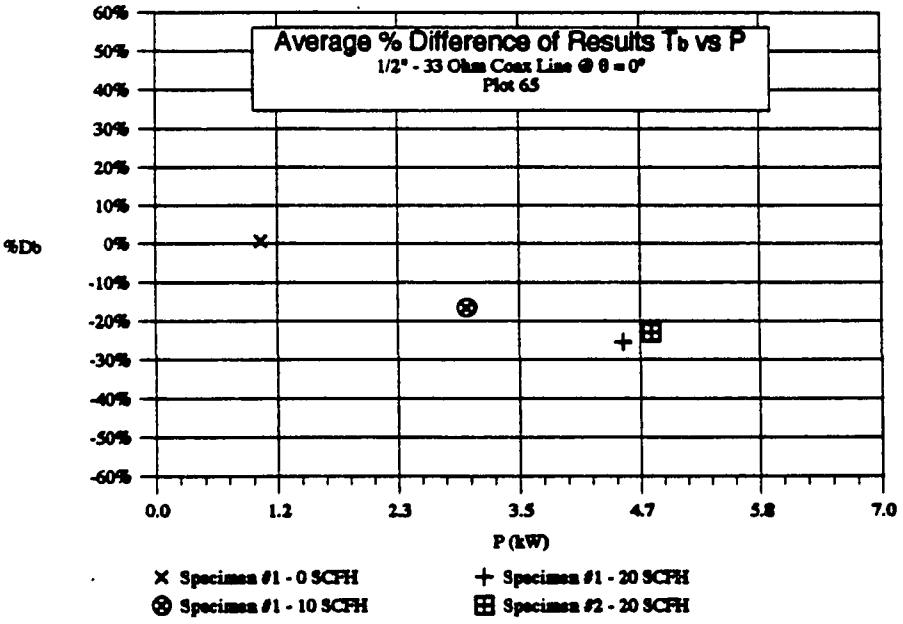

1/2" - 33-ohm @ θ = 90°

Figure 50 shows a plot of comparing test and calculated results of a specimen #2 oriented at θ = 90° and operating at P = 4.5 kW and Q = 20 SCFH.

Calculated results were made with COAX8. This model had the most complex boundary conditions of any model in this study and resulted in a 2-dimensional heat flow. Heat flow occurred in both an outward radial and longitudinal directions. The resulting longitudinal distribution for T_a is concave in shape and is slightly skewed. This distributions is attributed to the change in $\dot{q}_a''$ with position, y. Each section of line was assigned a value of $\dot{q}_a''$ which was unique for each change in impedance. The longitudinal distribution of T_b produced decreasing temperatures with increasing y. The most notable change in temperature occurred within the localized region, 0" ≤ y ≤ 12". This notable change is attributed to the large change in the convection coefficient, h_3, within this localized region.

It is noted, from the measured data, that the values for T_a and T_b did vary with position, y. The measured temperature distribution was slightly skewed.

The calculated difference for T_a and T_b between the calculated and measured results is: $\%D_a$ = -26.5% and $\%D_b$ = -50.9%. *In summary there was poor correlation for both Ta and T_b.* The difference associated with T_a and T_b were both heavily weighted below the 0% line. The measured effects due to line orientation tend to be secondary (and less then expected), and it is believed that a smaller difference could be realized if the previous model (1/2" - 33-ohm @ θ = 0°) were applied. It is thought that the major cause for this large difference can be attributed to expression (2-28) used to calculate h_3. It should also be pointed out for values of $N_{G_{k_y}} N_{P_R}$ for y > 30" exceed, Frank's [4], recommended limit of

10[9]. *In conclusion, further work needs to be done in developing any improved expression for calculating h_3 at $\theta = 90°$.*

FIGURE 50 — Comparison Results, Specimen #2 @ 4.5 kW & 20 SCFH

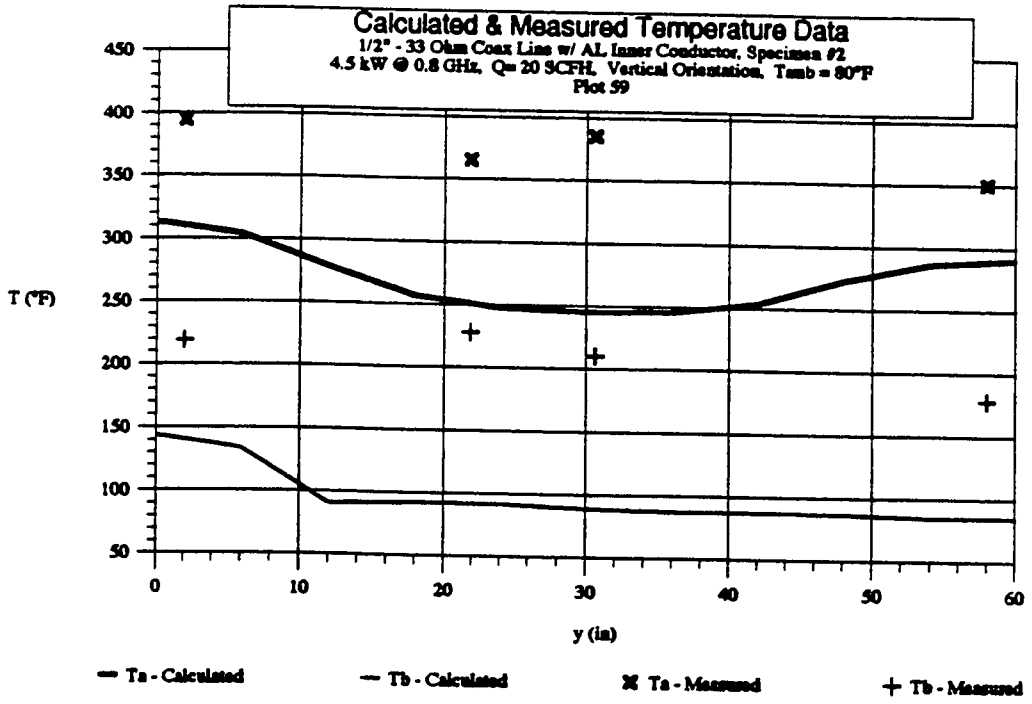

V. CONCLUSION

Summary

This study had three main objectives. The first was to further develop and evaluate an air-cooled low-loss coaxial transmission line, which would be suitable for use in high power UHF or L-Band radar systems. The second objective was to develop a thermal model to predict the steady state temperatures of the coaxial transmission line. The final objective was to identify a technique to accurately measure T_a.

Four air-cooled 1/2" diameter rigid coaxial lines were fabricated and tested. Testing was conducted at a fixed frequency of 0.8 GHz. Test specimens were instrumented with sensors to monitor both T_a and T_b. 50-ohm and 33-ohm specimens were fabricated. On average ΔT_a measured 6% higher and ΔT_b measured 35% higher for the 33-ohm specimens. Specimens were also fabricated with aluminum and copper inner conductors. Incorporation of the copper inner conductor reduced ΔT_a by 20% and ΔT_b by 9%. A forced air cooling system was evaluated where temperature measurements were taken at Q = 0, 10 and 20 SCFH. On average ΔT_a and ΔT_b decreased by 25% as Q was incrementally increased from 0 to 10 to 20 SCFH. Testing was conducted in both the horizontal and vertical position. The temperature gradient of the line was only slightly effected by line orientation, θ, changed. The measured cooling air exhaust stream temperatures are questionable, because of the measurement technique.

Fluoroptic Thermometry was used in the real time measurement of T_a. The fiber optic probe, which is non-metallic in construction, yielded non-intrusive temperature measurements of the inner conductor. For this study a 4-channel Luxtron Model 755 Fluoroptic Thermometer with both contacting and non-contacting probes was used.

Questionable measurements from the non-contacting probe were attributed to the application of the sensing material on the inner conductor. With further experimentation on the application of the sensing material, it is thought that the non-contacting probe could successfully be used in this application. Repeatability from contacting probe measurements was very good, ≤3%. A gasketed boss was designed into the line specimens which held the probe during testing.

Several FEA models were constructed and model results were compared against measured results. Good correlation was realized for both 50 and 33-ohm models where $\theta = 0°$. Bad correlation was realized for cases where $\theta = 90°$. This bad correlation was attributed to the simplified expression used to calculate h_3. However, results from the $\theta = 0°$ models were also in good agreement to measured results where $\theta = 90°$. Therefore, the models developed for horizontal line orientation, $\theta = 0°$, should yield acceptable results for any line orientation.

Recommendations

The following are recommendations which should be considered prior to incorporating the air-cooled coax design. The effects associated with changes in cooling air should be investigated. For this study the cooling air temperature was supplied over a rather limited range 70 - 80°F. Operational systems might not be able to consistently supply cooling air within this temperature range. Therefore, the first recommendation is to study the effects associated with the change in cooling air temperature.

In this study only a limited range of cooling air flow rates, Q, were evaluated. For systems where greater capacity is available increased line performance should be realized.

Therefore, where applicable, it is recommended that the effects related to higher Q be investigated. The effects of pressure drop versus Q should also be investigated.

This study did not address the issue of cooling air pressure drop. Some applications might have cooling air sources with a limited pressure head. The cooling sections used in this study had a length of 20". Therefore, measurements should be taken to determine what length of section can be realized. Also, the details such as the support beads, conductor surface finish and injection/exhaust ports on the test specimens were not optimized for a minimal pressure loss. So, the third recommendation is to study the effects associated with pressure losses; and how changes in parameters such as Q, L and line configuration can minimize pressure loss.

Lending [11] presents a curve which shows the increase in conductor's surface resistivity versus surface roughness at 3.0 GHz. Tables 12 presents his results at 0.45 and 1.6 GHz. From Table 12 it is apparent that a smoother conductor surface will yield lower line losses. A secondary benefit resulting from smoothing the conductor surfaces, is the increase in surface emissivity. This results in increased radiation cooling. Therefore, attention should be directed to fabricating lines with smooth conductor surfaces.

The requirements for certain applications specify light weight transmission lines. From this study the incorporation of a copper inner conductor was found substantially to improve the power capacity of the transmission line. The problem with copper is that its density is 3.3 times that of aluminum. Thus, for weight sensitive applications the choice of conductor materials should be further investigated. Table 13 lists the relative weights for several sizes of rigid air coaxial transmission lines constructed of different materials. From this table the

configurations with copper plated inner conductors will yield lower attenuation with only a slight (+3%) weight penalty.

Finally, further investigation might be required on the boundary condition at the outside surface of the outer conductor. In this study free air convection was assumed for all cases. In certain applications forced air convection might be available, which could increase the line capacity. However, other applications might have lines routed through passages where free air convection may not be realized; this could decrease line capacity. Therefore, for these cases further investigation is recommended.

TABLE 12 — Increase in Resistivity vs. Surface Roughness

Increase in Surface ρ	$\frac{RMS.Surface.Roughness}{\delta}$	RMS Surface Roughness (μ-inches)			
	[11]	0.45 GHz AL	0.45 GHz CU	1.6 GHz AL	1.6 GHz CU
10%	0.17	27	21	14	11
20%	0.69	108	85	58	45
30%	1.04	163	127	87	68
40%	1.38	217	169	115	90
50%	1.86	292	228	155	121
58%	2.80	440	343	233	182

TABLE 13— Weight Comparison of Different Rigid 50-ohm Air Coaxial Lines

Line Description	D (in)	b (in)	a (in)	d (in)	Weight[1] (lb/in)	Relative Weight
3/8"; AL = Outer; AL = Inner	0.375	0.312	0.135	0.072	0.0043	0.68
3/8"; AL=Outer; ALw/CU[2] Plating=Inner	0.375	0.312	0.135	0.072	0.0044	0.70
3/8"; AL = Outer; CU = Inner	0.375	0.312	0.135	0.072	0.0066	1.04
1/2"; AL = Outer; AL = Inner	0.50	0.433	0.188	0.125	0.0063	1.00
1/2"; AL=Outer; ALw/CU[2] Plating=Inner	0.50	0.433	0.188	0.125	0.0065	1.03
1/2"; AL = Outer; CU = Inner	0.50	0.433	0.188	0.125	0.0098	1.56
7/8"; AL = Outer; AL = Inner	0.842	0.778	0.388	0.325	0.0115	1.83
7/8"; AL=Outer; ALw/CU[2] Plating=Inner	0.842	0.778	0.388	0.325	0.0118	1.88
7/8"; AL = Outer; CU = Inner	0.842	0.778	0.388	0.325	0.0194	3.07
1-5/8"; AL = Outer; AL = Inner	1.625	1.562	0.680	0.618	0.0216	3.43
1-5/8"; AL=Outer; ALw/CU[2] Plating=In.	1.625	1.562	0.680	0.618	0.0223	3.54
1-5/8"; AL = Outer; AL = Inner	1.625	1.562	0.680	0.618	0.0358	5.69

Notes
1. Estimated weight does not include support beads.
2. 0.001" thick CU plating.

Conclusion

This study has shown that the 50-ohm air-cooled low-loss rigid coaxial transmission line has improved power capacity in comparison to the standard low-loss rigid coaxial transmission line. For certain radar applications this line design might be the preferred choice because of:

1. improved power capacity
2. minimal size
3. easy integration
4. simplified maintenance.

Also in this study, FEA models were constructed to predict the steady state performance of these lines. Using these models, power rating curves were calculated for 3/8", 1/2", 7/8" and 1-5/8" line sizes. From these curves the design engineer can quickly size lines for high power application. Figures 51 - 54 present these curves. The power rating limits were established by assuming $T_a = 392°F$ (200°C) and T_{amb} of 104°F. MIL-HDBK-216 [12] recommends this maximum value for T_a. At temperatures above this value materials tend to deteriorate i.e. conductors and spring contact members progressively lose their tensile strength, ductility, and flexibility.

From these curves it can be seen that power capacity decreases with increasing F. The air-cooled low-loss design shows a 38 to 75% increase in power capacity relative to the standard rigid design. A lower increase in power capacity was calculated for the larger line sizes. This can be attributed to lower cooling air flow velocities within the larger lines. Larger increases in power capacity could be realized if Q was increased. These power rating curves assume that the lines are perfectly matched (VSWR = 1.00:1). In real systems there will be some mismatch; so Figure 55 presents a derating curve for line

mismatch. Finally, appendices H, I, J and K include design curves which can be used by the design engineer to make line calculations for 3/8", 1/2", 7/8" and 1-5/8" lines at various values of F.

FIGURE 51 — Power Rating Curves 3/8" Coax Lines

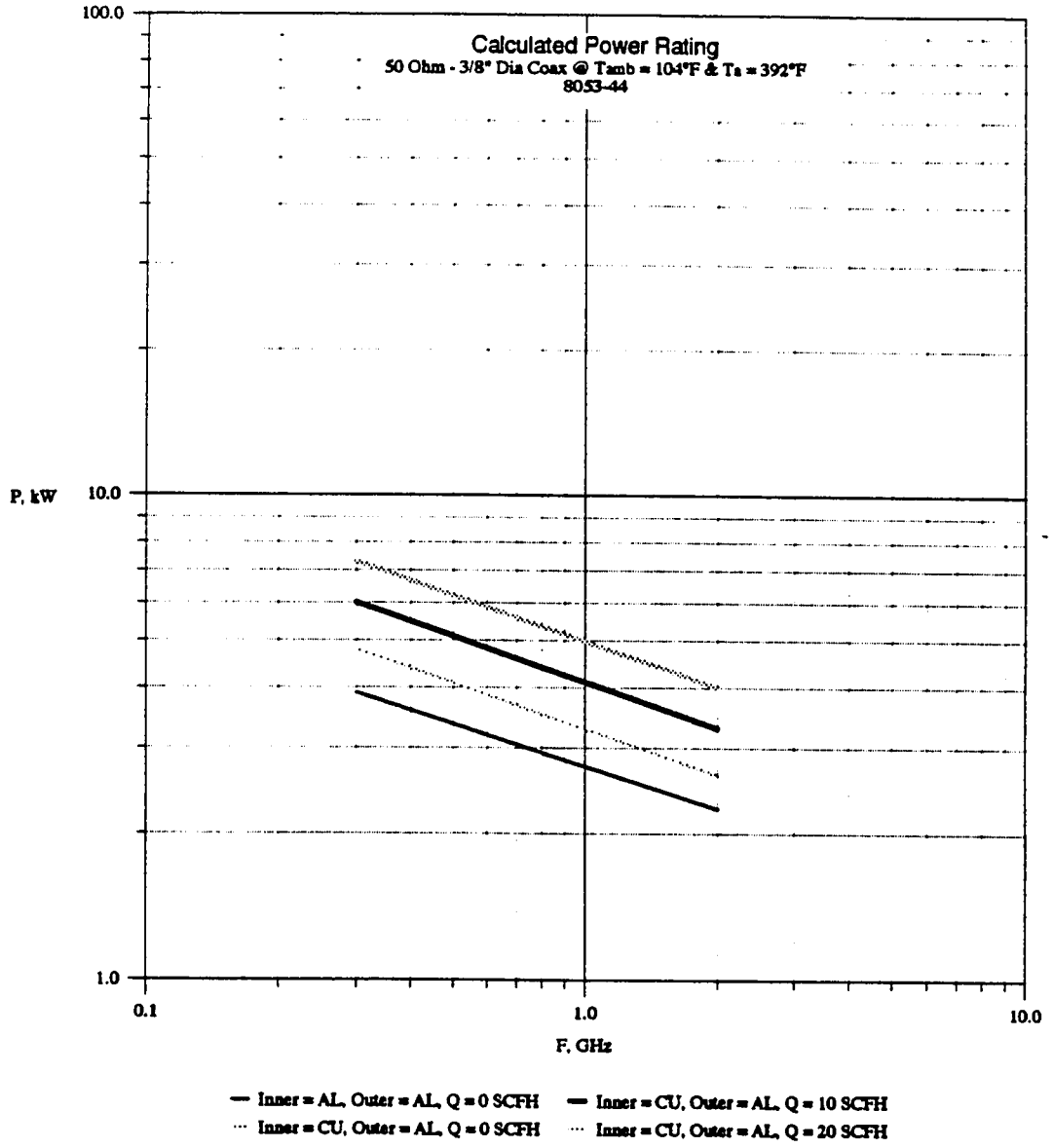

FIGURE 52 — Power Rating Curves 1/2" Coax Lines

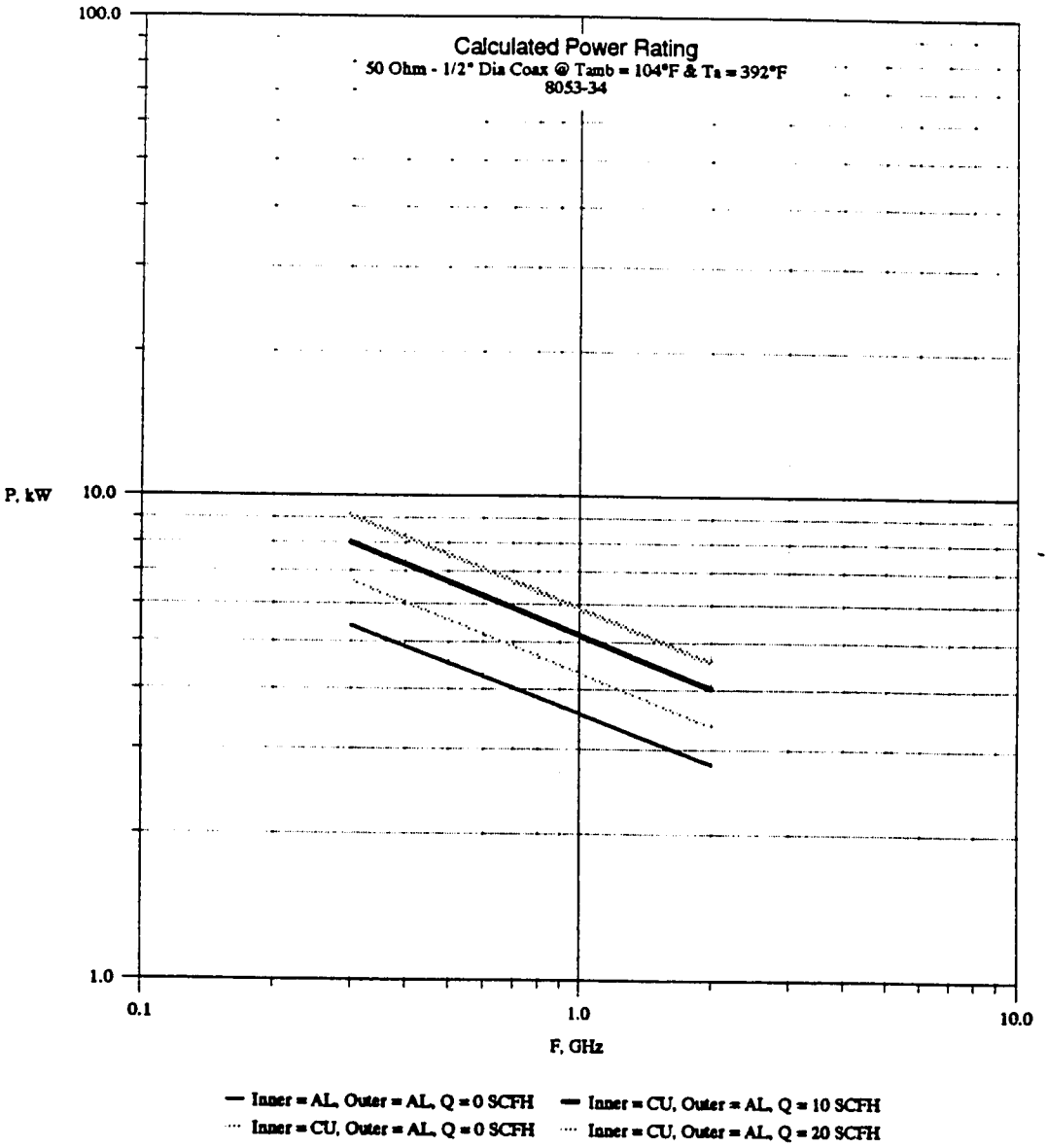

FIGURE 53 — Power Rating Curves 7/8" Coax Lines

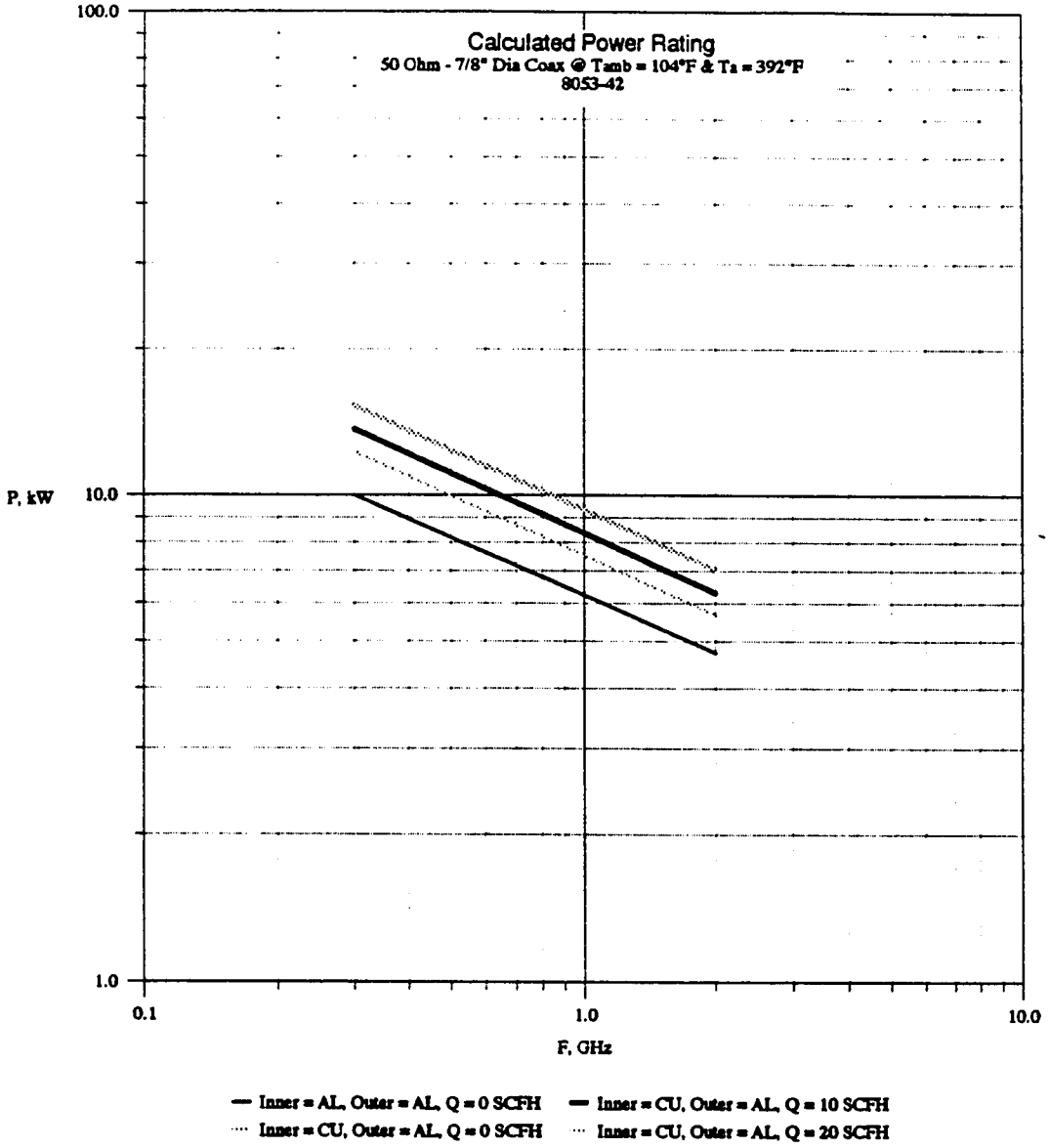

FIGURE 54 — Power Rating Curves 1-5/8" Coax Lines

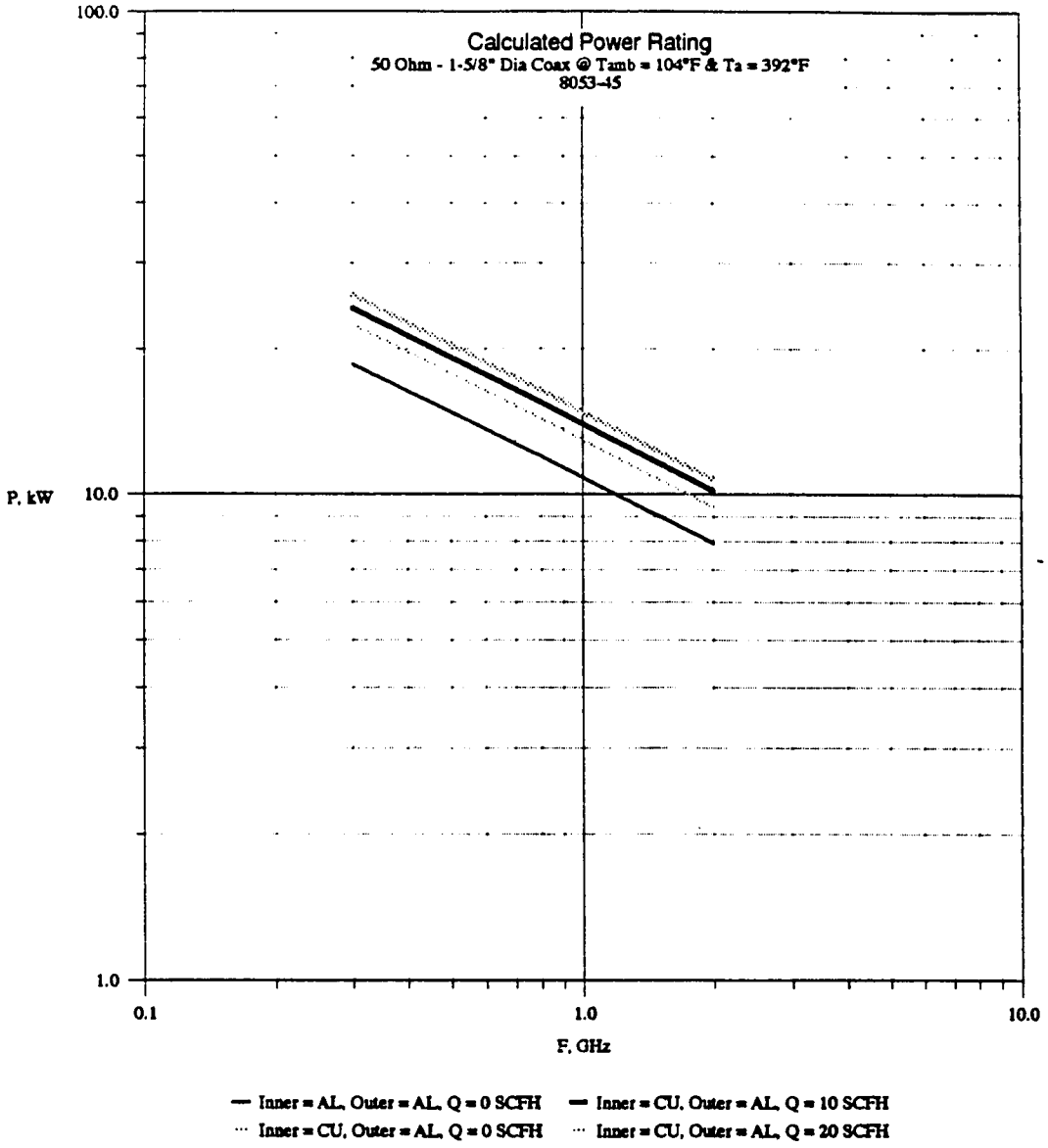

FIGURE 55 — Mismatch Derating Curve

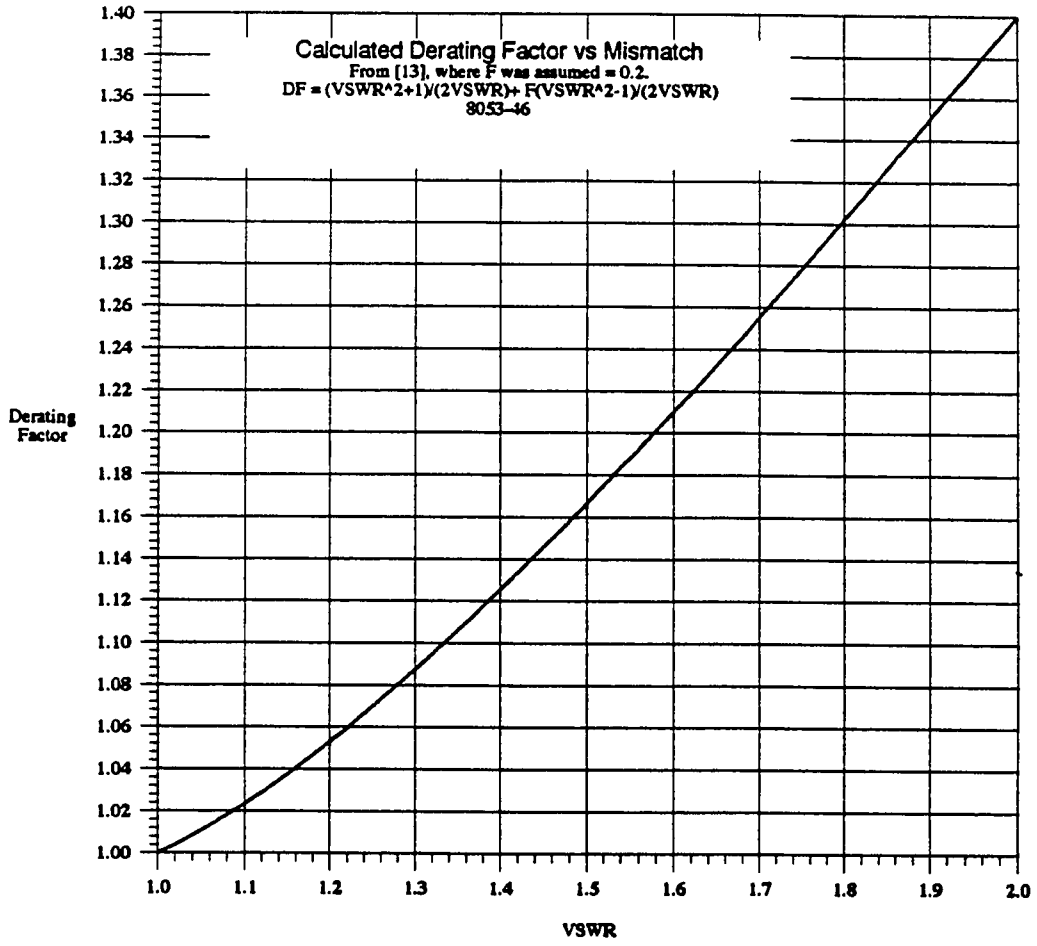

VI. REFERENCES

1. *Independent Research and Development Fiscal Year 1990*, Nero, M. ., "High Power, Multi-Channel Rotary Joint", Loral Randtron Systems, Menlo Park, 6/30/89, pp. 3.100-3.116.

2. *Medical Electronics*, K.A. Wickersheim and M.H. Sun, "Fluoroptic Thermometry", February 1987, pp. 84 - 91.

3. *IMAGES-Thermal*, Version 2.0, Berkeley, Celestial Software Inc. , 1990.

4. Frank Kreith, *Principles of Heat Transfer*,. 3rd Edition, San Francisco, Harper & Row, 1973.

5. Theodore Moreno, *Microwave Transmission Design Data*, Dover Publications Inc., New York, New York, 1958

6. George Regan, *Microwave Transmission Circuits*, 1st Edition, New York, McGraw Hill, 1948.

7. William McAdams, Heat Transfer, 3rd Edition, New York, McGraw Hill, 1954, pp. 165-182.

8. *RF Transmission Line The Complete Catalog & Handbook*, Times Fiber Communications Inc., Wallingford, Conn, 1983, pp. 7-8, 2.

9. W.W. Maccalpine, *Heating of Radio-Frequency Cables*, Electrical Communications, Volume 84, March 1948, pp. 84-99

10. H.E. King, *Rectangular Waveguide Theoretical CW Average Power Rating*, IRE Transactions on Microwave Theory and Techniques, July 1961, pp. 349-357

11. R. Lending, Vol. 11 Proceedings of National Electronics Conference.

12. MIL-HDBK-216, *RF Transmission Lines and Fittings*, Defense Supply Agency, Washington DC, January 4, 1962.

13. Catalog 35, *System Planning Product Specifications Services*, Andrew, Orland Park, ILL, 1991, pp. 423

Specimen #1 02-25-93
33 Ohm, Outer = AL / Inner = CU
Alpha = 0°

Measured Temperature

Time	RF Power	VSWR	I-Loss	Flow	Pos #1	Pos #2	Pos #3	Pos #4	Pos #5	Pos #6	Pos #7	Pos #8	Pos #9	Pos #10	Pos #11	Pos #12	Pos #13	Pos #14	Pos #15	Pos #16	Pos #17
	(Kw)	(dB)	(dB)	(SCFH)	(°F)	(°F)	(°F)	(°F)	(°F)	(°F)	(°F)	(°F)	(°F)	(°F)	(°F)	(°F)	(°F)	(°F)	(°F)	(°F)	(°F)
09:07	0.25	8.85	-29.22	0	86	92	101	93	73	74	78	85	87	83	74	74	73	75			
10:05	0.50	8.83	-28.22	0	105	114	134	112	74	74	88	97	99	92	75	75	74	74			
10:37	1.00	8.83	-28.19	0	134	156	190	142	76	79	102	130	134	107	79	78	75	75			
11:12	0.50	8.84	-30.87	0	105	111	126	112	75	77	89	99	101	94	77	77	76	76			
11:47	1.00	8.85	-28.31	0	134	157	192	143	77	80	101	131	135	107	79	78	76	76			
12:24	2.00	8.84	-26.61	0	196	233	308	204	79	85	129	176	188	134	81	80	77	83			
12:54	2.00	8.84	-29.38	10	196	197	232	197	80	86	130	159	159	134	81	80	77	77			
13:16	2.00	8.84	-31.95	20	171	170	196	179	80	85	123	142	142	129	82	80	77	77	79	82	81
13:53	3.00	8.84	-26.70	10	258	260	320	259	83	92	154	198	203	163	83	80	78	76	85	84	84
14:36	4.00	8.84	-26.87	20	282	273	321	282	86	98	172	210	209	177	85	83	78	76	80	80	80
15:06	4.50	8.83	-26.08	20	314	300	354	308	83	98	200	219	221	186	89	84	79	79	83	84	83
15:28	5.00	8.83	-25.07	20	348	330	392	340	82	93	216	244	241	197	94	85	79	79	81	81	81
15:36	5.00	8.77	-22.01	20*	262	234	324	274	80	81	131	130	137	120	78	78	76	76			
15:55	6.00	8.86	-22.39	20*	294	267	366	313	79	81	136	134	142	121	79	79	76	76			

Specimen #1 02-26-93
33 Ohm, Outer = AL / Inner = CU
Alpha = 90°

Measured Temperature

Time	RF Power	VSWR	I-Loss	Flow	Pos #1	Pos #2	Pos #3	Pos #4	Pos #5	Pos #6	Pos #7	Pos #8	Pos #9	Pos #10	Pos #11	Pos #12	Pos #13	Pos #14	Pos #15	Pos #16	Pos #17
	(Kw)	(dB)	(dB)	(SCFH)	(°F)	(°F)	(°F)	(°F)	(°F)	(°F)	(°F)	(°F)	(°F)	(°F)	(°F)	(°F)	(°F)	(°F)	(°F)	(°F)	(°F)
08:08	0.00				71	71	71	71	72	72	72	72	72	71	71	71	71	71			
08:31	0.50	8.94	-20.31	0	93	93	93	94	72	73	81	87	86	79	72	72	71	71			
09:16	1.00	8.91	-18.78	0	145	160	163	147	76	80	108	136	135	99	86	75	72	73			
09:48	2.00	8.88	-16.96	0	207	237	242	209	77	81	141	189	187	123	93	78	74	75			
10:18	3.00	8.85	-15.56	0	275	318	327	284	80	92	168	240	238	149	117	79	74	76			
10:46	3.00	8.86	-17.03	10	270	257	243	266	83	97	168	200	195	147	116	85	75	76	83	83	83
11:14	4.00	8.85	-16.23	10	334	314	298	333	81	93	201	236	228	177	131	85	75	75	84	84	84
11:48	5.00	8.85	-16.02	20	348	320	272	327	86	101	206	242	226	188	150	91	75	75	82	82	82
12:16	5.50	8.85	-15.79	20	385	351	300	360	86	104	214	267	246	207	93	86	75	76	79	79	79
12:38	5.50	8.86	-16.23	20*	285	248	204	304	79	80	127	152	146	163	86	81	76	76	79	79	79
13:12	7.00	8.85	-15.26	20*	361	314	253	385	80	81	145	179	170	195	83	78	77	78	81	81	81

* External cooling w/ fan.

Specimen #2
33 Ohm, Outer = AL / Inner = AL
Alpha = 0°

03-04-93

Measured Temperature

Time	RF Power (Kw)	VSWR (dB)	I-Loss (dB)	Flow (SCFH)	Pos #1 (°F)	Pos #2 (°F)	Pos #3 (°F)	Pos #4 (°F)	Pos #5 (°F)	Pos #6 (°F)	Pos #7 (°F)	Pos #8 (°F)	Pos #9 (°F)	Pos #10 (°F)	Pos #11 (°F)	Pos #12 (°F)	Pos #13 (°F)	Pos #14 (°F)	Pos #15 (°F)	Pos #16 (°F)	Pos #17 (°F)
12:15	-	-	-	-	82	77	78	83	79	79	81	79	78	83	79	79	78	78			
12:52	1.00	-18.47	8.66	0	137	165	169	155	80	80	92	132	142	108	85	84	79	80			
13:20	3.00	-15.34	8.61	0	259	334	350	298	81	81	119	235	264	160	100	94	81	83			
13:44	3.00	-16.93	8.62	10	273	308	275	303	81	82	124	206	220	168	101	93	81	80	88	89	89
14:04	4.00	-15.28	8.60	10	331	376	338	386	82	82	136	252	266	199	109	97	81	79	86	87	87
14:26	4.00	-16.64	8.61	20	316	330	262	337	82	82	140	219	225	188	103	95	81	80	86	86	85
14:52	4.78	-15.65	8.60	20	416	397	311	399	89	85	225	262	263	208	107	93	82	81	86	85	86
15:15	1.00	-18.88	8.66	0	165	165	164	166	85	83	121	135	139	116	92	87	81	82			
15:49	4.78	-15.60	8.60	20	425	400	309	405	93	87	235	266	259	206	116	98	83	86			
16:08	-	-	-	-	75	77	79	79	82	80	77	82	80	83	81	81	81	80			

Specimen #2
33 Ohm, Outer = AL / Inner = AL
Alpha = 90°

03-04-93

Measured Temperature

Time	RF Power (Kw)	VSWR (dB)	I-Loss (dB)	Flow (SCFH)	Pos #1 (°F)	Pos #2 (°F)	Pos #3 (°F)	Pos #4 (°F)	Pos #5 (°F)	Pos #6 (°F)	Pos #7 (°F)	Pos #8 (°F)	Pos #9 (°F)	Pos #10 (°F)	Pos #11 (°F)	Pos #12 (°F)	Pos #13 (°F)	Pos #14 (°F)	Pos #15 (°F)	Pos #16 (°F)	Pos #17 (°F)
08:46	0.00			0	73	73	73	72	74	74	75	74	74	74	73	73	74	75			
09:34	1.00	-30.35	8.66	0	151	167	165	154	80	77	115	134	137	108	83	80	75	77			
10:08	3.00	-16.88	8.61	0	311	348	348	295	85	82	191	253	267	167	96	86	76	77			
10:40	3.00	-18.57	8.62	10	324	309	264	295	89	85	203	218	213	172	98	85	77	78	82	81	82
10:58	4.00	-16.91	8.60	10	401	387	339	362	90	81	237	265	264	200	105	90	77	78	84	84	84
11:18	4.00	-18.65	8.62	20	353	328	258	319	88	81	217	229	220	180	104	92	78	79	82	83	82
11:34	4.50	-17.68	8.61	20	394	365	285	350	85	82	219	228	210	178	106	94	78	79	85	85	85

Specimen #3
50 Ohm, Outer = AL / Inner = CU
Alpha = 0°

03-05-92

Measured Temperature

Time	RF Power (Kw)	VSWR (dB)	I-Loss (dB)	Flow (SCFH)	Pos #1 (°F)	Pos #2 (°F)	Pos #3 (°F)	Pos #4 (°F)	Pos #5 (°F)	Pos #6 (°F)	Pos #7 (°F)	Pos #8 (°F)	Pos #9 (°F)	Pos #10 (°F)	Pos #11 (°F)	Pos #12 (°F)	Pos #13 (°F)	Pos #14 (°F)	Pos #15 (°F)	Pos #16 (°F)	Pos #17 (°F)
08:59	-	-	-	-	72	74	74	73	74	74	74	75	74	74	74		74	74			
09:32	1.00	-33.71	8.79	0	122	149	154	137	76	76	95	116	117	103	80	78	75	76			
10:06	3.00	-22.87	8.73	0	239	321	339	277	78	78	145	207	209	162	89	86	77	76			
10:26	3.00	-24.16	8.74	10	239	259	249	256	79	80	150	182	172	161	88	86	78	77	83	84	83
10:50	4.50	-22.70	8.74	10	324	361	347	342	81	83	187	242	227	195	96	92	80	78	83	84	83
11:18	4.50	-23.55	8.73	20	287	278	239	286	82	83	186	206	186	183	95	91	80	81	84	85	84
11:46	6.50	-22.47	8.70	20	408	380	322	395	87	94	227	254	219	220	103	99	81	80	83	84	83

Specimen #3
50 Ohm, Outer = AL / Inner = CU
Alpha = 90°

03-05-92

Measured Temperature

Time	RF Power (Kw)	VSWR (dB)	I-Loss (dB)	Flow (SCFH)	Pos #1 (°F)	Pos #2 (°F)	Pos #3 (°F)	Pos #4 (°F)	Pos #5 (°F)	Pos #6 (°F)	Pos #7 (°F)	Pos #8 (°F)	Pos #9 (°F)	Pos #10 (°F)	Pos #11 (°F)	Pos #12 (°F)	Pos #13 (°F)	Pos #14 (°F)	Pos #15 (°F)	Pos #16 (°F)	Pos #17 (°F)
12:42	3.00	-23.98	8.89	0	266	321	325	286	85	88	173	218	174	202	95	87	79	80			
13:12	3.00	-26.67	8.89	10	254	248	244	259	84	86	160	175	161	155	96	88	79	80	82	84	83
13:42	4.50	-24.59	8.78	10	355	351	346	359	87	89	207	241	197	199	104	94	80	80	80	81	81
14:06	4.50	-26.29	8.79	20	324	293	277	315	84	89	189	199	182	170	102	93	81	80	85	85	86
14:30	6.50	-25.31	8.82	20	404	363	343	385	88	90	235	269	226	177	110	99	81	82	83	83	84

Specimen #4
50 Ohm, Outer = AL / Inner = AL
Alpha = 90°

02-26-93

Measured Temperature

Time	RF Power (Kw)	VSWR (dB)	I-Loss (dB)	Flow (SCFH)	Pos #1 (°F)	Pos #2 (°F)	Pos #3 (°F)	Pos #4 (°F)	Pos #5 (°F)	Pos #6 (°F)	Pos #7 (°F)	Pos #8 (°F)	Pos #9 (°F)	Pos #10 (°F)	Pos #11 (°F)	Pos #12 (°F)	Pos #13 (°F)	Pos #14 (°F)	Pos #15 (°F)	Pos #16 (°F)	Pos #17 (°F)
15:10	1.00	-14.33	8.89	0	155	177	178	160	78	82	114	129	130	93	80	78	75	76			
15:33	3.00	-13.48	8.86	0	307	378	388	321	82	95	178	243	249	122	89	83	75	76			
15:50	3.00	-13.13	8.82	10	334	349	338	344	84	97	115	196	185	124	91	87	76	76	79	80	80
16:06	4.00	-13.73	8.82	10	397	374	347	405	83	95	124	231	219	125	93	83	76	76	78	78	78
16:26	4.00	-13.73	8.82	20	343	288	275	324	81	89	121	200	181	123	92	85	76	76	80	80	81
16:52	4.50	-13.33	8.81	20	364	320	294	353	80	89	118	210	192	133	92	87	76	76	78	78	79

Specimen #1
33 Ohm, Outer = AL / Inner = CU
Alpha = 0°

02-25-93

Calculated Delta Temperature

Time	RF Power (Kw)	VSWR (dB)	I-Loss (dB)	Flow (SCFH)	Pos #1 (°F)	Pos #2 (°F)	Pos #3 (°F)	Pos #4 (°F)	Pos #5 (°F)	Pos #6 (°F)	Pos #7 (°F)	Pos #8 (°F)	Pos #9 (°F)	Pos #10 (°F)	Pos #11 (°F)	Pos #12 (°F)	Pos #13 (°F)	Pos #14 (°F)	Pos #15 (°F)	Pos #16 (°F)	Pos #17 (°F)
09:07	0.25	8.85	-29.22	0	12	17	27	19	-1	-1.0	4	11	12	9	0	0	-2	0			
10:05	0.50	8.83	-28.22	0	30	39	60	38	-1.0	0	13	22	25	18	1.0	0	-1.0	0			
10:37	1.00	8.83	-28.19	0	59	81	115	66	1.0	4	27	55	59	31	4	2	0	0			
11:12	0.50	8.84	-30.87	0	29	35	50	36	-1.0	1.0	13	23	25	18	1	0	-1.0	0			
11:47	1.00	8.85	-28.31	0	58	80	116	67	1.0	3	25	54	59	31	3	2	0	0			
12:24	2.00	8.84	-26.61	0	113	150	225	122	-4	2	46	93	105	51	-1	-3	-6	0			
12:54	2.00	8.84	-29.38	10	120	121	155	120	4	9	53	82	82	57	5	3	0	0			
13:16	2.00	8.84	-31.95	20	94	93	119	102	4	9	47	65	66	52	5	3	0	0	2	5	4
13:53	3.00	8.84	-26.70	10	181	184	243	183	7	15	78	122	127	86	7	4	1	0	9	8	8
14:36	4.00	8.84	-26.87	20	206	197	245	206	10	22	96	134	133	101	9	7	2	0	4	4	4
15:06	4.50	8.83	-26.08	20	236	221	275	229	5	20	122	140	143	108	10	5	0	0	5	6	4
15:28	5.00	8.83	-25.07	20	269	251	313	261	3	13	137	164	162	118	14	6	0	0	2	2	2
15:36	5.00	8.77	-22.01	20*	186	158	248	199	4	5	55	54	61	44	3	2	0	0			
15:55	6.00	8.86	-22.39	20*	218	190	289	236	3	4	59	58	66	45	3	2	0	0			

Specimen #1
33 Ohm, Outer = AL / Inner = CU
Alpha = 90°

02-26-93

Calculated Delta Temperature

Time	RF Power (Kw)	VSWR (dB)	I-Loss (dB)	Flow (SCFH)	Pos #1 (°F)	Pos #2 (°F)	Pos #3 (°F)	Pos #4 (°F)	Pos #5 (°F)	Pos #6 (°F)	Pos #7 (°F)	Pos #8 (°F)	Pos #9 (°F)	Pos #10 (°F)	Pos #11 (°F)	Pos #12 (°F)	Pos #13 (°F)	Pos #14 (°F)	Pos #15 (°F)	Pos #16 (°F)	Pos #17 (°F)
08:08	0.00			0	0	0	0	0	1.0	1.0	1.0	1	1	0	0	0	0	0			
08:31	0.50	8.94	-20.31	0	22	21	22	23	0	1	10	16	15	7	1	0	0	0			
09:16	1.00	8.91	-18.78	0	72	87	89	73	3	6	35	63	62	26	12	2	-1	0			
09:48	2.00	8.88	-16.96	0	132	162	168	135	3	7	66	115	112	48	19	4	-1.0	0			
10:18	3.00	8.85	-15.56	0	200	242	251	208	4	16	92	164	162	74	42	4	-1	0			
10:46	3.00	8.86	-17.03	10	194	182	168	190	7	22	93	124	120	71	40	10	-1.0	0	7	7	7
11:14	4.00	8.85	-16.23	10	259	239	223	257	6	17	125	161	153	101	55	10	-1.0	0	9	8	8
11:48	5.00	8.85	-16.02	20	273	245	196	252	11	26	131	167	151	113	74	15	-1.0	0	7	7	7
12:16	5.50	8.85	-15.79	20	309	275	224	284	10	28	138	191	170	131	17	10	-1	0	3	3	3
12:38	5.50	8.86	-16.23	20*	209	172	128	228	3	4	51	76	69	86	10	5	-1.0	0	3	3	2
13:12	7.00	8.85	-15.26	20*	283	236	175	307	2	3	67	101	92	117	5	0	-2	0	3	3	3

* External cooling w/ fan.

Specimen #2 03-04-93
33 Ohm, Outer = AL / Inner = AL
Alpha = 0°

Calculated Delta Temperature

Time	RF Power (Kw)	VSWR (dB)	I-Loss (dB)	Flow (SCFH)	Pos #1 (°F)	Pos #2 (°F)	Pos #3 (°F)	Pos #4 (°F)	Pos #5 (°F)	Pos #6 (°F)	Pos #7 (°F)	Pos #8 (°F)	Pos #9 (°F)	Pos #10 (°F)	Pos #11 (°F)	Pos #12 (°F)	Pos #13 (°F)	Pos #14 (°F)	Pos #15 (°F)	Pos #16 (°F)	Pos #17 (°F)
12:15	-	-	-	-	4	-1.0	-1.0	5	1.0	1.0	3	0	0	5	1.0	0	0	0			
12:52	1.00	-18.47	8.66	0	57	86	89	75	0	0	12	53	62	28	6	4	-1.0	0			
13:20	3.00	-15.34	8.61	0	176	251	267	215	-2	-2	36	152	181	77	17	11	-2	0			
13:44	3.00	-16.93	8.62	10	193	228	195	224	2	2	44	127	140	88	21	14	1	0	9	9	9
14:04	4.00	-15.28	8.60	10	252	296	258	307	3	3	56	173	187	120	30	17	2	0	7	8	8
14:26	4.00	-16.64	8.61	20	236	250	183	258	2	2	60	139	146	108	23	15	2	0	6	7	6
14:52	4.78	-15.65	8.60	20	334	316	229	318	8	4	144	181	181	126	26	12	0	0	5	4	5
15:15	1.00	-18.88	8.66	0	83	84	82	85	4	1	39	53	58	34	10	5	-1.0	0			
15:49	4.78	-15.60	8.60	20	339	314	223	319	7	1	149	180	174	120	31	12	-3	0			
16:08	-	-	-	-	-5	-3	-1.0	-1.0	2	0	-3	2	0	3	1.0	1.0	1	0			

Specimen #2 03-04-93
33 Ohm, Outer = AL / Inner = AL
Alpha = 90°

Calculated Delta Temperature

Time	RF Power (Kw)	VSWR (dB)	I-Loss (dB)	Flow (SCFH)	Pos #1 (°F)	Pos #2 (°F)	Pos #3 (°F)	Pos #4 (°F)	Pos #5 (°F)	Pos #6 (°F)	Pos #7 (°F)	Pos #8 (°F)	Pos #9 (°F)	Pos #10 (°F)	Pos #11 (°F)	Pos #12 (°F)	Pos #13 (°F)	Pos #14 (°F)	Pos #15 (°F)	Pos #16 (°F)	Pos #17 (°F)
08:46	0.00			0	-2	-2	-1	-2	-1.0	-1.0	0	0	0	-1	-2	-2	-1.0	0			
09:34	1.00	-30.35	8.66	0	75	90	88	78	3	0	39	57	60	31	6	3	-2	0			
10:08	3.00	-16.88	8.61	0	234	271	271	217	8	4	113	176	189	89	19	9	-1	0			
10:40	3.00	-18.57	8.62	10	246	232	186	217	12	7	125	140	135	94	21	8	0	0	4	4	4
10:58	4.00	-16.91	8.60	10	323	309	261	284	12	3	159	187	186	122	27	12	-1.0	0	6	6	6
11:18	4.00	-18.65	8.62	20	274	249	179	240	9	2	138	150	141	101	25	13	-1	0	3	4	4
11:34	4.50	-17.68	8.61	20	315	286	206	271	7	4	141	149	132	100	27	15	0	0	7	6	6

Specimen #3 03-05-92
50 Ohm, Outer = AL / Inner = CU
Alpha = 0°

Calculated Delta Temperature

Time	RF Power (Kw)	VSWR (dB)	I-Loss (dB)	Flow (SCFH)	Pos #1 (°F)	Pos #2 (°F)	Pos #3 (°F)	Pos #4 (°F)	Pos #5 (°F)	Pos #6 (°F)	Pos #7 (°F)	Pos #8 (°F)	Pos #9 (°F)	Pos #10 (°F)	Pos #11 (°F)	Pos #12 (°F)	Pos #13 (°F)	Pos #14 (°F)	Pos #15 (°F)	Pos #16 (°F)	Pos #17 (°F)
08:59	-	-	-	-	-2	-1.0	0	-1	0	0	0	0	0	0	0	-74	0	0			
09:32	1.00	-33.71	8.79	0	46	73	79	62	0	0	20	40	41	27	4	3	-1.0	0			
10:06	3.00	-22.87	8.73	0	162	244	262	200	1	1	69	130	133	86	13	10	1	0			
10:26	3.00	-24.16	8.74	10	162	182	171	179	2	3	73	105	95	84	11	8	1.0	0	6	6	6
10:50	4.50	-22.70	8.74	10	246	283	269	264	3	5	109	164	149	117	18	14	2	0	5	6	5
11:18	4.50	-23.55	8.73	20	207	198	159	206	1	2	106	125	106	102	15	10	-1	0	3	4	3
11:46	6.50	-22.47	8.70	20	329	300	242	315	7	15	147	175	140	140	23	19	1.0	0	3	4	4

Specimen #3 03-05-92
50 Ohm, Outer = AL / Inner = CU
Alpha = 90°

Calculated Delta Temperature

Time	RF Power (Kw)	VSWR (dB)	I-Loss (dB)	Flow (SCFH)	Pos #1 (°F)	Pos #2 (°F)	Pos #3 (°F)	Pos #4 (°F)	Pos #5 (°F)	Pos #6 (°F)	Pos #7 (°F)	Pos #8 (°F)	Pos #9 (°F)	Pos #10 (°F)	Pos #11 (°F)	Pos #12 (°F)	Pos #13 (°F)	Pos #14 (°F)	Pos #15 (°F)	Pos #16 (°F)	Pos #17 (°F)
12:42	3.00	-23.98	8.89	0	186	241	246	207	5	8	93	138	94	122	15	7	-1.0	0			
13:12	3.00	-26.67	8.89	10	174	168	164	179	4	6	81	95	81	75	16	8	-1.0	0	3	4	3
13:42	4.50	-24.59	8.78	10	276	271	266	280	7	10	127	161	118	119	24	14	0	0	1.0	1	1
14:06	4.50	-26.29	8.79	20	244	213	197	235	4	9	109	119	102	90	22	12	0	0	5	4	6
14:30	6.50	-25.31	8.82	20	322	281	261	303	7	9	153	188	144	96	29	17	0	0	1	2	3

Specimen #4
50 Ohm, Outer = AL / Inner = AL
Alpha = 90°

02-26-93

Calculated Delta Temperature

Time	RF Power (Kw)	VSWR (dB)	I-Loss (dB)	Flow (SCFH)	Pos #1 (°F)	Pos #2 (°F)	Pos #3 (°F)	Pos #4 (°F)	Pos #5 (°F)	Pos #6 (°F)	Pos #7 (°F)	Pos #8 (°F)	Pos #9 (°F)	Pos #10 (°F)	Pos #11 (°F)	Pos #12 (°F)	Pos #13 (°F)	Pos #14 (°F)	Pos #15 (°F)	Pos #16 (°F)	Pos #17 (°F)
15:10	1.00	-14.33	8.89	0	79	101	102	83	2	5	38	52	54	17	4	2	-1	0			
15:33	3.00	-13.48	8.86	0	231	302	312	244	6	19	101	167	173	46	13	7	-1.0	0			
15:50	3.00	-13.13	8.82	10	258	273	261	268	8	21	39	120	109	48	15	11	0	0	3	3	4
16:06	4.00	-13.73	8.82	10	321	298	271	329	7	19	48	155	143	49	17	7	0	0	2	2	2
16:26	4.00	-13.73	8.82	20	266	211	198	247	4	13	44	123	105	47	16	8	0	0	4	4	4
16:52	4.50	-13.33	8.81	20	288	243	218	276	4	13	42	134	115	56	16	11	-1.0	0	2	2	2

APPENDIX C — Plots Test Data (ΔT @ y = 21.9" vs. P)

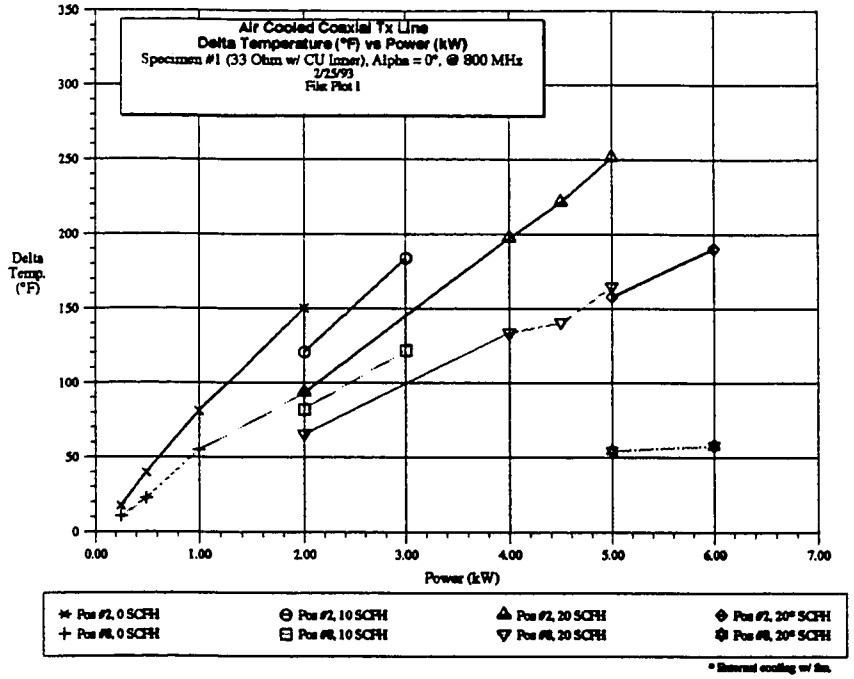

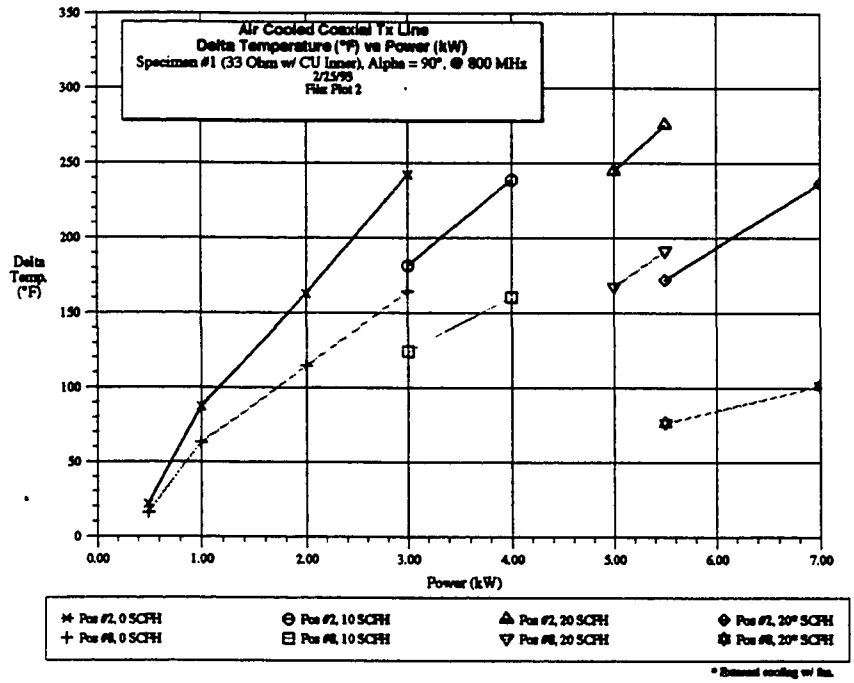

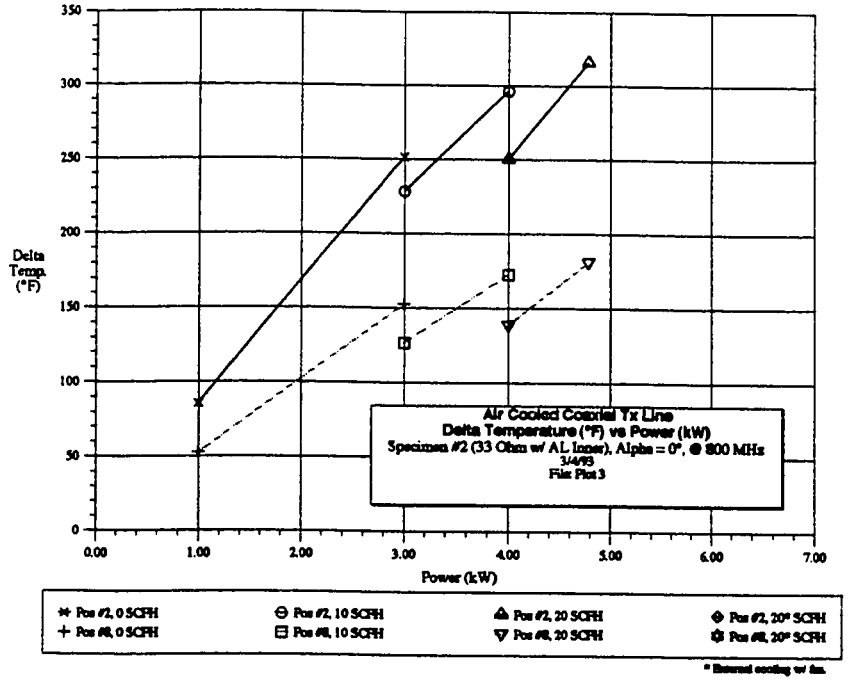
Air Cooled Coaxial Tx Line
Delta Temperature (°F) vs Power (kW)
Specimen #2 (33 Ohm w/ AL Inner), Alpha = 0°, @ 800 MHz
3/4/93
File: Plot 3
Delta Temp. (°F)
Power (kW)
0
50
100
150
200
250
300
350
0.00
1.00
2.00
3.00
4.00
5.00
6.00
7.00
Pos #2, 0 SCFH
Pos #8, 0 SCFH
Pos #2, 10 SCFH
Pos #8, 10 SCFH
Pos #2, 20 SCFH
Pos #8, 20 SCFH
Pos #2, 20* SCFH
Pos #8, 20* SCFH

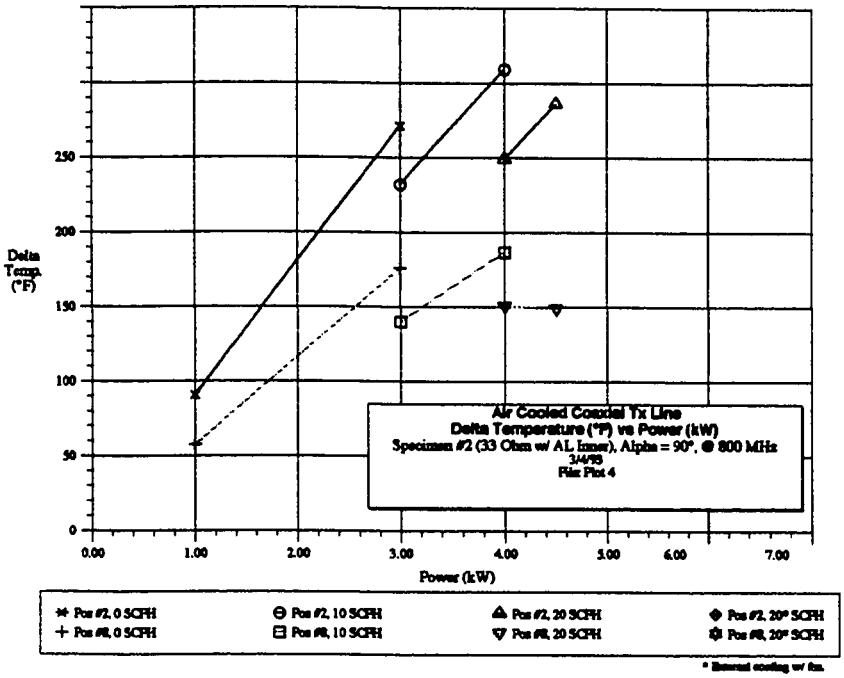
Air Cooled Coaxial Tx Line
Delta Temperature (°F) vs Power (kW)
Specimen #2 (33 Ohm w/ AL Inner), Alpha = 90°, @ 800 MHz
3/4/93
File: Plot 4
Delta Temp. (°F)
Power (kW)
0
50
100
150
200
250
0.00
1.00
2.00
3.00
4.00
5.00
6.00
7.00
Pos #2, 0 SCFH
Pos #8, 0 SCFH
Pos #2, 10 SCFH
Pos #8, 10 SCFH
Pos #2, 20 SCFH
Pos #8, 20 SCFH
Pos #2, 20* SCFH
Pos #8, 20* SCFH

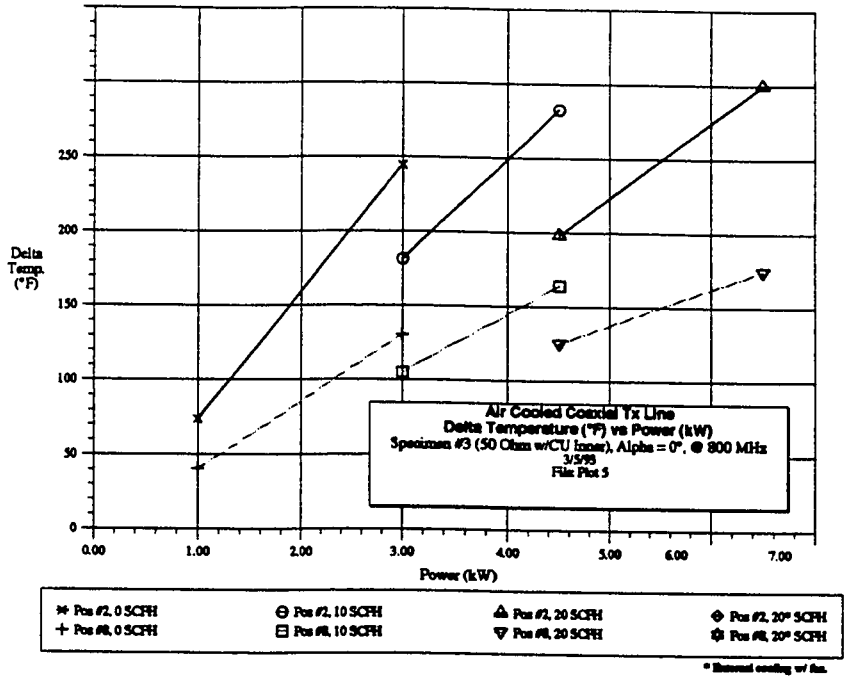
Delta Temp. (°F)
250
200
150
100
50
0
0.00
1.00
2.00
3.00
4.00
5.00
6.00
7.00
Power (kW)
Air Cooled Coaxial Tx Line
Delta Temperature (°F) vs Power (kW)
Specimen #3 (50 Ohm w/CU Inner), Alpha = 0°, @ 800 MHz
3/5/98
File: Plot 5
Pos #2, 0 SCFH
Pos #8, 0 SCFH
Pos #2, 10 SCFH
Pos #8, 10 SCFH
Pos #2, 20 SCFH
Pos #8, 20 SCFH
Pos #2, 20* SCFH
Pos #8, 20* SCFH

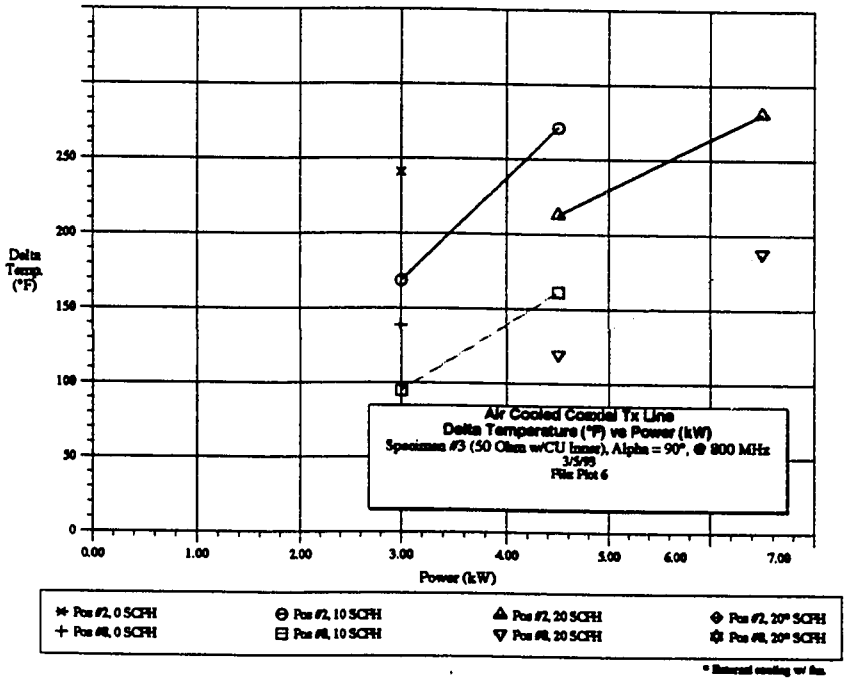
Delta Temp. (°F)
250
200
150
100
50
0
0.00
1.00
2.00
3.00
4.00
5.00
6.00
7.00
Power (kW)
Air Cooled Coaxial Tx Line
Delta Temperature (°F) vs Power (kW)
Specimen #3 (50 Ohm w/CU Inner), Alpha = 90°, @ 800 MHz
3/5/98
File: Plot 6
Pos #2, 0 SCFH
Pos #8, 0 SCFH
Pos #2, 10 SCFH
Pos #8, 10 SCFH
Pos #2, 20 SCFH
Pos #8, 20 SCFH
Pos #2, 20* SCFH
Pos #8, 20* SCFH

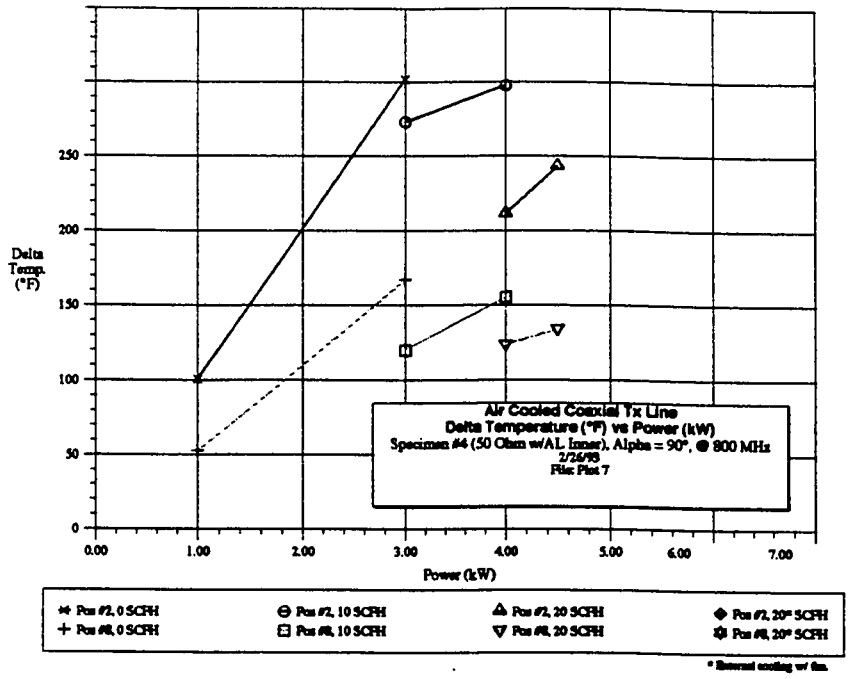
Air Cooled Coaxial Tx Line
Delta Temperature (°F) vs Power (kW)
Specimen #4 (50 Ohm w/AL Inner), Alpha = 90°, @ 800 MHz
2/26/98
File: Plot 7
Delta Temp. (°F)
0
50
100
150
200
250
0.00
1.00
2.00
3.00
4.00
5.00
6.00
7.00
Power (kW)
Pos #2, 0 SCFH
Pos #8, 0 SCFH
Pos #2, 10 SCFH
Pos #8, 10 SCFH
Pos #2, 20 SCFH
Pos #8, 20 SCFH
Pos #2, 20* SCFH
Pos #8, 20* SCFH

APPENDIX D — Plots Test Data (ΔT of Inner Conductor vs. y)

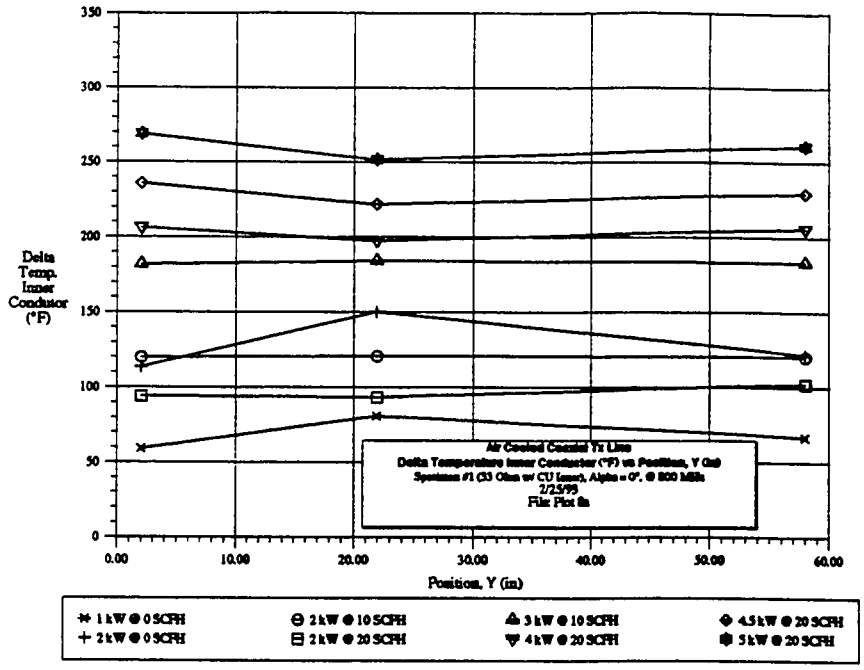

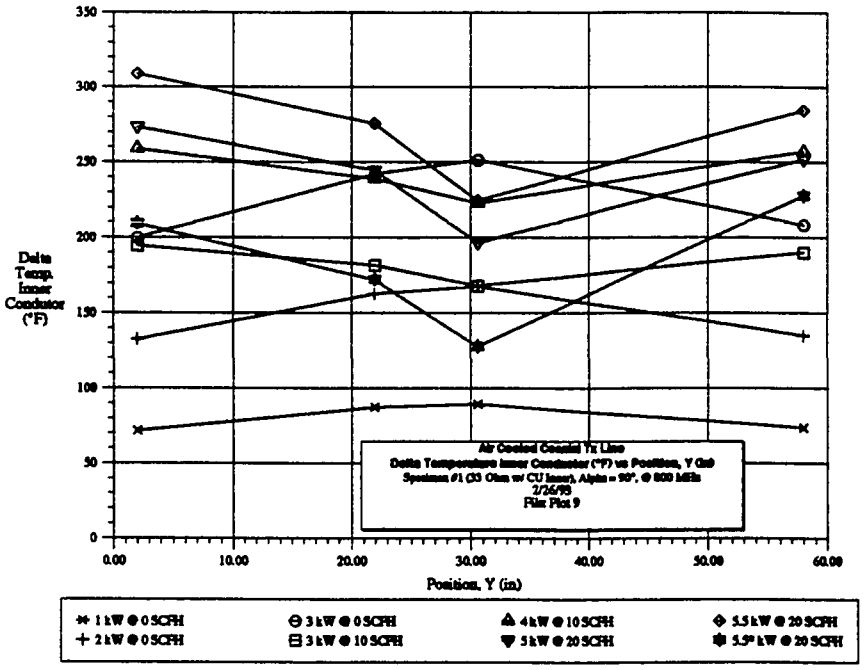

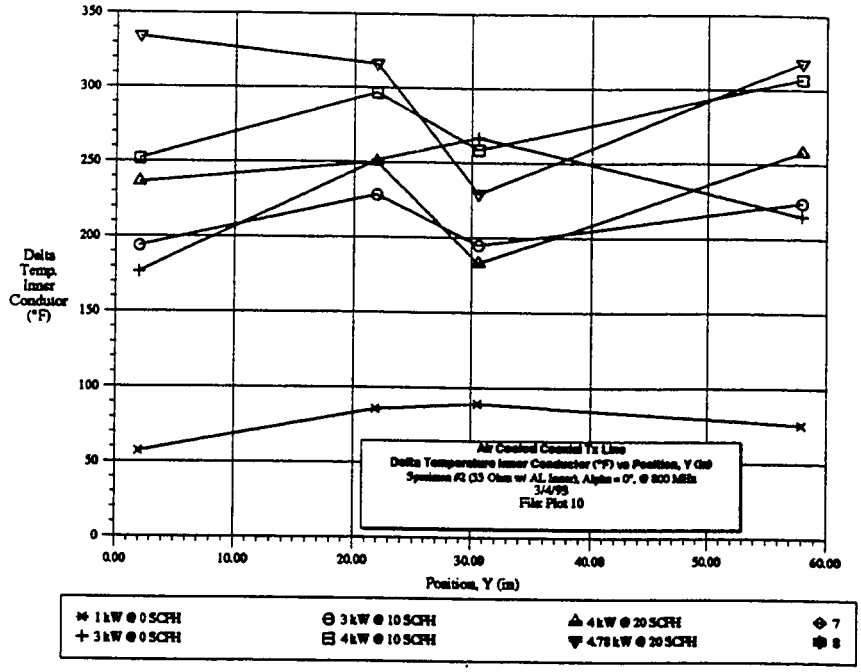
Delta Temp. Inner Conductor (°F)
Position, Y (in)
0.00
10.00
20.00
30.00
40.00
50.00
60.00
0
50
100
150
200
250
300
350
Air Cooled Coaxial Tx Line
Delta Temperature Inner Conductor (°F) vs Position, Y (in)
Specimen #2 (33 Ohm w/ AL Inner), Alpha = 0°, @ 800 MHz
3/4/98
File: Plot 10
1 kW @ 0 SCFH
3 kW @ 0 SCFH
3 kW @ 10 SCFH
4 kW @ 10 SCFH
4 kW @ 20 SCFH
4.78 kW @ 20 SCFH
7
8

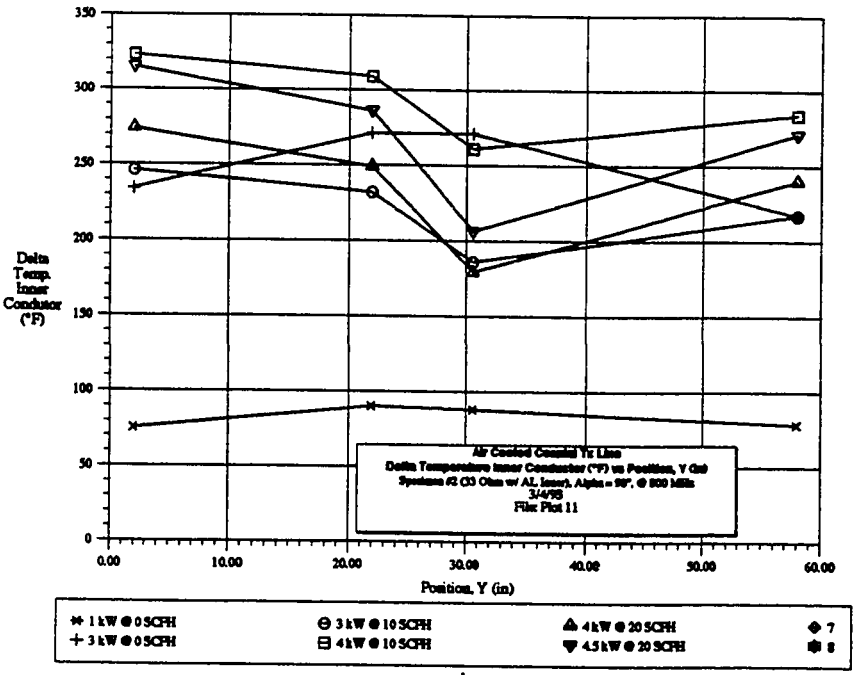
Delta Temp. Inner Conductor (°F)
Position, Y (in)
0.00
10.00
20.00
30.00
40.00
50.00
60.00
0
50
100
150
200
250
300
350
Air Cooled Coaxial Tx Line
Delta Temperature Inner Conductor (°F) vs Position, Y (in)
Specimen #2 (33 Ohm w/ AL Inner), Alpha = 90°, @ 800 MHz
3/4/98
File: Plot 11
1 kW @ 0 SCFH
3 kW @ 0 SCFH
3 kW @ 10 SCFH
4 kW @ 10 SCFH
4 kW @ 20 SCFH
4.5 kW @ 20 SCFH
7
8

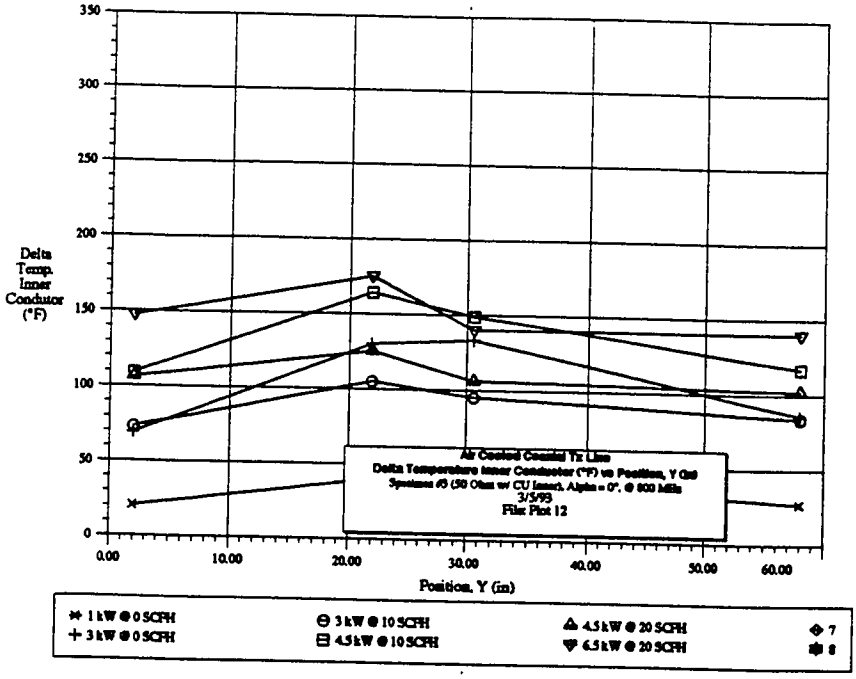
Delta Temp. Inner Conductor (°F)
Position, Y (in)
Air Cooled Coaxial Tx Line
3/5/95
File: Plot 12
1 kW @ 0 SCFH
3 kW @ 0 SCFH
3 kW @ 10 SCFH
4.5 kW @ 10 SCFH
4.5 kW @ 20 SCFH
6.5 kW @ 20 SCFH
7
8

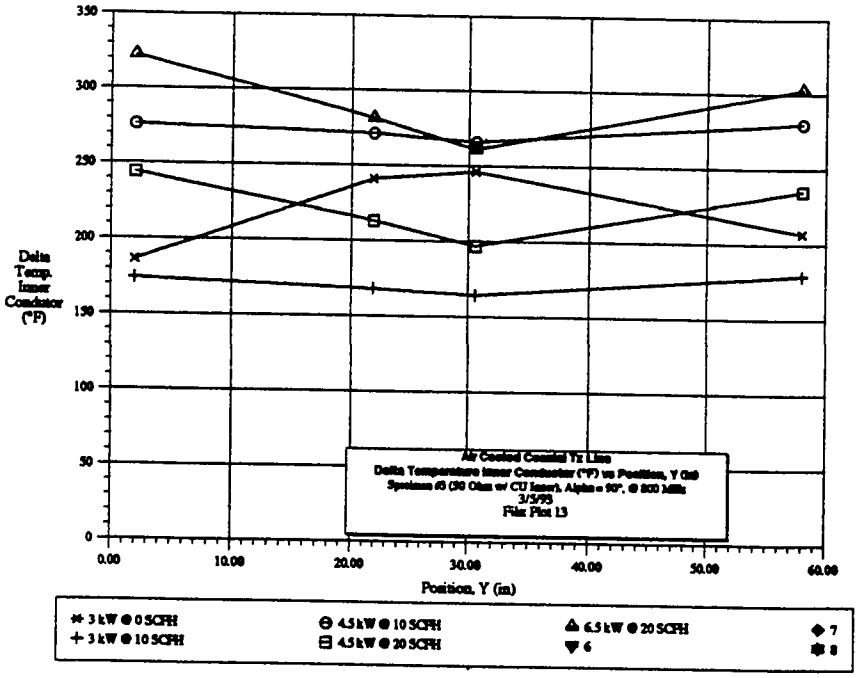
Delta Temp. Inner Conductor (°F)
Position, Y (in)
Air Cooled Coaxial Tx Line
3/5/95
File: Plot 13
3 kW @ 0 SCFH
3 kW @ 10 SCFH
4.5 kW @ 10 SCFH
4.5 kW @ 20 SCFH
6.5 kW @ 20 SCFH
6
7
8

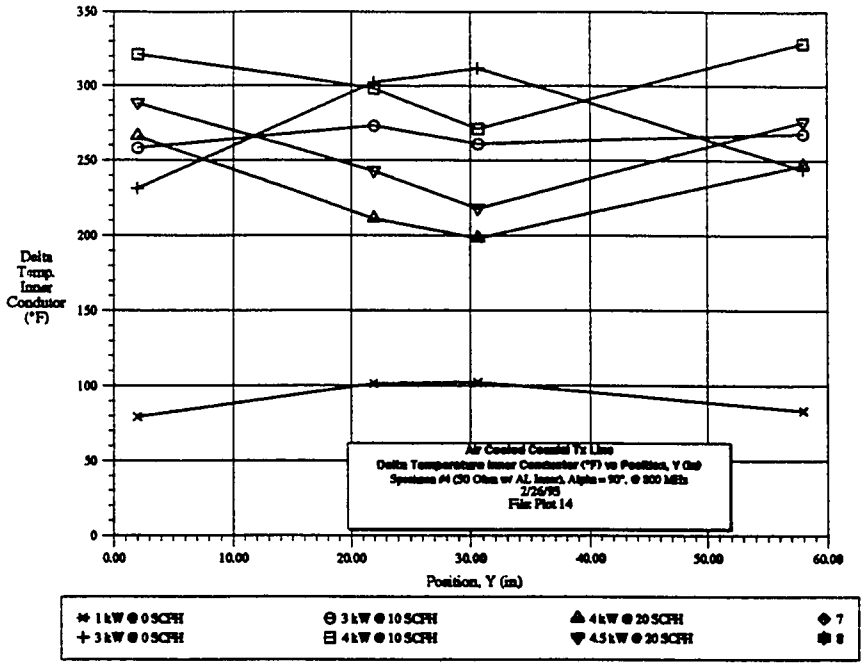
350
300
250
200
150
100
50
0
Delta Temp. Inner Conductor (°F)
0.00
10.00
20.00
30.00
40.00
50.00
60.00
Position, Y (in)
Air Cooled Coaxial Tx Line
Delta Temperature Inner Conductor (°F) vs Position, Y (in)
Specimen #4 (50 Ohm w/ AL Inner), Alpha = 90°, @ 800 MHz
2/26/95
File: Plot 14
1 kW @ 0 SCFH
3 kW @ 0 SCFH
3 kW @ 10 SCFH
4 kW @ 10 SCFH
4 kW @ 20 SCFH
4.5 kW @ 20 SCFH
7
8

APPENDIX E — Plots Test Data (ΔT of Outer Conductor vs. y)

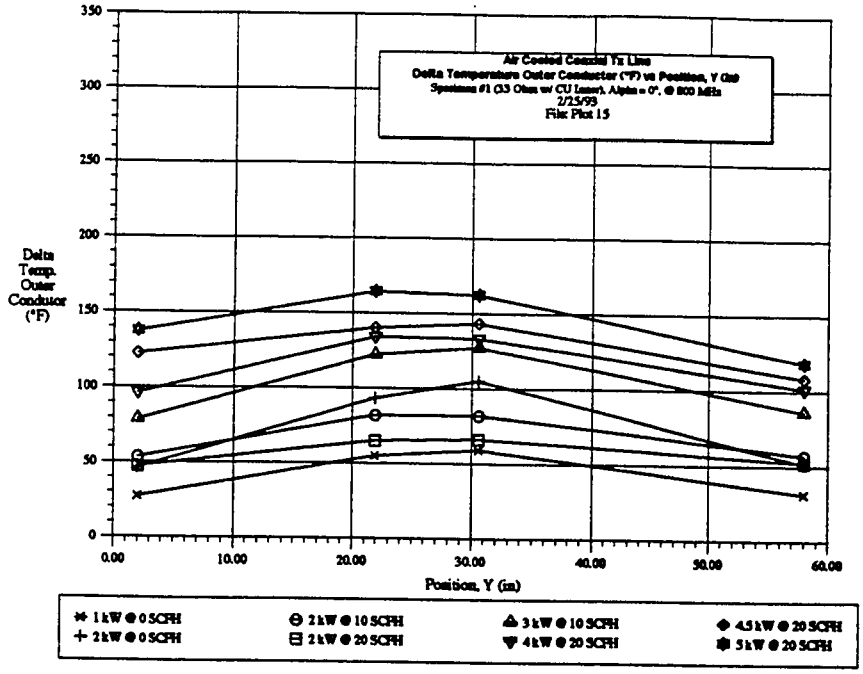

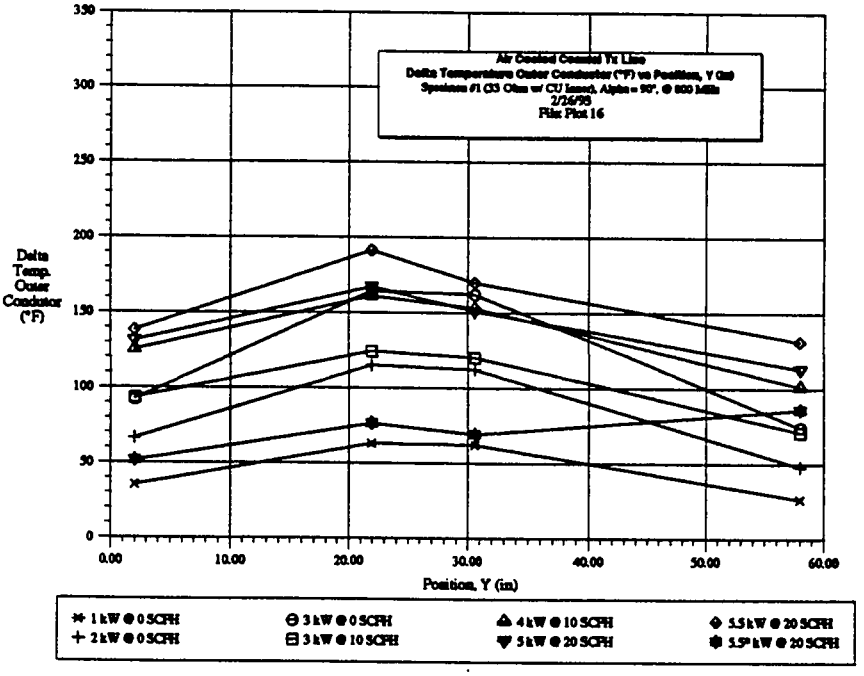

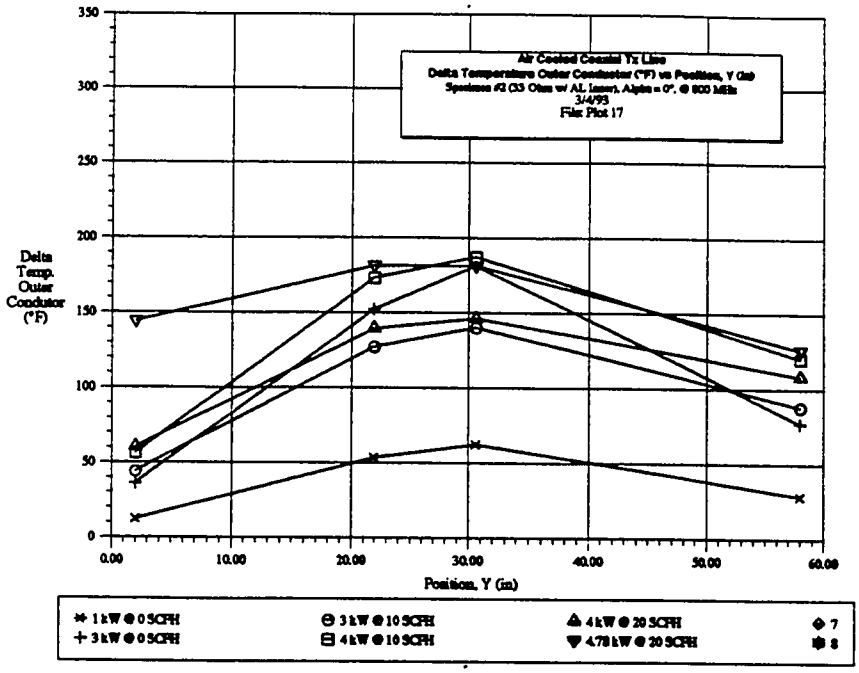
Air Cooled Coaxial Yz Line
3/4/95
Plot 17
Delta Temp. Outer Conductor (°F)
Position, Y (in)
1 kW @ 0 SCFH
3 kW @ 0 SCFH
3 kW @ 10 SCFH
4 kW @ 10 SCFH
4 kW @ 20 SCFH
4.78 kW @ 20 SCFH
7
8

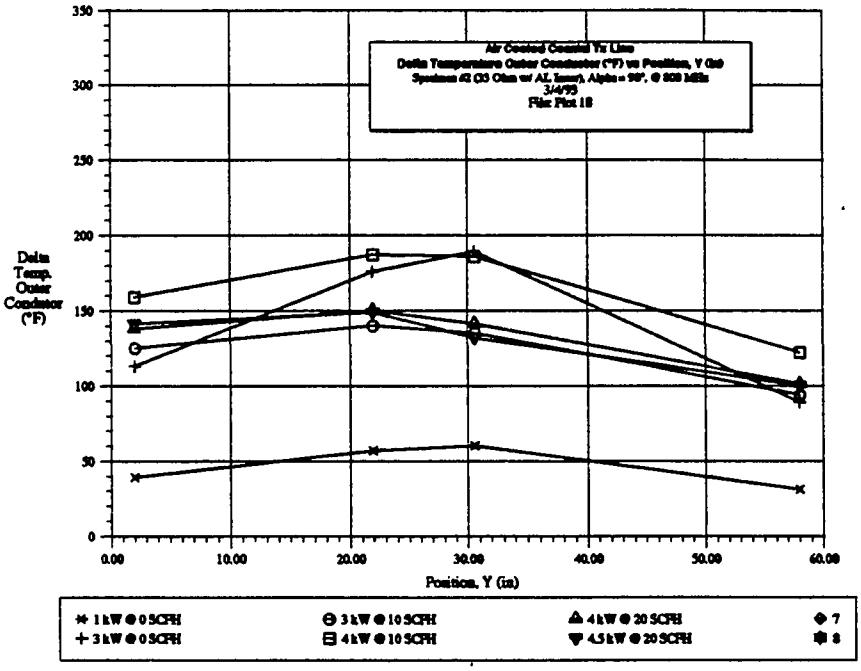
Air Cooled Coaxial Yz Line
3/4/95
Plot 18
Delta Temp. Outer Conductor (°F)
Position, Y (in)
1 kW @ 0 SCFH
3 kW @ 0 SCFH
3 kW @ 10 SCFH
4 kW @ 10 SCFH
4 kW @ 20 SCFH
4.5 kW @ 20 SCFH
7
8

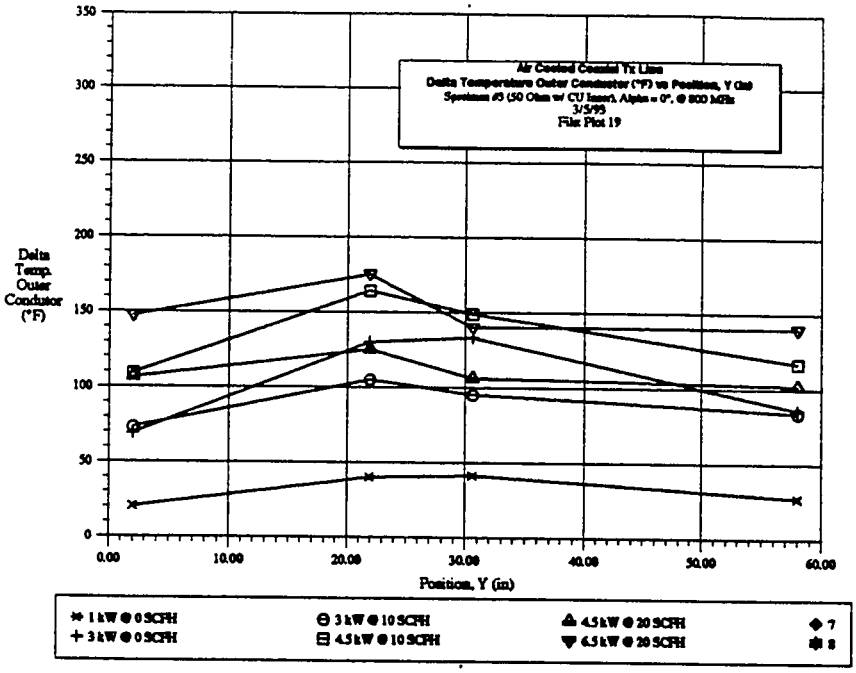
Air Cooled Coaxial Tx Line
3/5/95
Plot Plot 19
Delta Temp. Outer Conductor (°F)
Position, Y (in)
1 kW @ 0 SCFH
3 kW @ 0 SCFH
3 kW @ 10 SCFH
4.5 kW @ 10 SCFH
4.5 kW @ 20 SCFH
6.5 kW @ 20 SCFH
7
8

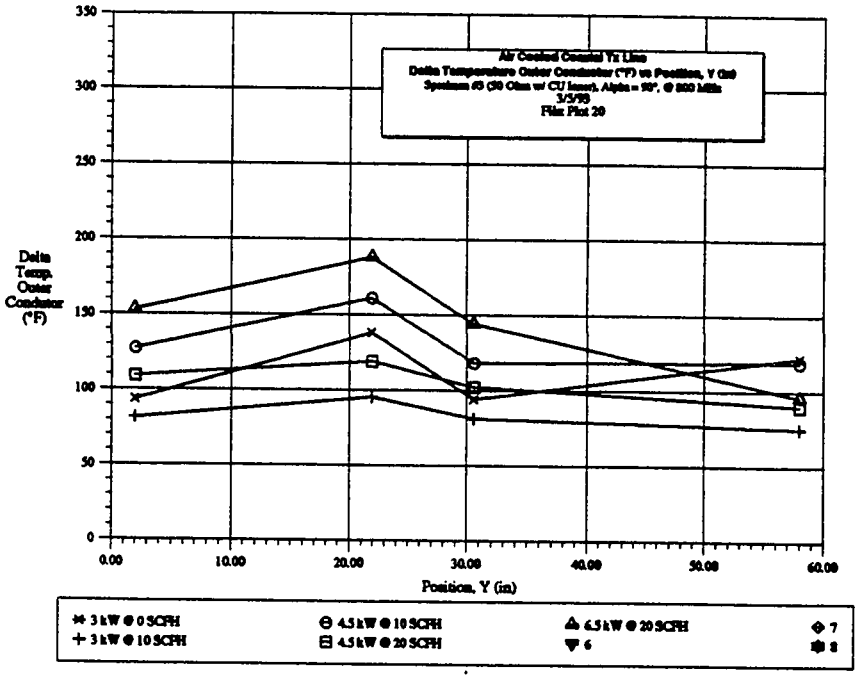
Air Cooled Coaxial Tx Line
3/5/95
Plot Plot 20
Delta Temp. Outer Conductor (°F)
Position, Y (in)
3 kW @ 0 SCFH
3 kW @ 10 SCFH
4.5 kW @ 10 SCFH
4.5 kW @ 20 SCFH
6.5 kW @ 20 SCFH
6
7
8

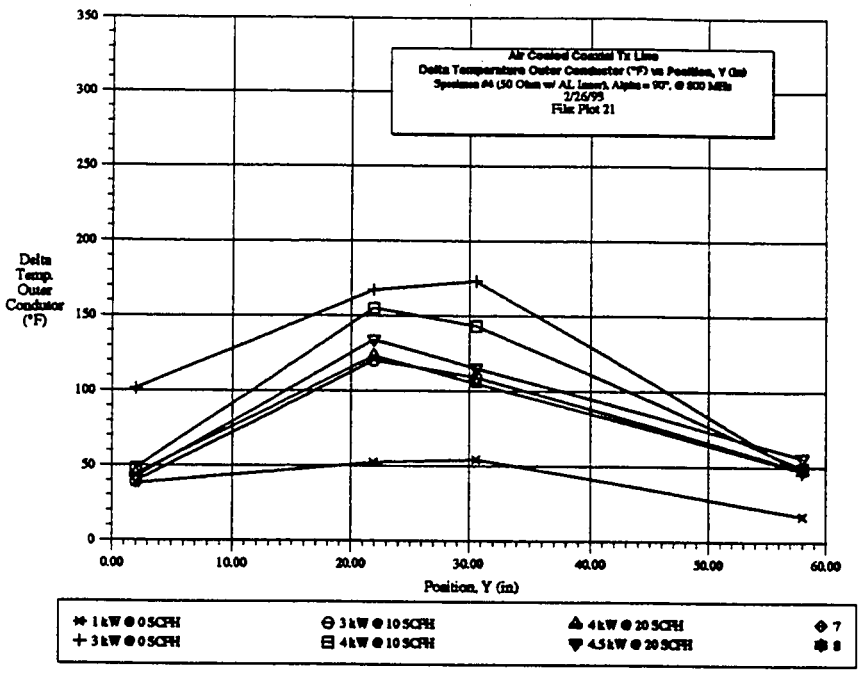
Air Cooled Coaxial Tx Line
Delta Temperature Outer Conductor (°F) vs Position, Y (in)
Specimen #4 (50 Ohm w/ AL Inner), Alpha = 90°, @ 800 MHz
2/26/95
File: Plot 21
Delta Temp. Outer Conductor (°F)
350
300
250
200
150
100
50
0
0.00
10.00
20.00
30.00
40.00
50.00
60.00
Position, Y (in)
1 kW @ 0 SCFH
3 kW @ 0 SCFH
3 kW @ 10 SCFH
4 kW @ 10 SCFH
4 kW @ 20 SCFH
4.5 kW @ 20 SCFH
7
8

APPENDIX F — FEA Model, COAX7

RANDTRON SYSTEMS S/N:400132 05/11/93
PAGE 1 RUN ID=BI94220 08:05:37

========== I M A G E S T H E R M A L ==========
= Copyright (c) 1989 Celestial Software Inc. =
==========

CHECK GEOMETRY Version 2.0 07/01/90

50 OHM X 60" TX LINE

MATERIAL PROPERTIES

Material No	Coefficients of Thermal Conductivity K1	K2	K3	Emittance
1	8.33300E+00	3.92200E-03	0.00000E+00	0.00000E+00
2	1.86160E+01	-1.57400E-03	0.00000E+00	0.00000E+00
3	1.10800E-03	1.55000E-06	0.00000E+00	0.00000E+00

NODE COORDINATES

Node	X-Coord.	Y-Coord.	Z-Coord.
1	0.00000E+00	0.00000E+00	0.00000E+00
2	9.40000E-02	0.00000E+00	0.00000E+00
3	2.15000E-01	0.00000E+00	0.00000E+00
4	2.50000E-01	0.00000E+00	0.00000E+00
5	0.00000E+00	3.00000E+00	0.00000E+00
6	9.40000E-02	3.00000E+00	0.00000E+00
7	2.15000E-01	3.00000E+00	0.00000E+00
8	2.50000E-01	3.00000E+00	0.00000E+00
9	0.00000E+00	6.00000E+00	0.00000E+00
10	9.40000E-02	6.00000E+00	0.00000E+00
11	2.15000E-01	6.00000E+00	0.00000E+00
12	2.50000E-01	6.00000E+00	0.00000E+00
13	0.00000E+00	9.00000E+00	0.00000E+00
14	9.40000E-02	9.00000E+00	0.00000E+00
15	2.15000E-01	9.00000E+00	0.00000E+00
16	2.50000E-01	9.00000E+00	0.00000E+00
17	0.00000E+00	1.20000E+01	0.00000E+00
18	9.40000E-02	1.20000E+01	0.00000E+00
19	2.15000E-01	1.20000E+01	0.00000E+00
20	2.50000E-01	1.20000E+01	0.00000E+00
21	0.00000E+00	1.50000E+01	0.00000E+00
22	9.40000E-02	1.50000E+01	0.00000E+00
23	2.15000E-01	1.50000E+01	0.00000E+00
24	2.50000E-01	1.50000E+01	0.00000E+00
25	0.00000E+00	1.80000E+01	0.00000E+00
26	9.40000E-02	1.80000E+01	0.00000E+00
27	2.15000E-01	1.80000E+01	0.00000E+00
28	2.50000E-01	1.80000E+01	0.00000E+00

========== I M A G E S T H E R M A L ==========
= Copyright (c) 1989 Celestial Software Inc. =
==========

CHECK GEOMETRY Version 2.0 07/01/90

50 OHM X 60" TX LINE

Node	X-Coord.	Y-Coord.	Z-Coord.
29	0.00000E+00	2.10000E+01	0.00000E+00
30	9.40000E-02	2.10000E+01	0.00000E+00
31	2.15000E-01	2.10000E+01	0.00000E+00
32	2.50000E-01	2.10000E+01	0.00000E+00
33	0.00000E+00	2.40000E+01	0.00000E+00
34	9.40000E-02	2.40000E+01	0.00000E+00
35	2.15000E-01	2.40000E+01	0.00000E+00
36	2.50000E-01	2.40000E+01	0.00000E+00
37	0.00000E+00	2.70000E+01	0.00000E+00
38	9.40000E-02	2.70000E+01	0.00000E+00
39	2.15000E-01	2.70000E+01	0.00000E+00
40	2.50000E-01	2.70000E+01	0.00000E+00
41	0.00000E+00	3.00000E+01	0.00000E+00
42	9.40000E-02	3.00000E+01	0.00000E+00
43	2.15000E-01	3.00000E+01	0.00000E+00
44	2.50000E-01	3.00000E+01	0.00000E+00
45	0.00000E+00	3.30000E+01	0.00000E+00
46	9.40000E-02	3.30000E+01	0.00000E+00
47	2.15000E-01	3.30000E+01	0.00000E+00
48	2.50000E-01	3.30000E+01	0.00000E+00
49	0.00000E+00	3.60000E+01	0.00000E+00
50	9.40000E-02	3.60000E+01	0.00000E+00
51	2.15000E-01	3.60000E+01	0.00000E+00
52	2.50000E-01	3.60000E+01	0.00000E+00
53	0.00000E+00	3.90000E+01	0.00000E+00
54	9.40000E-02	3.90000E+01	0.00000E+00
55	2.15000E-01	3.90000E+01	0.00000E+00
56	2.50000E-01	3.90000E+01	0.00000E+00
57	0.00000E+00	4.20000E+01	0.00000E+00
58	9.40000E-02	4.20000E+01	0.00000E+00
59	2.15000E-01	4.20000E+01	0.00000E+00
60	2.50000E-01	4.20000E+01	0.00000E+00
61	0.00000E+00	4.50000E+01	0.00000E+00
62	9.40000E-02	4.50000E+01	0.00000E+00
63	2.15000E-01	4.50000E+01	0.00000E+00
64	2.50000E-01	4.50000E+01	0.00000E+00
65	0.00000E+00	4.80000E+01	0.00000E+00
66	9.40000E-02	4.80000E+01	0.00000E+00
67	2.15000E-01	4.80000E+01	0.00000E+00
68	2.50000E-01	4.80000E+01	0.00000E+00
69	0.00000E+00	5.10000E+01	0.00000E+00
70	9.40000E-02	5.10000E+01	0.00000E+00

========== I M A G E S T H E R M A L ==========
= Copyright (c) 1989 Celestial Software Inc. =
==========

CHECK GEOMETRY Version 2.0 07/01/90

50 OHM X 60" TX LINE

Node	X-Coord.	Y-Coord.	Z-Coord.
71	2.15000E-01	5.10000E+01	0.00000E+00
72	2.50000E-01	5.10000E+01	0.00000E+00
73	0.00000E+00	5.40000E+01	0.00000E+00
74	9.40000E-02	5.40000E+01	0.00000E+00
75	2.15000E-01	5.40000E+01	0.00000E+00
76	2.50000E-01	5.40000E+01	0.00000E+00
77	0.00000E+00	5.70000E+01	0.00000E+00
78	9.40000E-02	5.70000E+01	0.00000E+00
79	2.15000E-01	5.70000E+01	0.00000E+00
80	2.50000E-01	5.70000E+01	0.00000E+00
81	0.00000E+00	6.00000E+01	0.00000E+00
82	9.40000E-02	6.00000E+01	0.00000E+00
83	2.15000E-01	6.00000E+01	0.00000E+00
84	2.50000E-01	6.00000E+01	0.00000E+00

AXI-SOLID ELEMENT CONNECTIVITY

Axi-Solid No.	NODES I	J	K	L	Mat No.	Volume per rad.
1	3	4	8	7	1	2.441E-02
2	7	8	12	11	1	2.441E-02
3	11	12	16	15	1	2.441E-02
4	15	16	20	19	1	2.441E-02
5	19	20	24	23	1	2.441E-02
6	23	24	28	27	1	2.441E-02
7	27	28	32	31	1	2.441E-02
8	31	32	36	35	1	2.441E-02
9	35	36	40	39	1	2.441E-02
10	39	40	44	43	1	2.441E-02
11	43	44	48	47	1	2.441E-02
12	47	48	52	51	1	2.441E-02
13	51	52	56	55	1	2.441E-02
14	55	56	60	59	1	2.441E-02
15	59	60	64	63	1	2.441E-02
16	63	64	68	67	1	2.441E-02
17	67	68	72	71	1	2.441E-02
18	71	72	76	75	1	2.441E-02
19	75	76	80	79	1	2.441E-02
20	79	80	84	83	1	2.441E-02

========== I M A G E S T H E R M A L ==========
= Copyright (c) 1989 Celestial Software Inc. =
==========

CHECK GEOMETRY Version 2.0 07/01/90

50 OHM X 60" TX LINE

Axi-Solid No.	NODES I	J	K	L	Mat No.	Volume per rad.
21	2	3	7	6	3	5.608E-02
22	6	7	11	10	3	5.608E-02
23	10	11	15	14	3	5.608E-02
24	14	15	19	18	3	5.608E-02
25	18	19	23	22	3	5.608E-02
26	22	23	27	26	3	5.608E-02
27	26	27	31	30	3	5.608E-02
28	30	31	35	34	3	5.608E-02
29	34	35	39	38	3	5.608E-02
30	38	39	43	42	3	5.608E-02
31	42	43	47	46	3	5.608E-02
32	46	47	51	50	3	5.608E-02
33	50	51	55	54	3	5.608E-02
34	54	55	59	58	3	5.608E-02
35	58	59	63	62	3	5.608E-02
36	62	63	67	66	3	5.608E-02
37	66	67	71	70	3	5.608E-02
38	70	71	75	74	3	5.608E-02
39	74	75	79	78	3	5.608E-02
40	78	79	83	82	3	5.608E-02
41	1	2	6	5	2	1.325E-02
42	5	6	10	9	2	1.325E-02
43	9	10	14	13	2	1.325E-02
44	13	14	18	17	2	1.325E-02
45	17	18	22	21	2	1.325E-02
46	21	22	26	25	2	1.325E-02
47	25	26	30	29	2	1.325E-02
48	29	30	34	33	2	1.325E-02
49	33	34	38	37	2	1.325E-02
50	37	38	42	41	2	1.325E-02
51	41	42	46	45	2	1.325E-02
52	45	46	50	49	2	1.325E-02
53	49	50	54	53	2	1.325E-02
54	53	54	58	57	2	1.325E-02
55	57	58	62	61	2	1.325E-02
56	61	62	66	65	2	1.325E-02
57	65	66	70	69	2	1.325E-02
58	69	70	74	73	2	1.325E-02
59	73	74	78	77	2	1.325E-02
60	77	78	82	81	2	1.325E-02

APPENDIX G — FEA Model, COAX8

RANDTRON SYSTEMS S/N:400132
PAGE 1 RUN ID=XX74065 05/12/93 07:52:10

========== I M A G E S T H E R M A L ==========
= Copyright (c) 1989 Celestial Software Inc. =
==========

CHECK GEOMETRY Version 2.0 07/01/90

33 OHM TX LINE

MATERIAL PROPERTIES

Material No	Coefficients of Thermal Conductivity K1	K2	K3	Emittance
1	8.33300E+00	3.92200E-03	0.00000E+00	0.00000E+00
2	1.86160E+01	-1.57400E-03	0.00000E+00	0.00000E+00
3	1.10800E-03	1.55000E-06	0.00000E+00	0.00000E+00

NODE COORDINATES

Node	X-Coord.	Y-Coord.	Z-Coord.
1	0.00000E+00	0.00000E+00	0.00000E+00
2	0.00000E+00	3.00000E+00	0.00000E+00
3	0.00000E+00	6.00000E+00	0.00000E+00
4	0.00000E+00	8.00000E+00	0.00000E+00
5	0.00000E+00	8.00100E+00	0.00000E+00
6	0.00000E+00	9.00000E+00	0.00000E+00
7	0.00000E+00	1.20000E+01	0.00000E+00
8	0.00000E+00	1.25440E+01	0.00000E+00
9	0.00000E+00	1.25450E+01	0.00000E+00
10	0.00000E+00	1.50000E+01	0.00000E+00
11	0.00000E+00	1.70880E+01	0.00000E+00
12	0.00000E+00	1.70890E+01	0.00000E+00
13	0.00000E+00	1.80000E+01	0.00000E+00
14	0.00000E+00	2.10000E+01	0.00000E+00
15	0.00000E+00	2.40000E+01	0.00000E+00
16	0.00000E+00	2.70000E+01	0.00000E+00
17	0.00000E+00	3.00000E+01	0.00000E+00
18	0.00000E+00	3.30000E+01	0.00000E+00
19	0.00000E+00	3.60000E+01	0.00000E+00
20	0.00000E+00	3.90000E+01	0.00000E+00
21	0.00000E+00	4.20000E+01	0.00000E+00
22	0.00000E+00	4.29110E+01	0.00000E+00
23	0.00000E+00	4.29120E+01	0.00000E+00
24	0.00000E+00	4.50000E+01	0.00000E+00
25	0.00000E+00	4.74550E+01	0.00000E+00
26	0.00000E+00	4.74560E+01	0.00000E+00
27	0.00000E+00	4.80000E+01	0.00000E+00
28	0.00000E+00	5.10000E+01	0.00000E+00

========== I M A G E S T H E R M A L ==========
= Copyright (c) 1989 Celestial Software Inc. =
==========

CHECK GEOMETRY Version 2.0 07/01/90

33 OHM TX LINE

Node	X-Coord.	Y-Coord.	Z-Coord.
29	0.00000E+00	5.19990E+01	0.00000E+00
30	0.00000E+00	5.20000E+01	0.00000E+00
31	0.00000E+00	5.40000E+01	0.00000E+00
32	0.00000E+00	5.70000E+01	0.00000E+00
33	0.00000E+00	6.00000E+01	0.00000E+00
34	9.40000E-02	0.00000E+00	0.00000E+00
35	9.40000E-02	3.00000E+00	0.00000E+00
36	9.40000E-02	6.00000E+00	0.00000E+00
37	9.40000E-02	8.00000E+00	0.00000E+00
38	1.05000E-01	8.00100E+00	0.00000E+00
39	1.05000E-01	9.00000E+00	0.00000E+00
40	1.05000E-01	1.20000E+01	0.00000E+00
41	1.05000E-01	1.25440E+01	0.00000E+00
42	1.14500E-01	1.25450E+01	0.00000E+00
43	1.14500E-01	1.50000E+01	0.00000E+00
44	1.14500E-01	1.70880E+01	0.00000E+00
45	1.24000E-01	1.70890E+01	0.00000E+00
46	1.24000E-01	1.80000E+01	0.00000E+00
47	1.24000E-01	2.10000E+01	0.00000E+00
48	1.24000E-01	2.40000E+01	0.00000E+00
49	1.24000E-01	2.70000E+01	0.00000E+00
50	1.24000E-01	3.00000E+01	0.00000E+00
51	1.24000E-01	3.30000E+01	0.00000E+00
52	1.24000E-01	3.60000E+01	0.00000E+00
53	1.24000E-01	3.90000E+01	0.00000E+00
54	1.24000E-01	4.20000E+01	0.00000E+00
55	1.24000E-01	4.29110E+01	0.00000E+00
56	1.14500E-01	4.29120E+01	0.00000E+00
57	1.14500E-01	4.50000E+01	0.00000E+00
58	1.14500E-01	4.74550E+01	0.00000E+00
59	1.05000E-01	4.74560E+01	0.00000E+00
60	1.05000E-01	4.80000E+01	0.00000E+00
61	1.05000E-01	5.10000E+01	0.00000E+00
62	1.05000E-01	5.19990E+01	0.00000E+00
63	9.40000E-02	5.20000E+01	0.00000E+00
64	9.40000E-02	5.40000E+01	0.00000E+00
65	9.40000E-02	5.70000E+01	0.00000E+00
66	9.40000E-02	6.00000E+01	0.00000E+00
67	2.15000E-01	0.00000E+00	0.00000E+00
68	2.15000E-01	3.00000E+00	0.00000E+00
69	2.15000E-01	6.00000E+00	0.00000E+00
70	2.15000E-01	8.00000E+00	0.00000E+00

========== I M A G E S T H E R M A L ==========
= Copyright (c) 1989 Celestial Software Inc. =
==========

CHECK GEOMETRY Version 2.0 07/01/90

33 OHM TX LINE

Node	X-Coord.	Y-Coord.	Z-Coord.
71	2.15000E-01	8.00100E+00	0.00000E+00
72	2.15000E-01	9.00000E+00	0.00000E+00
73	2.15000E-01	1.20000E+01	0.00000E+00
74	2.15000E-01	1.25440E+01	0.00000E+00
75	2.15000E-01	1.25450E+01	0.00000E+00
76	2.15000E-01	1.50000E+01	0.00000E+00
77	2.15000E-01	1.70880E+01	0.00000E+00
78	2.15000E-01	1.70890E+01	0.00000E+00
79	2.15000E-01	1.80000E+01	0.00000E+00
80	2.15000E-01	2.10000E+01	0.00000E+00
81	2.15000E-01	2.40000E+01	0.00000E+00
82	2.15000E-01	2.70000E+01	0.00000E+00
83	2.15000E-01	3.00000E+01	0.00000E+00
84	2.15000E-01	3.30000E+01	0.00000E+00
85	2.15000E-01	3.60000E+01	0.00000E+00
86	2.15000E-01	3.90000E+01	0.00000E+00
87	2.15000E-01	4.20000E+01	0.00000E+00
88	2.15000E-01	4.29110E+01	0.00000E+00
89	2.15000E-01	4.29120E+01	0.00000E+00
90	2.15000E-01	4.50000E+01	0.00000E+00
91	2.15000E-01	4.74550E+01	0.00000E+00
92	2.15000E-01	4.74560E+01	0.00000E+00
93	2.15000E-01	4.80000E+01	0.00000E+00
94	2.15000E-01	5.10000E+01	0.00000E+00
95	2.15000E-01	5.19990E+01	0.00000E+00
96	2.15000E-01	5.20000E+01	0.00000E+00
97	2.15000E-01	5.40000E+01	0.00000E+00
98	2.15000E-01	5.70000E+01	0.00000E+00
99	2.15000E-01	6.00000E+01	0.00000E+00
100	2.50000E-01	0.00000E+00	0.00000E+00
101	2.50000E-01	3.00000E+00	0.00000E+00
102	2.50000E-01	6.00000E+00	0.00000E+00
103	2.50000E-01	8.00000E+00	0.00000E+00
104	2.50000E-01	8.00100E+00	0.00000E+00
105	2.50000E-01	9.00000E+00	0.00000E+00
106	2.50000E-01	1.20000E+01	0.00000E+00
107	2.50000E-01	1.25440E+01	0.00000E+00
108	2.50000E-01	1.25450E+01	0.00000E+00
109	2.50000E-01	1.50000E+01	0.00000E+00
110	2.50000E-01	1.70880E+01	0.00000E+00
111	2.50000E-01	1.70890E+01	0.00000E+00
112	2.50000E-01	1.80000E+01	0.00000E+00

========== I M A G E S T H E R M A L ==========
= Copyright (c) 1989 Celestial Software Inc. =
==========

CHECK GEOMETRY Version 2.0 07/01/90

33 OHM TX LINE

Node	X-Coord.	Y-Coord.	Z-Coord.
113	2.50000E-01	2.10000E+01	0.00000E+00
114	2.50000E-01	2.40000E+01	0.00000E+00
115	2.50000E-01	2.70000E+01	0.00000E+00
116	2.50000E-01	3.00000E+01	0.00000E+00
117	2.50000E-01	3.30000E+01	0.00000E+00
118	2.50000E-01	3.60000E+01	0.00000E+00
119	2.50000E-01	3.90000E+01	0.00000E+00
120	2.50000E-01	4.20000E+01	0.00000E+00
121	2.50000E-01	4.29110E+01	0.00000E+00
122	2.50000E-01	4.29120E+01	0.00000E+00
123	2.50000E-01	4.50000E+01	0.00000E+00
124	2.50000E-01	4.74550E+01	0.00000E+00
125	2.50000E-01	4.74560E+01	0.00000E+00
126	2.50000E-01	4.80000E+01	0.00000E+00
127	2.50000E-01	5.10000E+01	0.00000E+00
128	2.50000E-01	5.19990E+01	0.00000E+00
129	2.50000E-01	5.20000E+01	0.00000E+00
130	2.50000E-01	5.40000E+01	0.00000E+00
131	2.50000E-01	5.70000E+01	0.00000E+00
132	2.50000E-01	6.00000E+01	0.00000E+00

AXI-SOLID ELEMENT CONNECTIVITY

Axi-Solid No.	NODES I	J	K	L	Mat No.	Volume per rad.
1	1	34	35	2	1	1.325E-02
2	2	35	36	3	1	1.325E-02
3	3	36	37	4	1	8.836E-03
4	4	37	38	5	1	4.952E-06
5	5	38	39	6	1	5.507E-03
6	6	39	40	7	1	1.654E-02
7	7	40	41	8	1	2.999E-03
8	8	41	42	9	1	6.025E-06
9	9	42	43	10	1	1.609E-02
10	10	43	44	11	1	1.369E-02
11	11	44	45	12	1	7.120E-06
12	12	45	46	13	1	7.004E-03
13	13	46	47	14	1	2.306E-02
14	14	47	48	15	1	2.306E-02

========== I M A G E S T H E R M A L ==========
= Copyright (c) 1989 Celestial Software Inc. =
==========

CHECK GEOMETRY Version 2.0 07/01/90

33 OHM TX LINE

Axi-Solid No.	N O D E S I	J	K	L	Mat No.	Volume per rad.
15	15	48	49	16	1	2.306E-02
16	16	49	50	17	1	2.306E-02
17	17	50	51	18	1	2.306E-02
18	18	51	52	19	1	2.306E-02
19	19	52	53	20	1	2.306E-02
20	20	53	54	21	1	2.306E-02
21	21	54	55	22	1	7.004E-03
22	22	55	56	23	1	7.106E-06
23	23	56	57	24	1	1.369E-02
24	24	57	58	25	1	1.609E-02
25	25	58	59	26	1	6.019E-06
26	26	59	60	27	1	2.999E-03
27	27	60	61	28	1	1.654E-02
28	28	61	62	29	1	5.507E-03
29	29	62	63	30	1	4.947E-06
30	30	63	64	31	1	8.836E-03
31	31	64	65	32	1	1.325E-02
32	32	65	66	33	1	1.325E-02
33	34	67	68	35	3	5.608E-02
34	35	68	69	36	3	5.608E-02
35	36	69	70	37	3	3.739E-02
36	37	70	71	38	3	1.817E-05
37	38	71	72	39	3	1.758E-02
38	39	72	73	40	3	5.280E-02
39	40	73	74	41	3	9.574E-03
40	41	74	75	42	3	1.710E-05
41	42	75	76	43	3	4.065E-02
42	43	76	77	44	3	3.457E-02
43	44	77	78	45	3	1.602E-05
44	45	78	79	46	3	1.405E-02
45	46	79	80	47	3	4.627E-02
46	47	80	81	48	3	4.627E-02
47	48	81	82	49	3	4.627E-02
48	49	82	83	50	3	4.627E-02
49	50	83	84	51	3	4.627E-02
50	51	84	85	52	3	4.627E-02
51	52	85	86	53	3	4.627E-02
52	53	86	87	54	3	4.627E-02
53	54	87	88	55	3	1.405E-02
54	55	88	89	56	3	1.599E-05
55	56	89	90	57	3	3.457E-02

========== I M A G E S T H E R M A L ==========
= Copyright (c) 1989 Celestial Software Inc. =
==========

CHECK GEOMETRY Version 2.0 07/01/90

33 OHM TX LINE

Axi-Solid No.	NODES I	J	K	L	Mat No.	Volume per rad.
56	57	90	91	58	3	4.065E-02
57	58	91	92	59	3	1.708E-05
58	59	92	93	60	3	9.574E-03
59	60	93	94	61	3	5.280E-02
60	61	94	95	62	3	1.758E-02
61	62	95	96	63	3	1.815E-05
62	63	96	97	64	3	3.739E-02
63	64	97	98	65	3	5.608E-02
64	65	98	99	66	3	5.608E-02
65	67	100	101	68	1	2.441E-02
66	68	101	102	69	1	2.441E-02
67	69	102	103	70	1	1.627E-02
68	70	103	104	71	1	8.141E-06
69	71	104	105	72	1	8.129E-03
70	72	105	106	73	1	2.441E-02
71	73	106	107	74	1	4.427E-03
72	74	107	108	75	1	8.141E-06
73	75	108	109	76	1	1.998E-02
74	76	109	110	77	1	1.699E-02
75	77	110	111	78	1	8.149E-06
76	78	111	112	79	1	7.413E-03
77	79	112	113	80	1	2.441E-02
78	80	113	114	81	1	2.441E-02
79	81	114	115	82	1	2.441E-02
80	82	115	116	83	1	2.441E-02
81	83	116	117	84	1	2.441E-02
82	84	117	118	85	1	2.441E-02
83	85	118	119	86	1	2.441E-02
84	86	119	120	87	1	2.441E-02
85	87	120	121	88	1	7.413E-03
86	88	121	122	89	1	8.133E-06
87	89	122	123	90	1	1.699E-02
88	90	123	124	91	1	1.998E-02
89	91	124	125	92	1	8.133E-06
90	92	125	126	93	1	4.427E-03
91	93	126	127	94	1	2.441E-02
92	94	127	128	95	1	8.129E-03
93	95	128	129	96	1	8.133E-06
94	96	129	130	97	1	1.627E-02
95	97	130	131	98	1	2.441E-02
96	98	131	132	99	1	2.441E-02

IMAGES-THERMAL

RENUMBER NODES Version 2.0 07/01/90

33 OHM TX LINE

Node Renumbering Cross Reference List

Was	Is	Was	Is	Was	Is	Was	Is	Was	Is
1	1	2	5	3	9	4	13	5	17
6	21	7	25	8	29	9	33	10	37
11	41	12	45	13	49	14	53	15	57
16	61	17	65	18	69	19	73	20	77
21	81	22	85	23	89	24	93	25	97
26	101	27	105	28	109	29	113	30	117
31	121	32	125	33	129	34	2	35	6
36	10	37	14	38	18	39	22	40	26
41	30	42	34	43	38	44	42	45	46
46	50	47	54	48	58	49	62	50	66
51	70	52	74	53	78	54	82	55	86
56	90	57	94	58	98	59	102	60	106
61	110	62	114	63	118	64	122	65	126
66	130	67	3	68	7	69	11	70	15
71	19	72	23	73	27	74	31	75	35
76	39	77	43	78	47	79	51	80	55
81	59	82	63	83	67	84	71	85	75
86	79	87	83	88	87	89	91	90	95
91	99	92	103	93	107	94	111	95	115
96	119	97	123	98	127	99	131	100	4
101	8	102	12	103	16	104	20	105	24
106	28	107	32	108	36	109	40	110	44
111	48	112	52	113	56	114	60	115	64
116	68	117	72	118	76	119	80	120	84
121	88	122	92	123	96	124	100	125	104
126	108	127	112	128	116	129	120	130	124
131	128	132	132						

APPENDIX H — 3/8"- 50 Ohm Coax, Design Curves

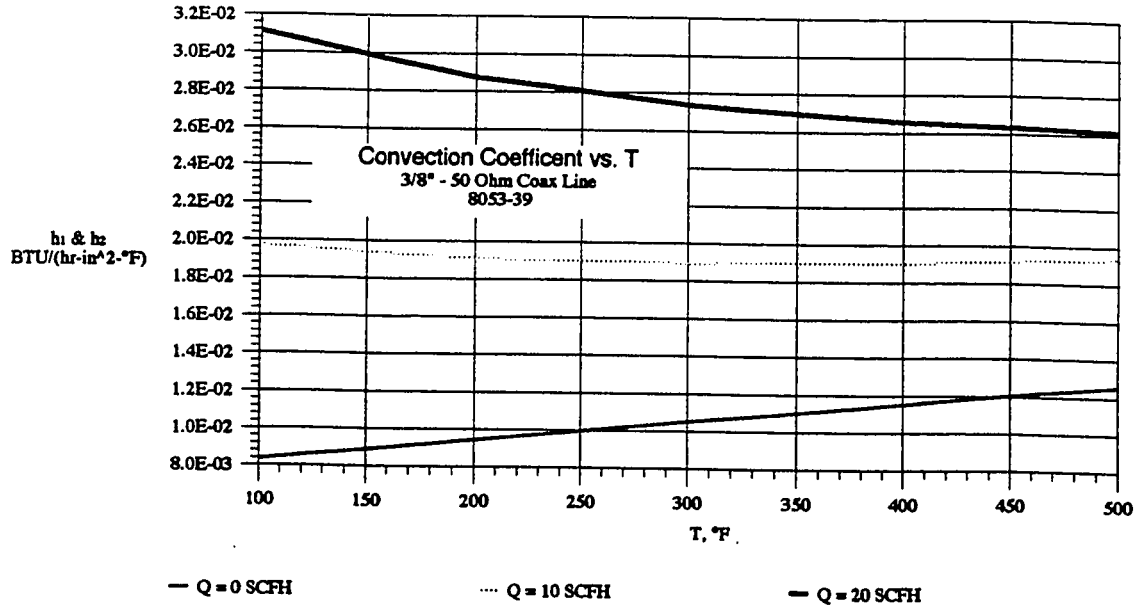

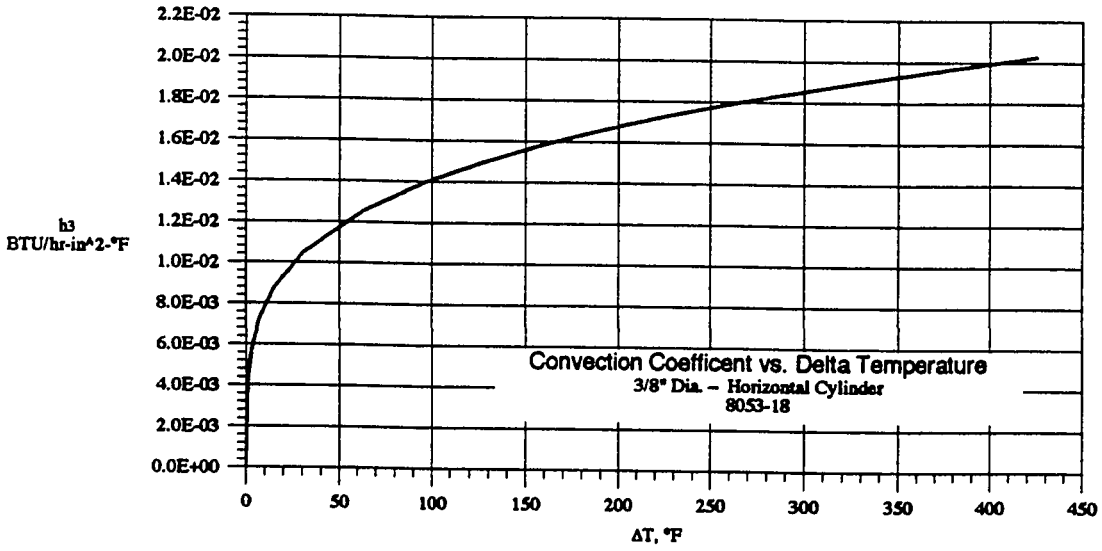

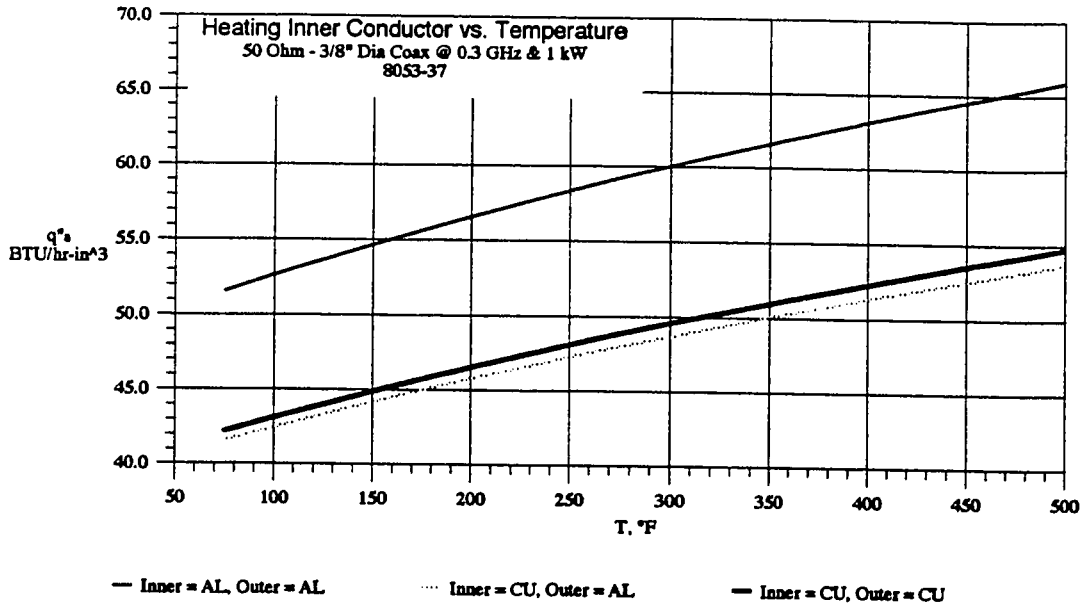
Heating Inner Conductor vs. Temperature
50 Ohm - 3/8" Dia Coax @ 0.3 GHz & 1 kW
8053-37
q'a
BTU/hr-in^3
70.0
65.0
60.0
55.0
50.0
45.0
40.0
50
100
150
200
250
300
350
400
450
500
T, °F
Inner = AL, Outer = AL
Inner = CU, Outer = AL
Inner = CU, Outer = CU

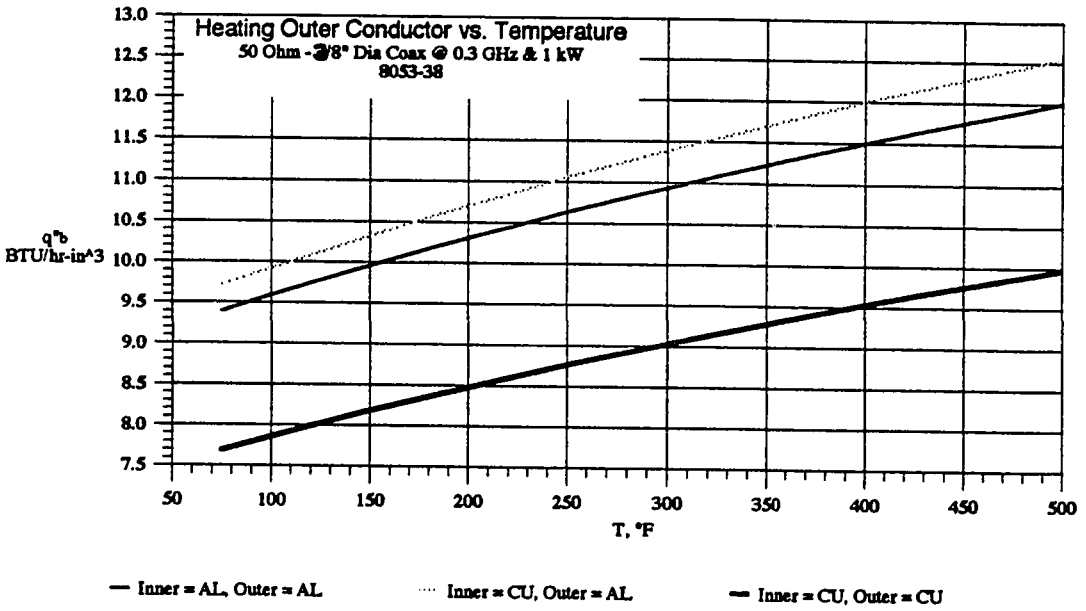
Heating Outer Conductor vs. Temperature
50 Ohm - 3/8" Dia Coax @ 0.3 GHz & 1 kW
8053-38
q'b
BTU/hr-in^3
13.0
12.5
12.0
11.5
11.0
10.5
10.0
9.5
9.0
8.5
8.0
7.5
50
100
150
200
250
300
350
400
450
500
T, °F
Inner = AL, Outer = AL
Inner = CU, Outer = AL
Inner = CU, Outer = CU

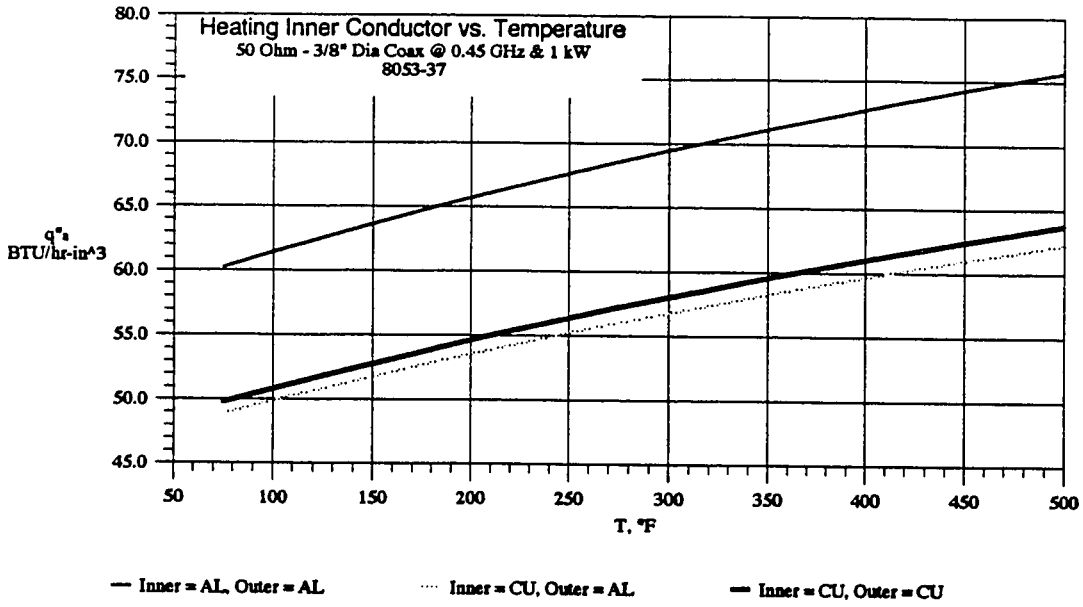
Heating Inner Conductor vs. Temperature
50 Ohm - 3/8" Dia Coax @ 0.45 GHz & 1 kW
8053-37
q"a
BTU/hr-in^3
80.0
75.0
70.0
65.0
60.0
55.0
50.0
45.0
50
100
150
200
250
300
350
400
450
500
T, °F
Inner = AL, Outer = AL
Inner = CU, Outer = AL
Inner = CU, Outer = CU

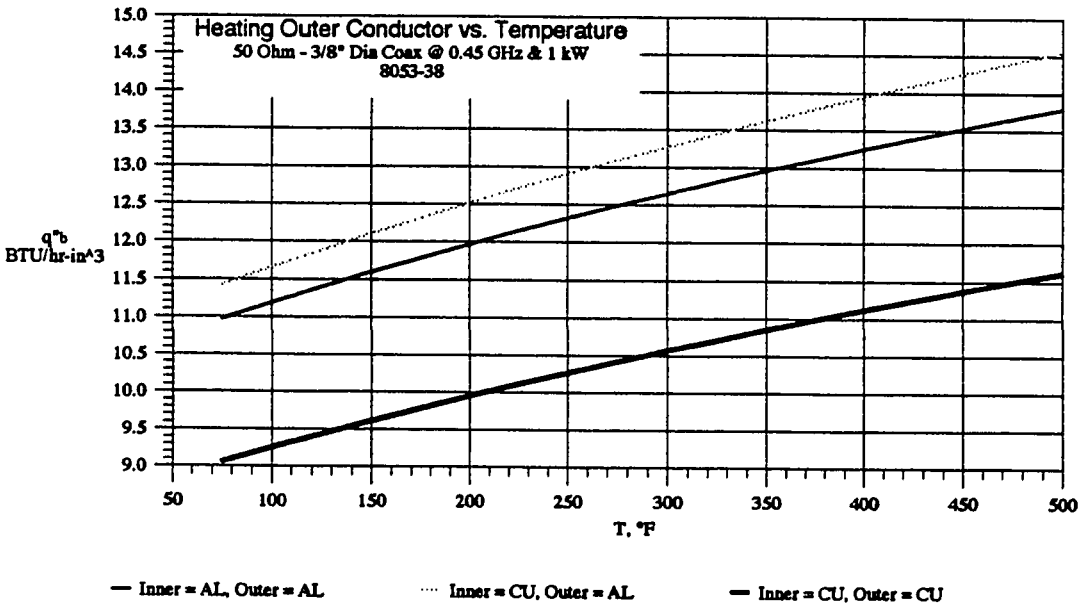
Heating Outer Conductor vs. Temperature
50 Ohm - 3/8" Dia Coax @ 0.45 GHz & 1 kW
8053-38
q"b
BTU/hr-in^3
15.0
14.5
14.0
13.5
13.0
12.5
12.0
11.5
11.0
10.5
10.0
9.5
9.0
50
100
150
200
250
300
350
400
450
500
T, °F
Inner = AL, Outer = AL
Inner = CU, Outer = AL
Inner = CU, Outer = CU

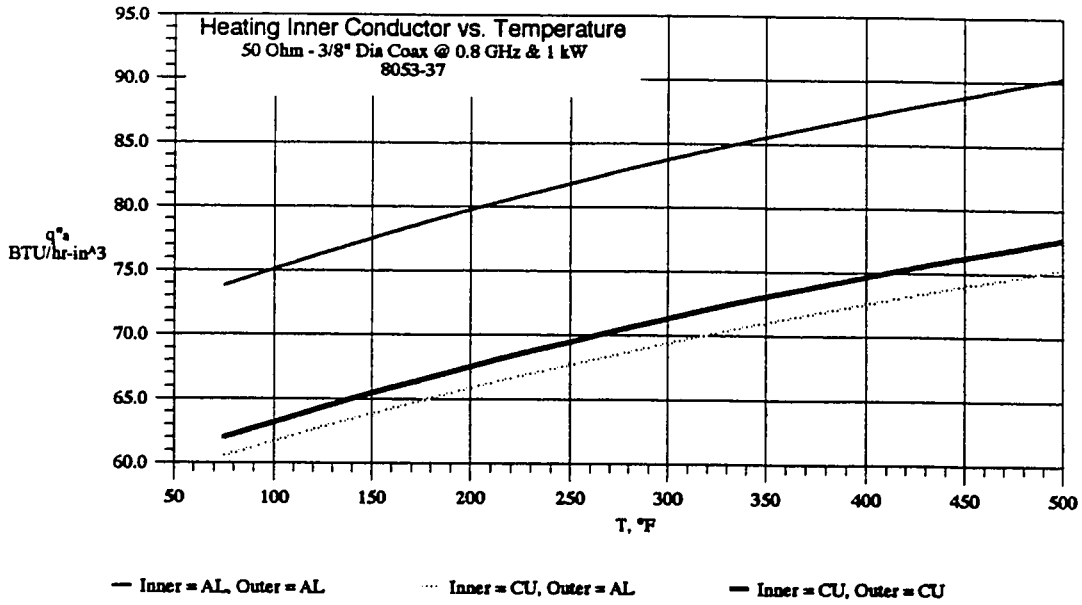
Heating Inner Conductor vs. Temperature
50 Ohm - 3/8" Dia Coax @ 0.8 GHz & 1 kW
8053-37
q"a
BTU/hr-in^3
95.0
90.0
85.0
80.0
75.0
70.0
65.0
60.0
50
100
150
200
250
300
350
400
450
500
T, °F
Inner = AL, Outer = AL
Inner = CU, Outer = AL
Inner = CU, Outer = CU

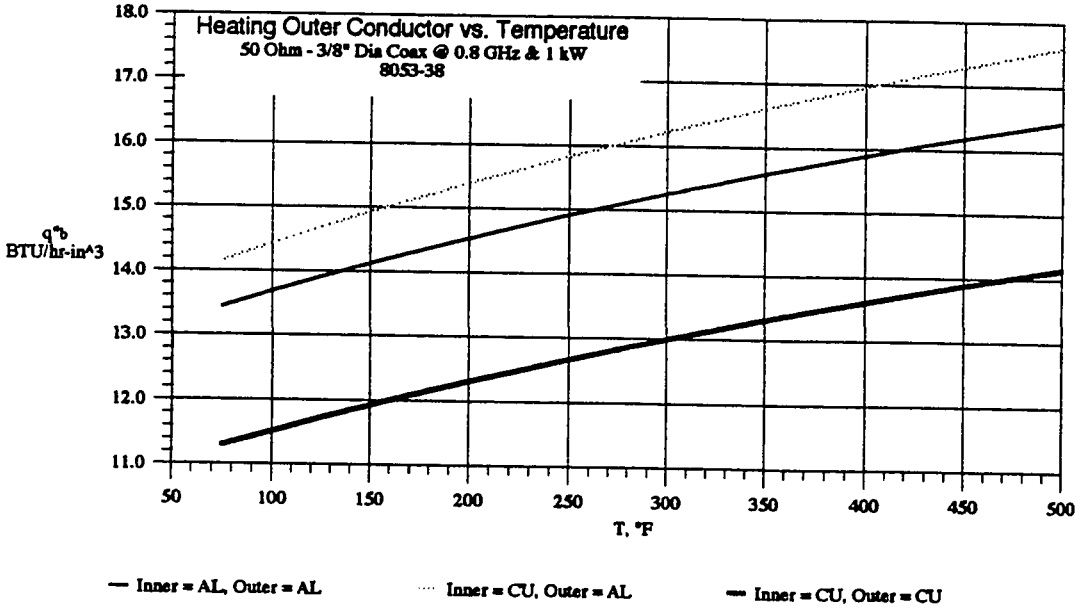
Heating Outer Conductor vs. Temperature
50 Ohm - 3/8" Dia Coax @ 0.8 GHz & 1 kW
8053-38
q"b
BTU/hr-in^3
18.0
17.0
16.0
15.0
14.0
13.0
12.0
11.0
50
100
150
200
250
300
350
400
450
500
T, °F
Inner = AL, Outer = AL
Inner = CU, Outer = AL
Inner = CU, Outer = CU

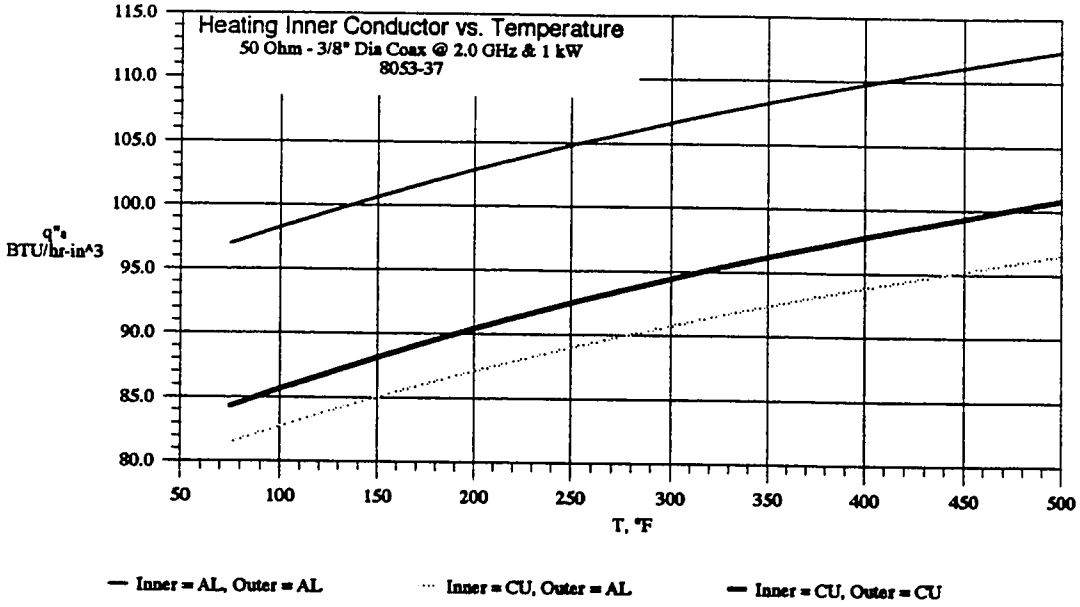
Heating Inner Conductor vs. Temperature
50 Ohm - 3/8" Dia Coax @ 2.0 GHz & 1 kW
8053-37
q"a
BTU/hr-in^3
115.0
110.0
105.0
100.0
95.0
90.0
85.0
80.0
50
100
150
200
250
300
350
400
450
500
T, °F
Inner = AL, Outer = AL
Inner = CU, Outer = AL
Inner = CU, Outer = CU

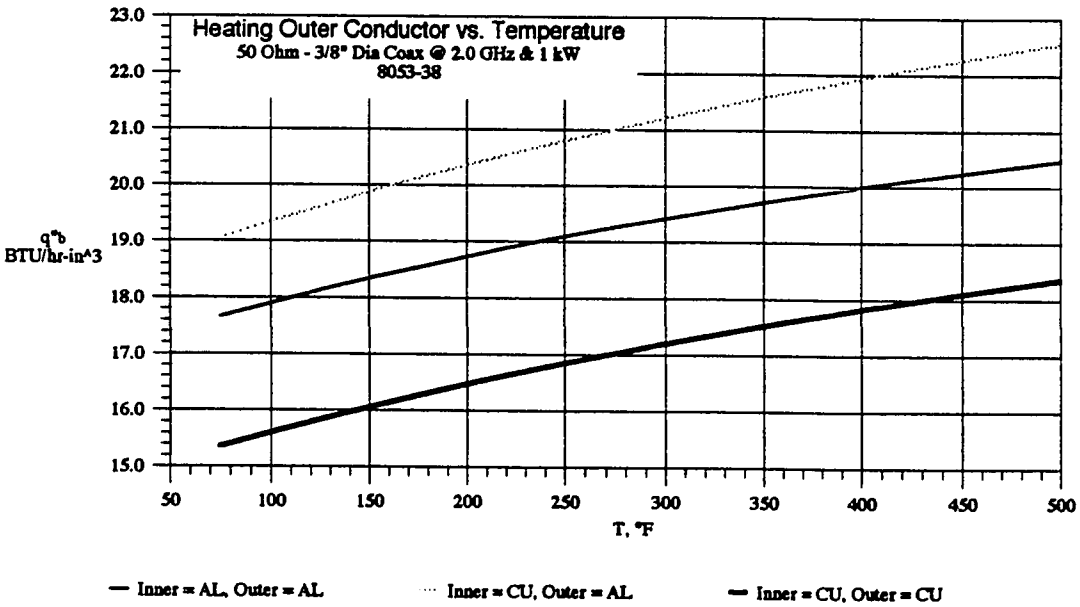
Heating Outer Conductor vs. Temperature
50 Ohm - 3/8" Dia Coax @ 2.0 GHz & 1 kW
8053-38
q"b
BTU/hr-in^3
23.0
22.0
21.0
20.0
19.0
18.0
17.0
16.0
15.0
50
100
150
200
250
300
350
400
450
500
T, °F
Inner = AL, Outer = AL
Inner = CU, Outer = AL
Inner = CU, Outer = CU

APPENDIX I — 1/2"- 50 Ohm Coax, Design Curves

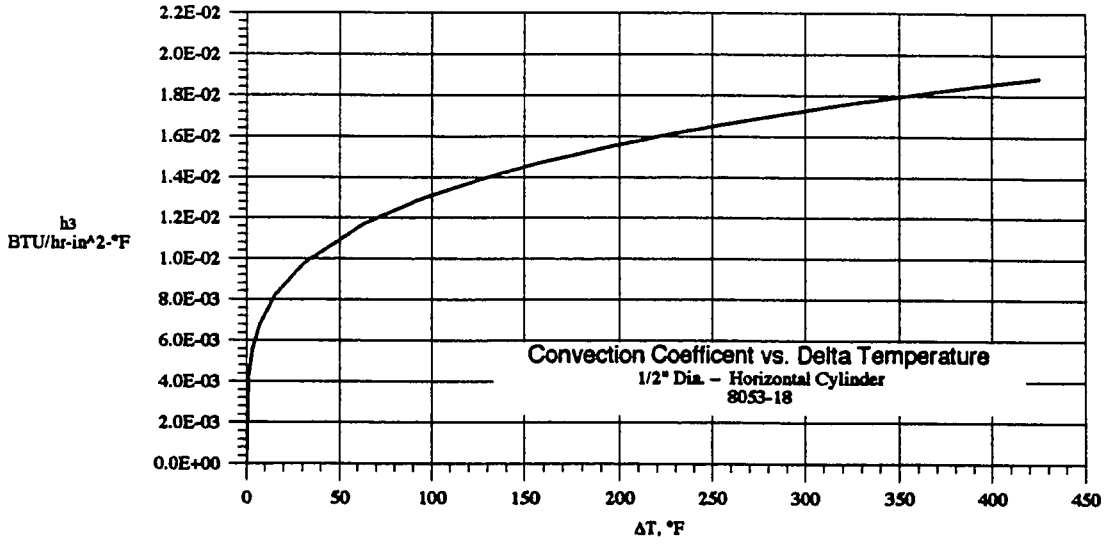

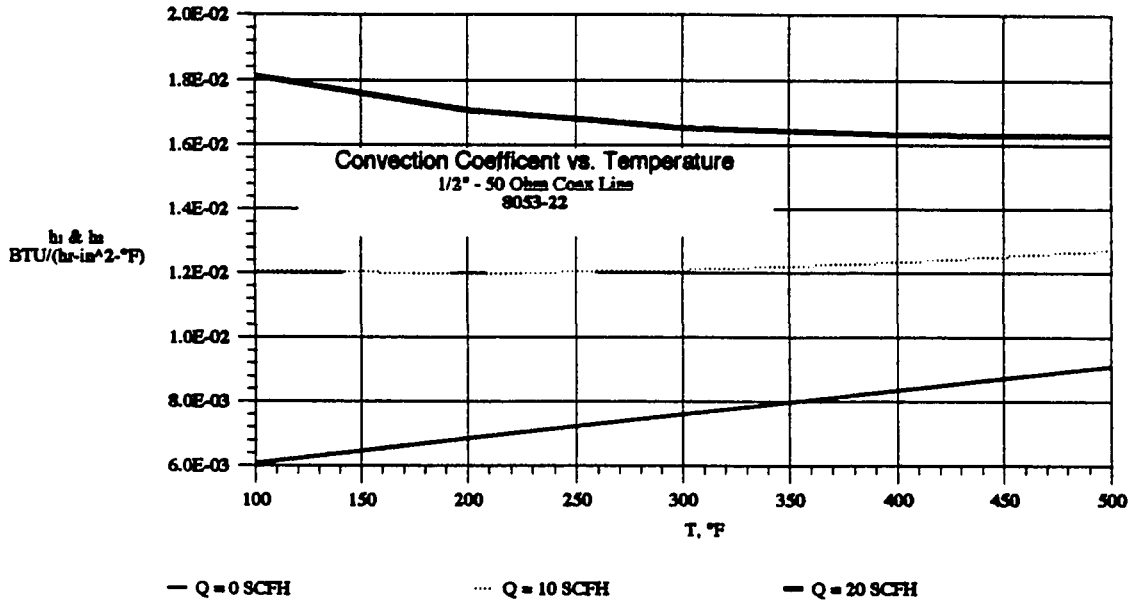

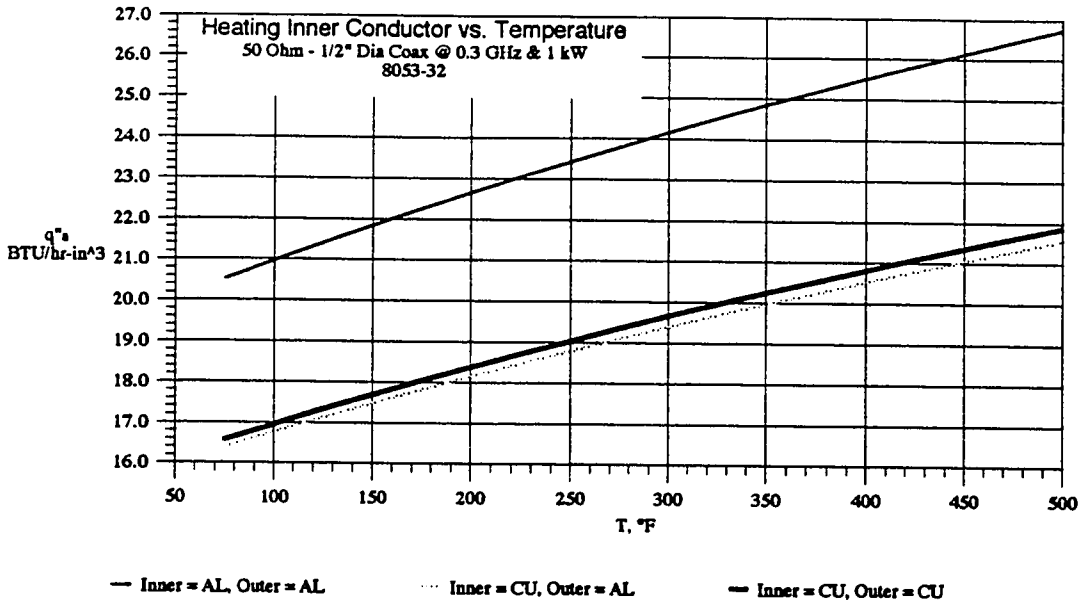
Heating Inner Conductor vs. Temperature
50 Ohm - 1/2" Dia Coax @ 0.3 GHz & 1 kW
8053-32
q"a
BTU/hr-in^3
27.0
26.0
25.0
24.0
23.0
22.0
21.0
20.0
19.0
18.0
17.0
16.0
50
100
150
200
250
300
350
400
450
500
T, °F
Inner = AL, Outer = AL
Inner = CU, Outer = AL
Inner = CU, Outer = CU

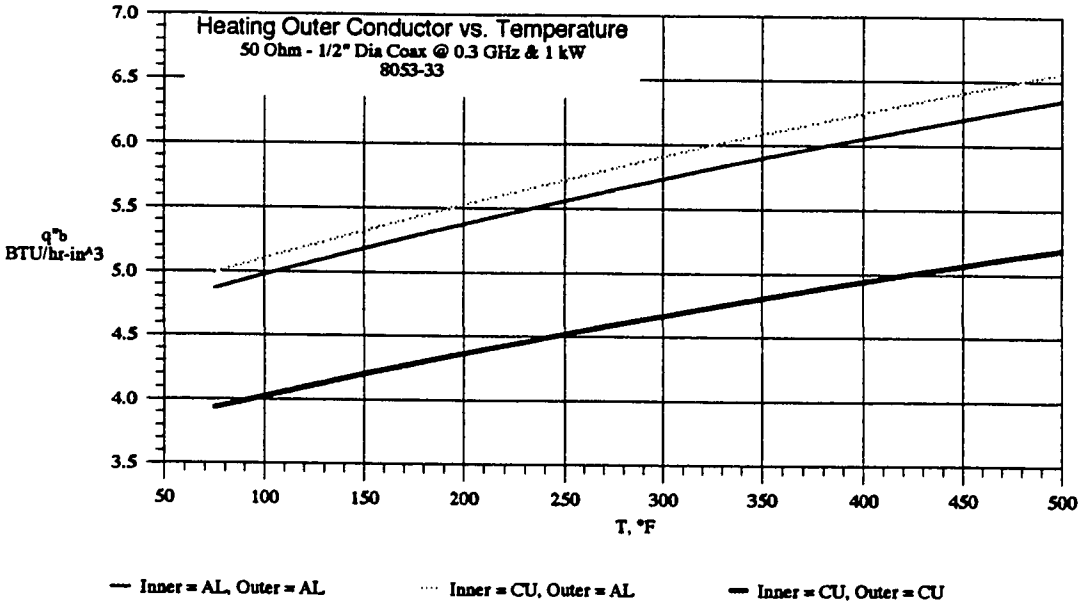
Heating Outer Conductor vs. Temperature
50 Ohm - 1/2" Dia Coax @ 0.3 GHz & 1 kW
8053-33
q"b
BTU/hr-in^3
7.0
6.5
6.0
5.5
5.0
4.5
4.0
3.5
50
100
150
200
250
300
350
400
450
500
T, °F
Inner = AL, Outer = AL
Inner = CU, Outer = AL
Inner = CU, Outer = CU

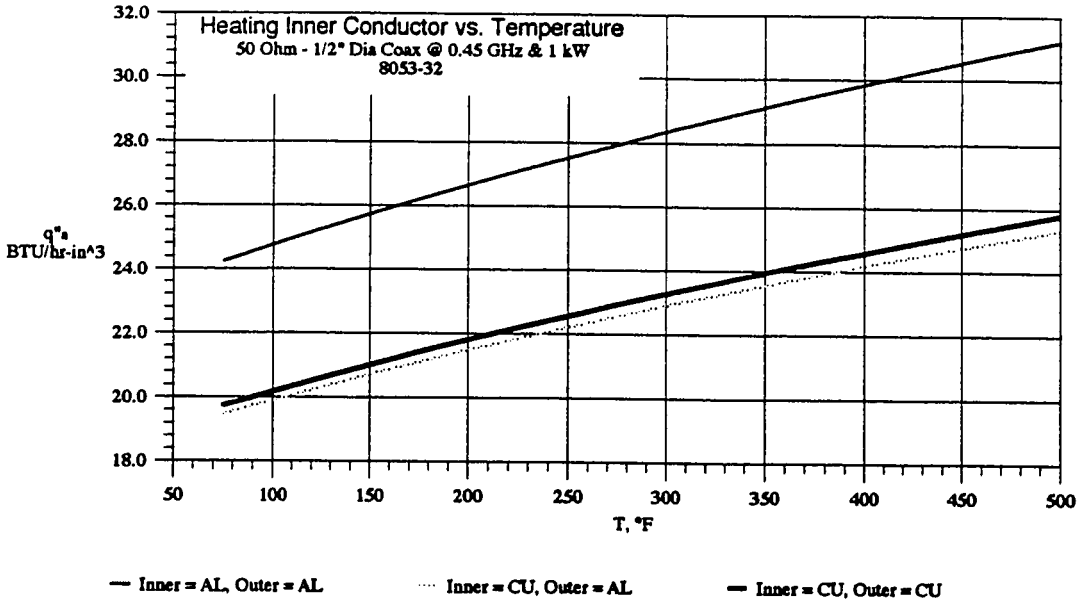
Heating Inner Conductor vs. Temperature
50 Ohm - 1/2" Dia Coax @ 0.45 GHz & 1 kW
8053-32
q"a
BTU/hr-in^3
32.0
30.0
28.0
26.0
24.0
22.0
20.0
18.0
50
100
150
200
250
300
350
400
450
500
T, °F
Inner = AL, Outer = AL
Inner = CU, Outer = AL
Inner = CU, Outer = CU

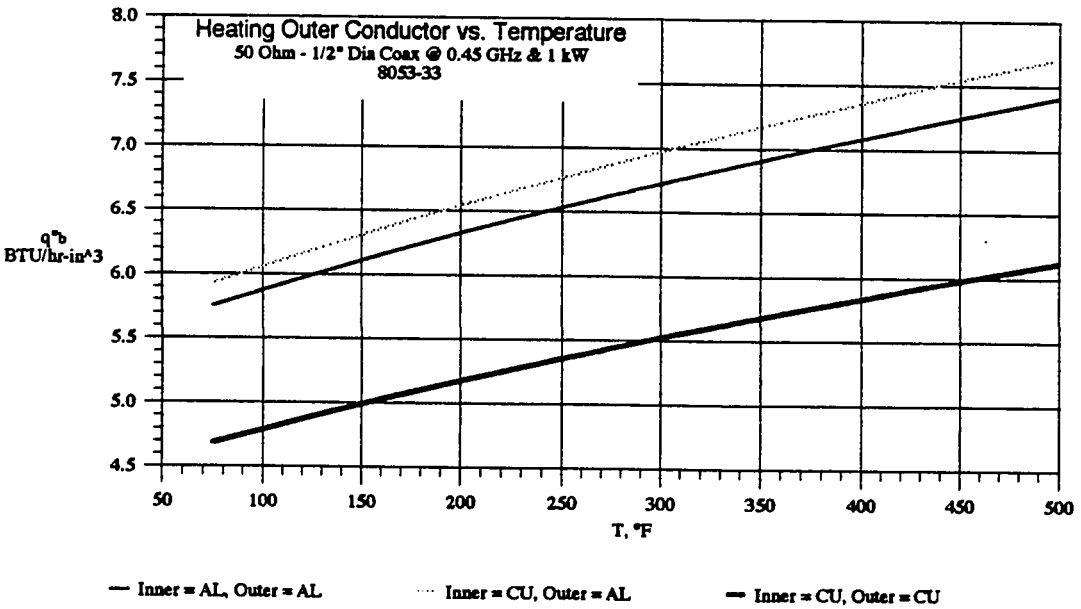
Heating Outer Conductor vs. Temperature
50 Ohm - 1/2" Dia Coax @ 0.45 GHz & 1 kW
8053-33
q"b
BTU/hr-in^3
8.0
7.5
7.0
6.5
6.0
5.5
5.0
4.5
50
100
150
200
250
300
350
400
450
500
T, °F
Inner = AL, Outer = AL
Inner = CU, Outer = AL
Inner = CU, Outer = CU

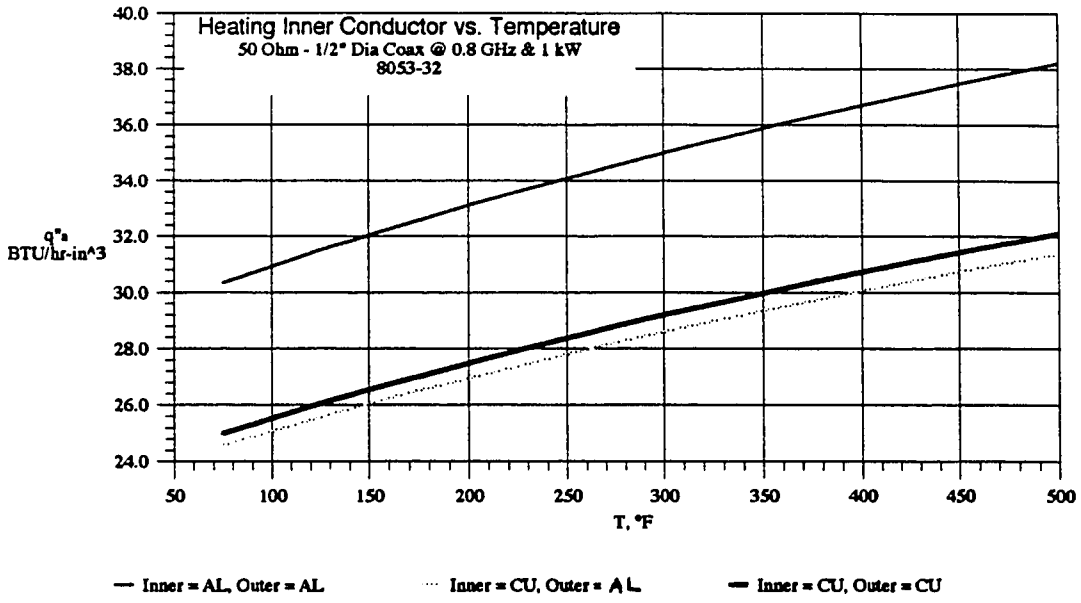
Heating Inner Conductor vs. Temperature
50 Ohm - 1/2" Dia Coax @ 0.8 GHz & 1 kW
8053-32
q"a
BTU/hr-in^3
40.0
38.0
36.0
34.0
32.0
30.0
28.0
26.0
24.0
50
100
150
200
250
300
350
400
450
500
T, °F
Inner = AL, Outer = AL
Inner = CU, Outer = AL
Inner = CU, Outer = CU

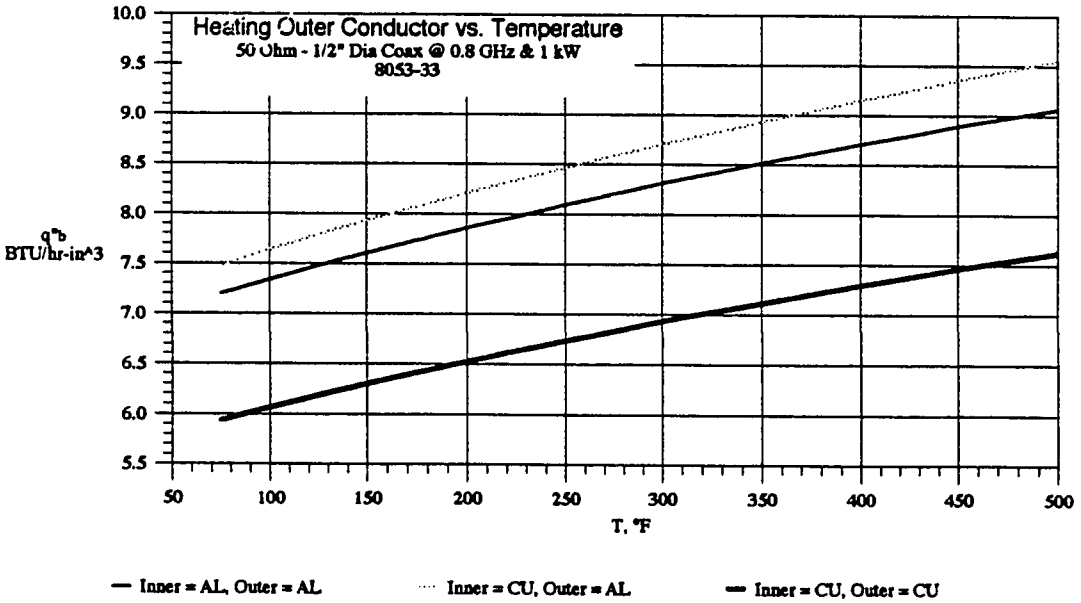
Heating Outer Conductor vs. Temperature
50 Ohm - 1/2" Dia Coax @ 0.8 GHz & 1 kW
8053-33
q"b
BTU/hr-in^3
10.0
9.5
9.0
8.5
8.0
7.5
7.0
6.5
6.0
5.5
50
100
150
200
250
300
350
400
450
500
T, °F
Inner = AL, Outer = AL
Inner = CU, Outer = AL
Inner = CU, Outer = CU

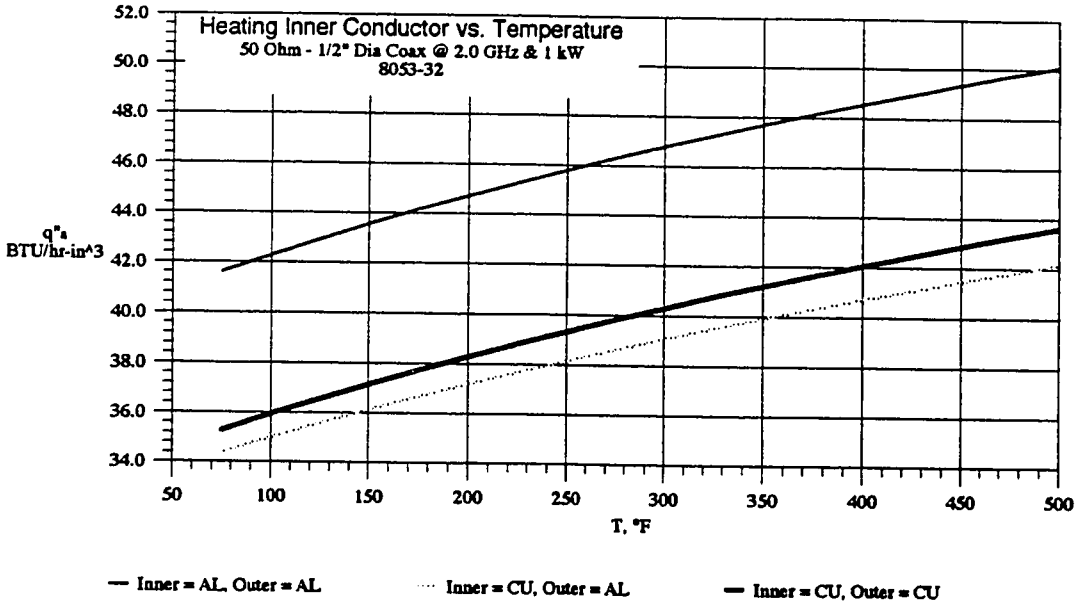
Heating Inner Conductor vs. Temperature
50 Ohm - 1/2" Dia Coax @ 2.0 GHz & 1 kW
8053-32
q"a
BTU/hr-in^3
52.0
50.0
48.0
46.0
44.0
42.0
40.0
38.0
36.0
34.0
50
100
150
200
250
300
350
400
450
500
T, °F
Inner = AL, Outer = AL
Inner = CU, Outer = AL
Inner = CU, Outer = CU

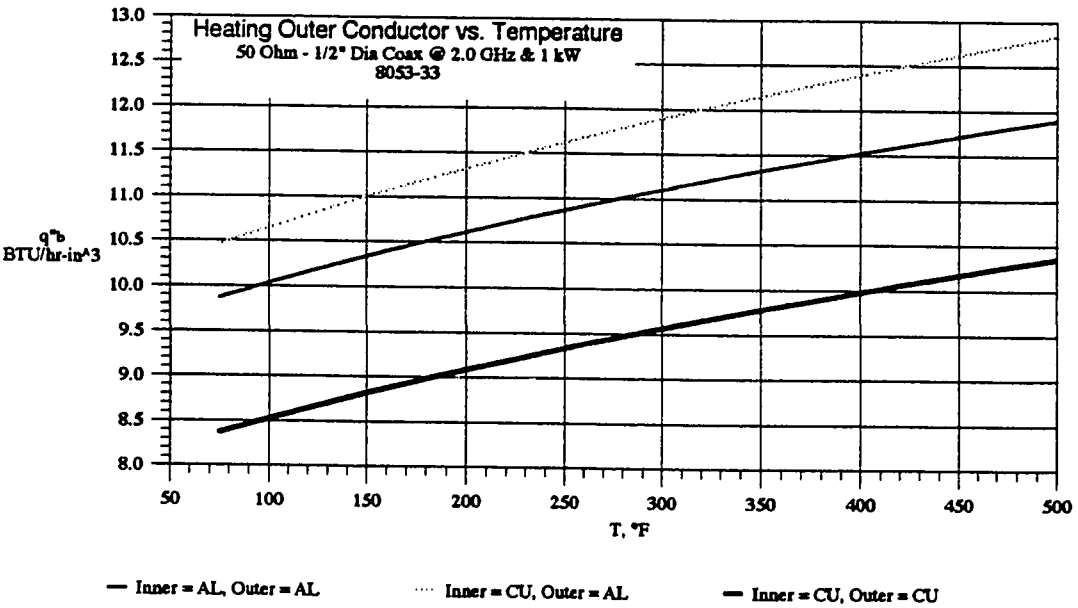
Heating Outer Conductor vs. Temperature
50 Ohm - 1/2" Dia Coax @ 2.0 GHz & 1 kW
8053-33
q"b
BTU/hr-in^3
13.0
12.5
12.0
11.5
11.0
10.5
10.0
9.5
9.0
8.5
8.0
50
100
150
200
250
300
350
400
450
500
T, °F
Inner = AL, Outer = AL
Inner = CU, Outer = AL
Inner = CU, Outer = CU

APPENDIX J — 7/8"- 50 Ohm Coax, Design Curves

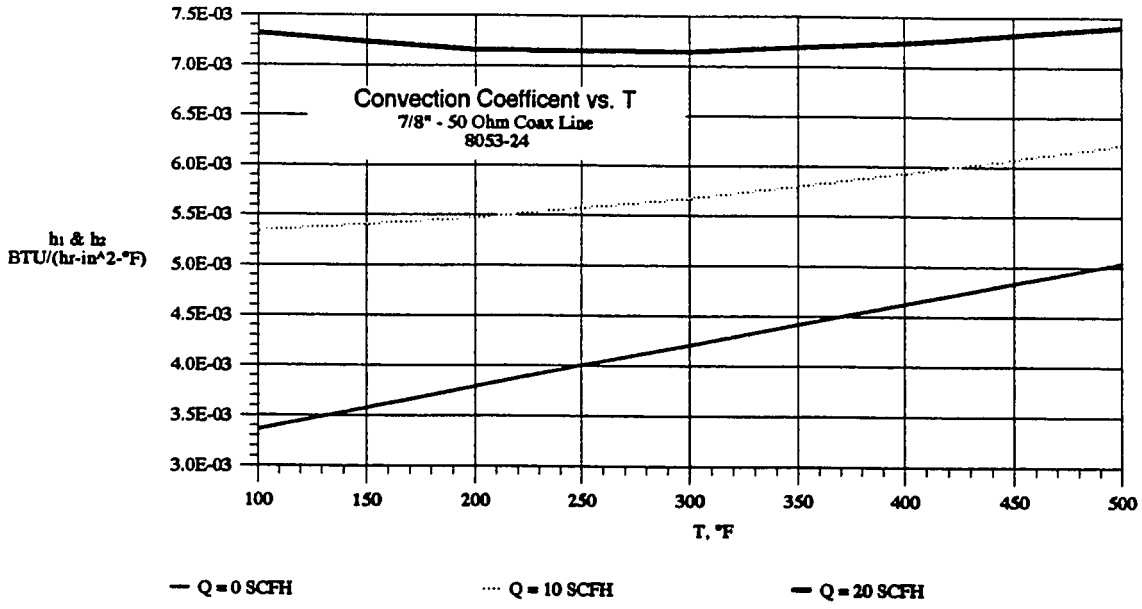

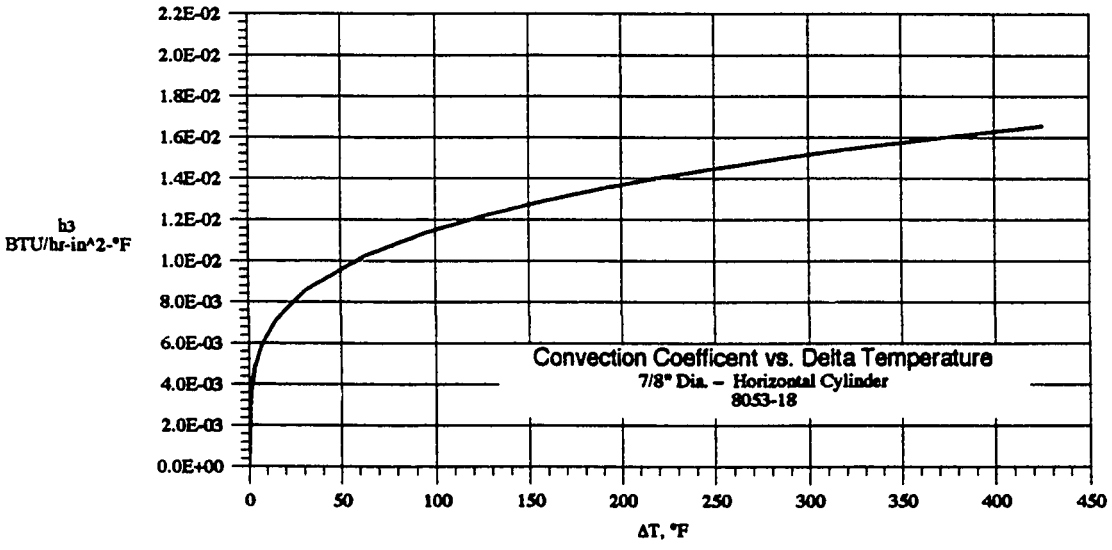

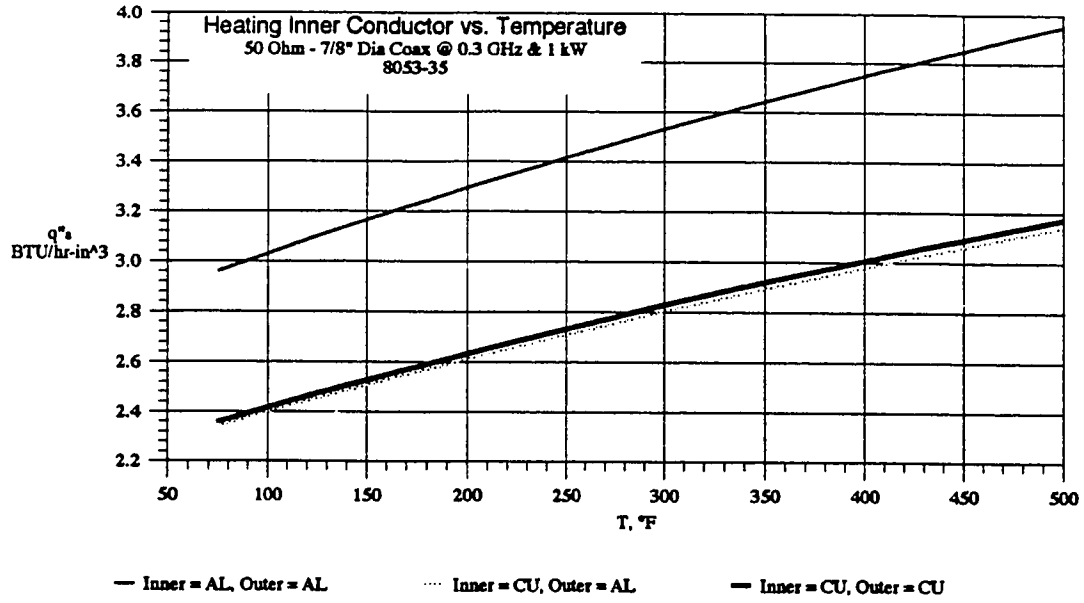
Heating Inner Conductor vs. Temperature
50 Ohm - 7/8" Dia Coax @ 0.3 GHz & 1 kW
8053-35
q"a
BTU/hr-in^3
4.0
3.8
3.6
3.4
3.2
3.0
2.8
2.6
2.4
2.2
50
100
150
200
250
300
350
400
450
500
T, °F
Inner = AL, Outer = AL
Inner = CU, Outer = AL
Inner = CU, Outer = CU

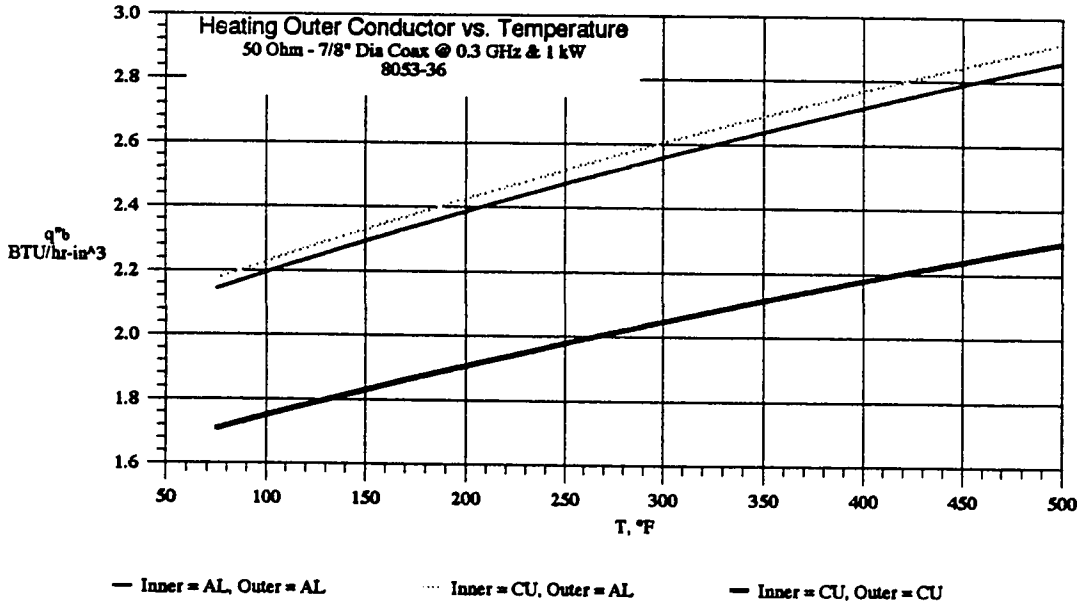
Heating Outer Conductor vs. Temperature
50 Ohm - 7/8" Dia Coax @ 0.3 GHz & 1 kW
8053-36
q"b
BTU/hr-in^3
3.0
2.8
2.6
2.4
2.2
2.0
1.8
1.6
50
100
150
200
250
300
350
400
450
500
T, °F
Inner = AL, Outer = AL
Inner = CU, Outer = AL
Inner = CU, Outer = CU

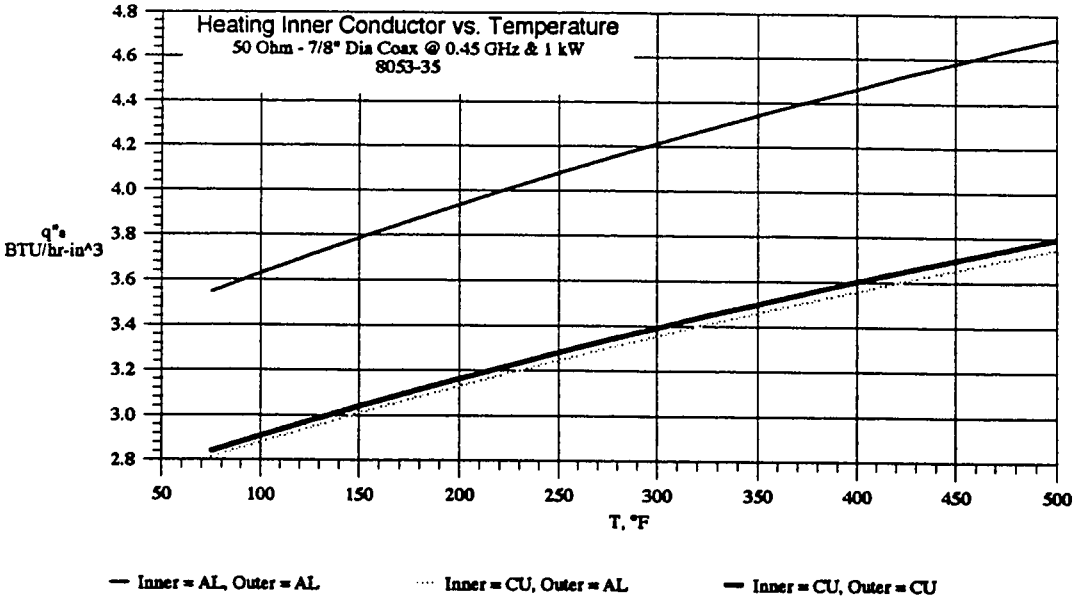
Heating Inner Conductor vs. Temperature
50 Ohm - 7/8" Dia Coax @ 0.45 GHz & 1 kW
8053-35
q'a
BTU/hr-in^3
4.8
4.6
4.4
4.2
4.0
3.8
3.6
3.4
3.2
3.0
2.8
50
100
150
200
250
300
350
400
450
500
T, °F
Inner = AL, Outer = AL
Inner = CU, Outer = AL
Inner = CU, Outer = CU

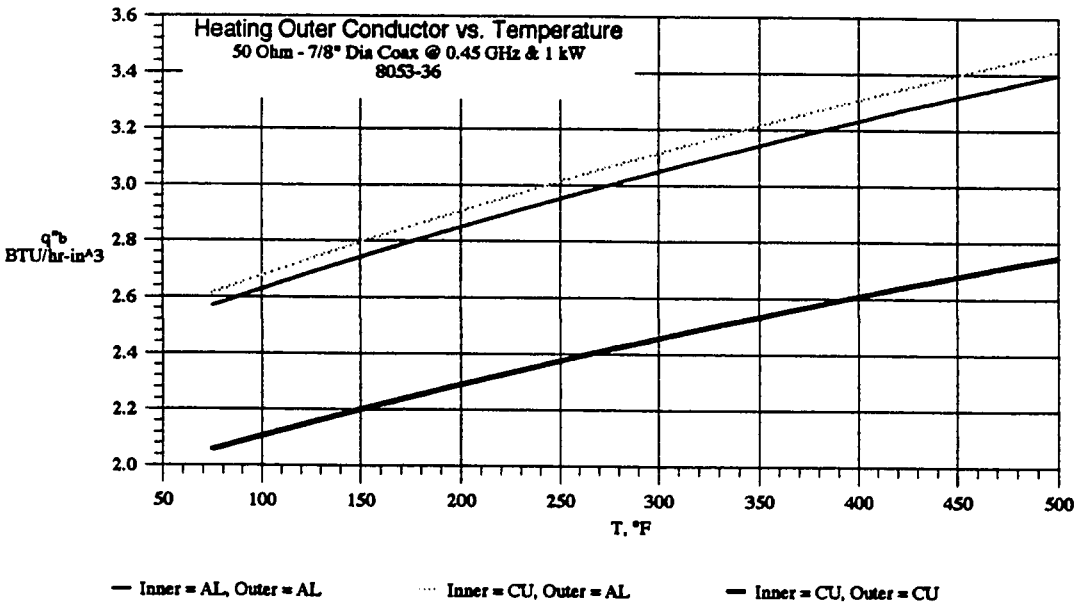
Heating Outer Conductor vs. Temperature
50 Ohm - 7/8" Dia Coax @ 0.45 GHz & 1 kW
8053-36
q'b
BTU/hr-in^3
3.6
3.4
3.2
3.0
2.8
2.6
2.4
2.2
2.0
50
100
150
200
250
300
350
400
450
500
T, °F
Inner = AL, Outer = AL
Inner = CU, Outer = AL
Inner = CU, Outer = CU

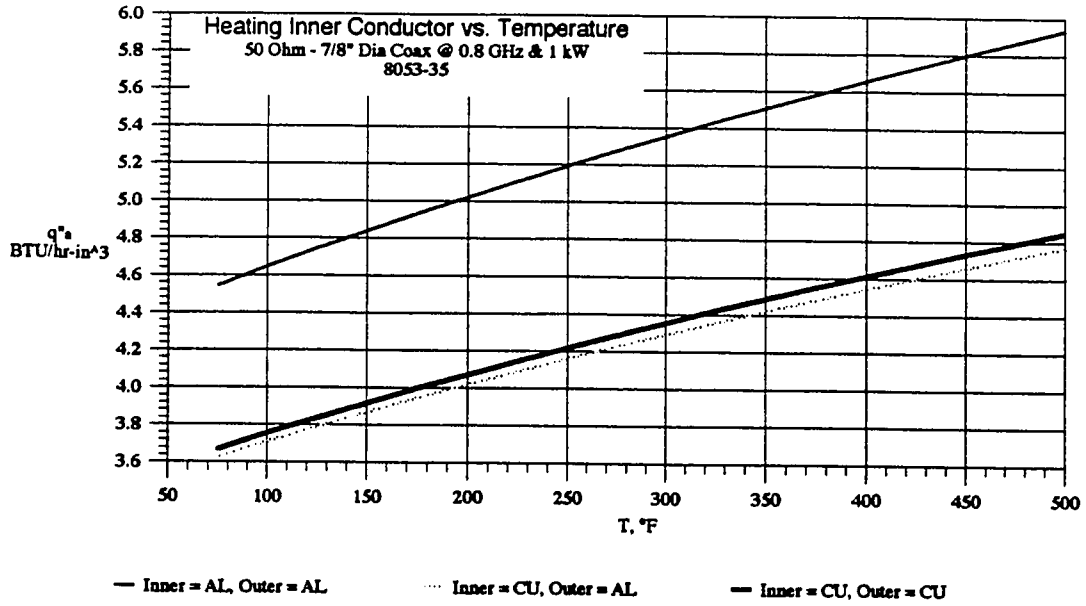
Heating Inner Conductor vs. Temperature
50 Ohm - 7/8" Dia Coax @ 0.8 GHz & 1 kW
8053-35
q'a
BTU/hr-in^3
6.0
5.8
5.6
5.4
5.2
5.0
4.8
4.6
4.4
4.2
4.0
3.8
3.6
50
100
150
200
250
300
350
400
450
500
T, °F
Inner = AL, Outer = AL
Inner = CU, Outer = AL
Inner = CU, Outer = CU

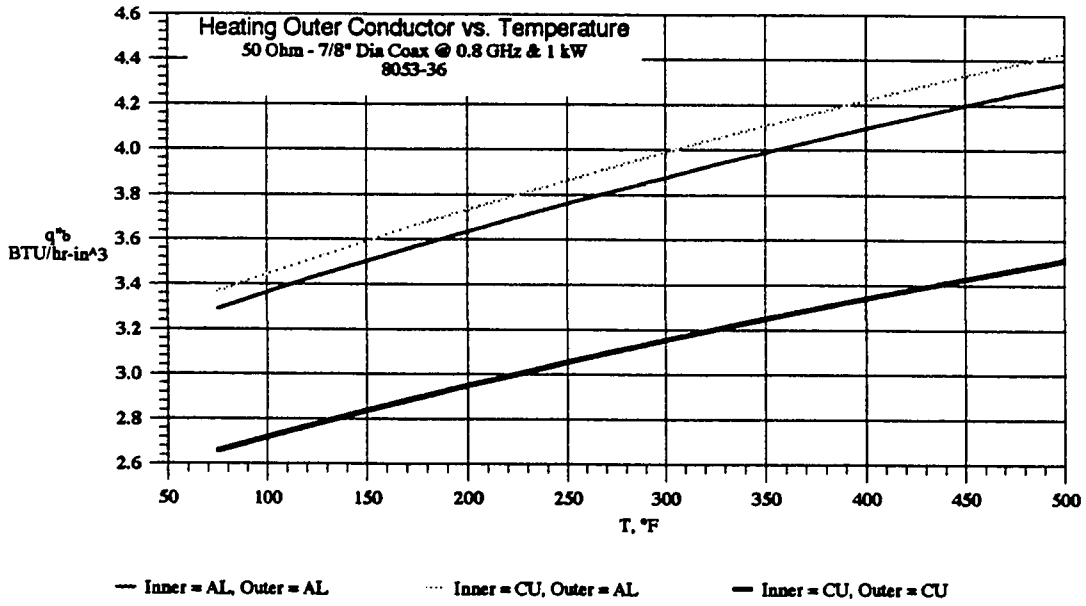
Heating Outer Conductor vs. Temperature
50 Ohm - 7/8" Dia Coax @ 0.8 GHz & 1 kW
8053-36
q'b
BTU/hr-in^3
4.6
4.4
4.2
4.0
3.8
3.6
3.4
3.2
3.0
2.8
2.6
50
100
150
200
250
300
350
400
450
500
T, °F
Inner = AL, Outer = AL
Inner = CU, Outer = AL
Inner = CU, Outer = CU

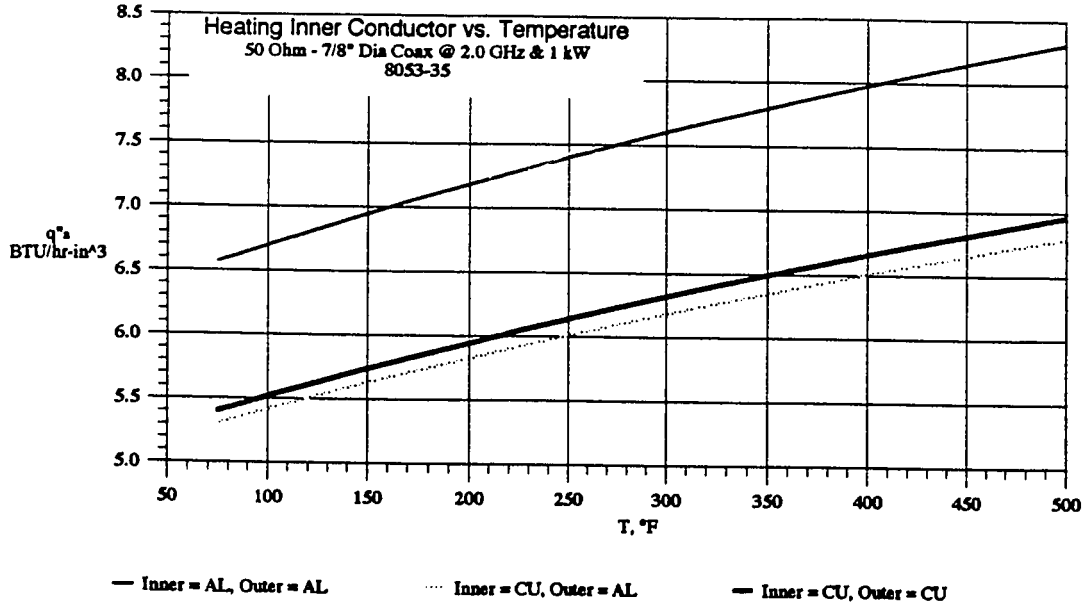
Heating Inner Conductor vs. Temperature
50 Ohm - 7/8" Dia Coax @ 2.0 GHz & 1 kW
8053-35
q'a
BTU/hr-in^3
8.5
8.0
7.5
7.0
6.5
6.0
5.5
5.0
50
100
150
200
250
300
350
400
450
500
T, °F
Inner = AL, Outer = AL
Inner = CU, Outer = AL
Inner = CU, Outer = CU

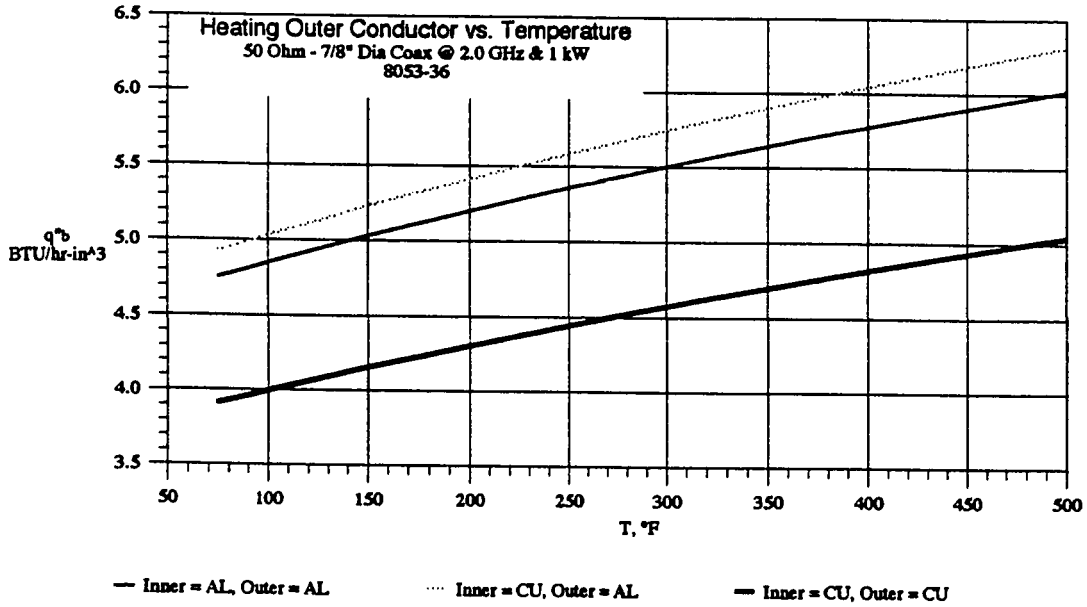
Heating Outer Conductor vs. Temperature
50 Ohm - 7/8" Dia Coax @ 2.0 GHz & 1 kW
8053-36
q'b
BTU/hr-in^3
6.5
6.0
5.5
5.0
4.5
4.0
3.5
50
100
150
200
250
300
350
400
450
500
T, °F
Inner = AL, Outer = AL
Inner = CU, Outer = AL
Inner = CU, Outer = CU

APPENDIX K — 1-5/8"- 50 Ohm Coax, Design Curves

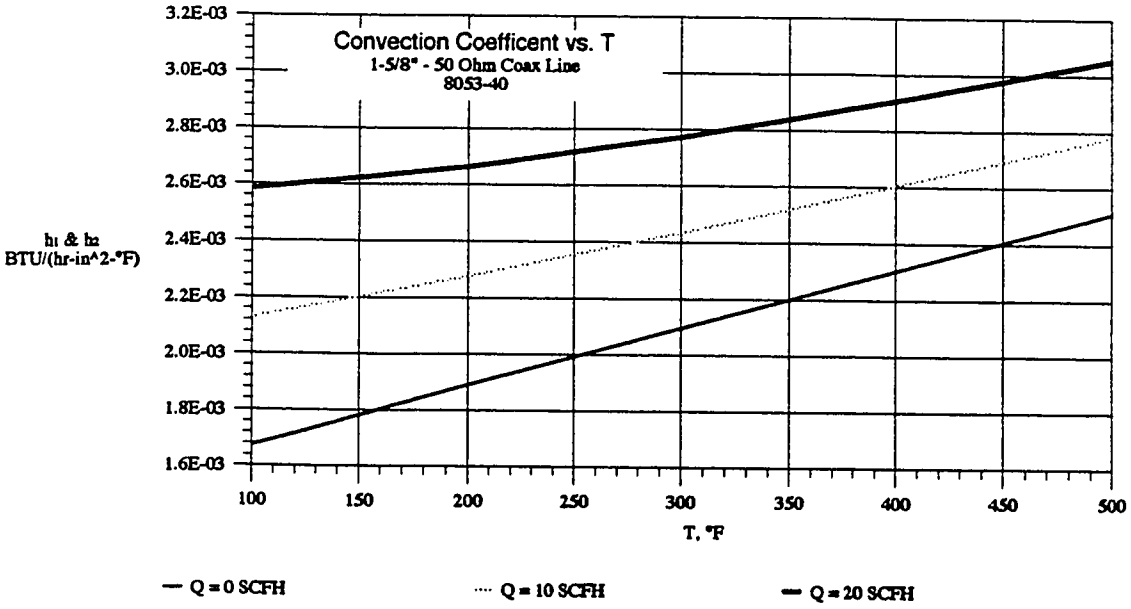

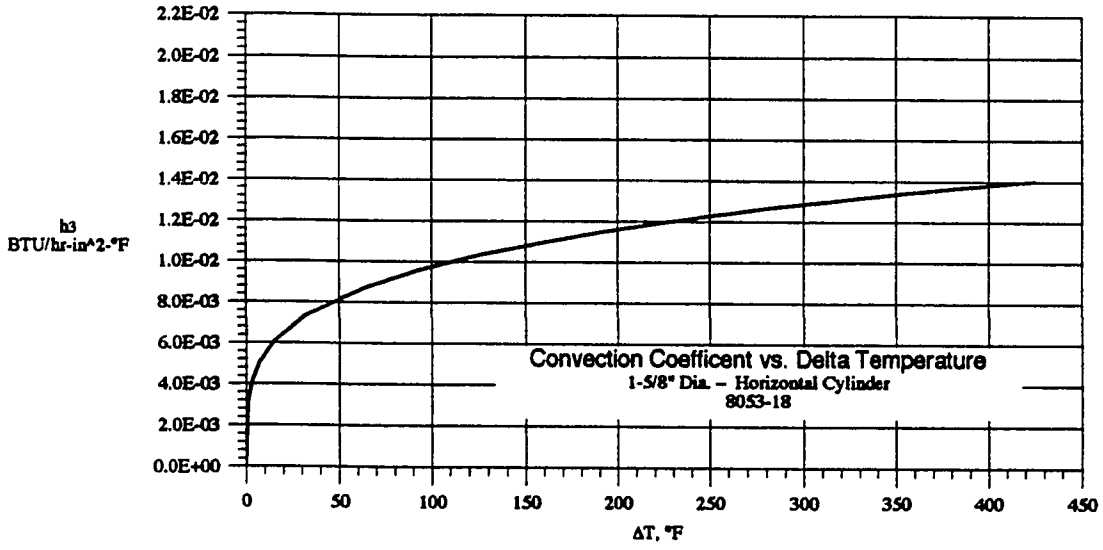

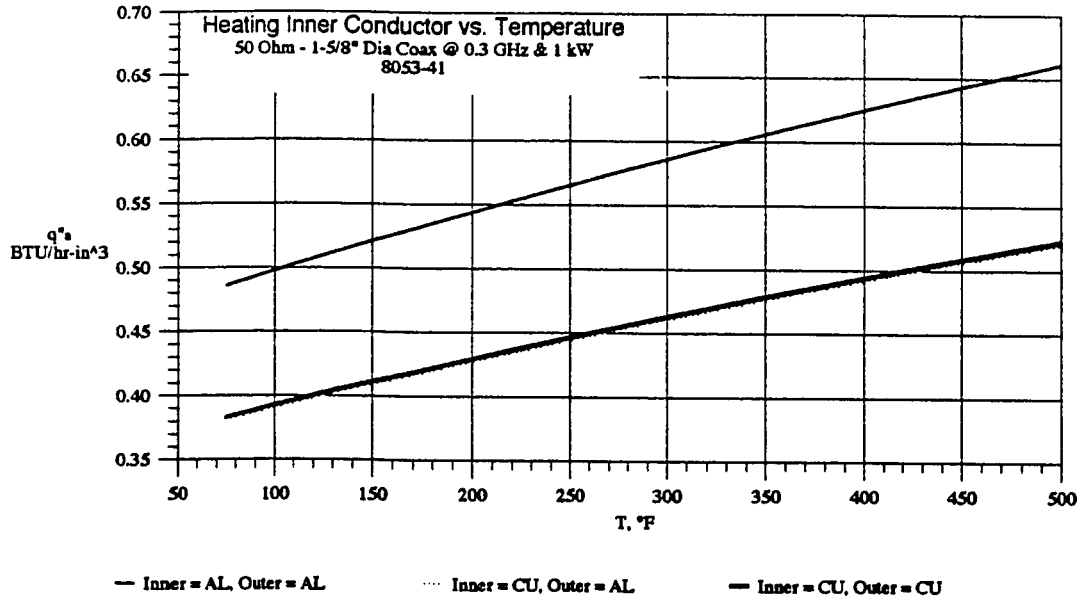
Heating Inner Conductor vs. Temperature
50 Ohm - 1-5/8" Dia Coax @ 0.3 GHz & 1 kW
8053-41
q'a
BTU/hr-in^3
0.70
0.65
0.60
0.55
0.50
0.45
0.40
0.35
50
100
150
200
250
300
350
400
450
500
T, °F
Inner = AL, Outer = AL
Inner = CU, Outer = AL
Inner = CU, Outer = CU

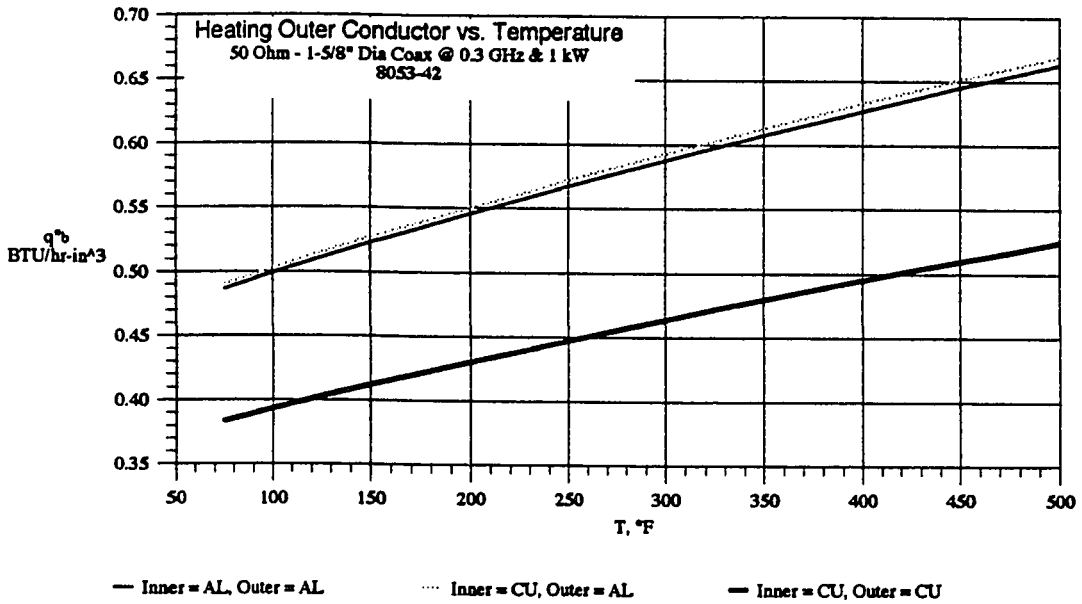
Heating Outer Conductor vs. Temperature
50 Ohm - 1-5/8" Dia Coax @ 0.3 GHz & 1 kW
8053-42
q'b
BTU/hr-in^3
0.70
0.65
0.60
0.55
0.50
0.45
0.40
0.35
50
100
150
200
250
300
350
400
450
500
T, °F
Inner = AL, Outer = AL
Inner = CU, Outer = AL
Inner = CU, Outer = CU

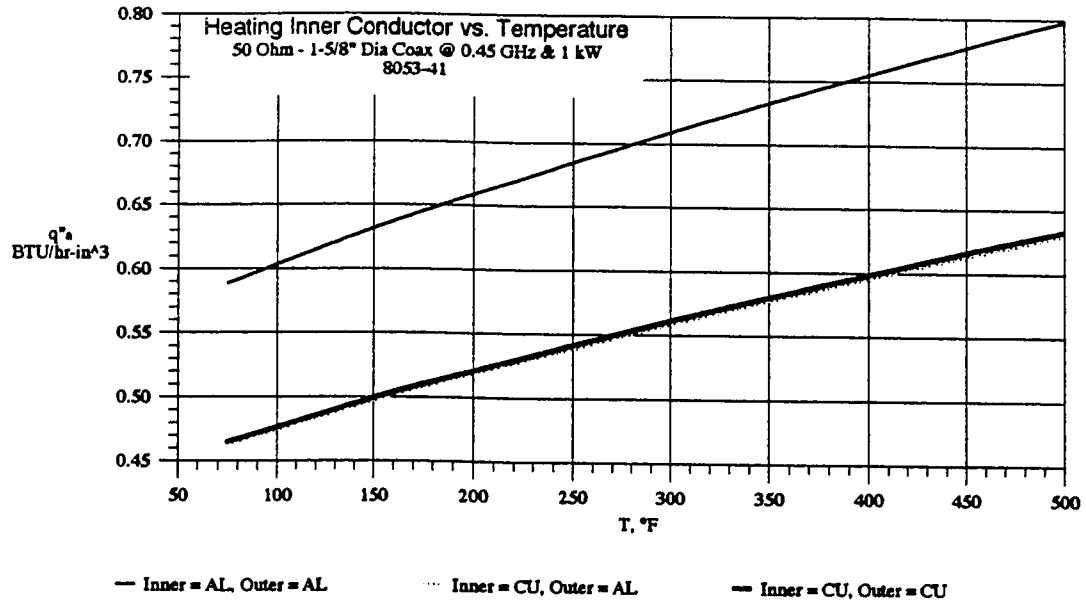
Heating Inner Conductor vs. Temperature
50 Ohm - 1-5/8" Dia Coax @ 0.45 GHz & 1 kW
8053-41
q"a
BTU/hr-in^3
0.80
0.75
0.70
0.65
0.60
0.55
0.50
0.45
50
100
150
200
250
300
350
400
450
500
T, °F
Inner = AL, Outer = AL
Inner = CU, Outer = AL
Inner = CU, Outer = CU

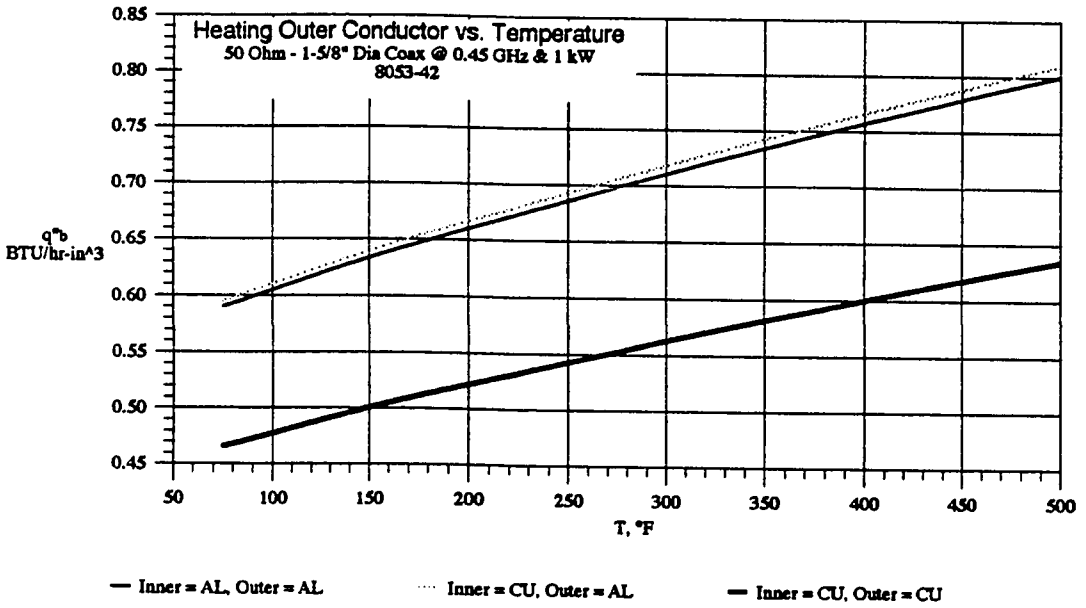
Heating Outer Conductor vs. Temperature
50 Ohm - 1-5/8" Dia Coax @ 0.45 GHz & 1 kW
8053-42
q"b
BTU/hr-in^3
0.85
0.80
0.75
0.70
0.65
0.60
0.55
0.50
0.45
50
100
150
200
250
300
350
400
450
500
T, °F
Inner = AL, Outer = AL
Inner = CU, Outer = AL
Inner = CU, Outer = CU

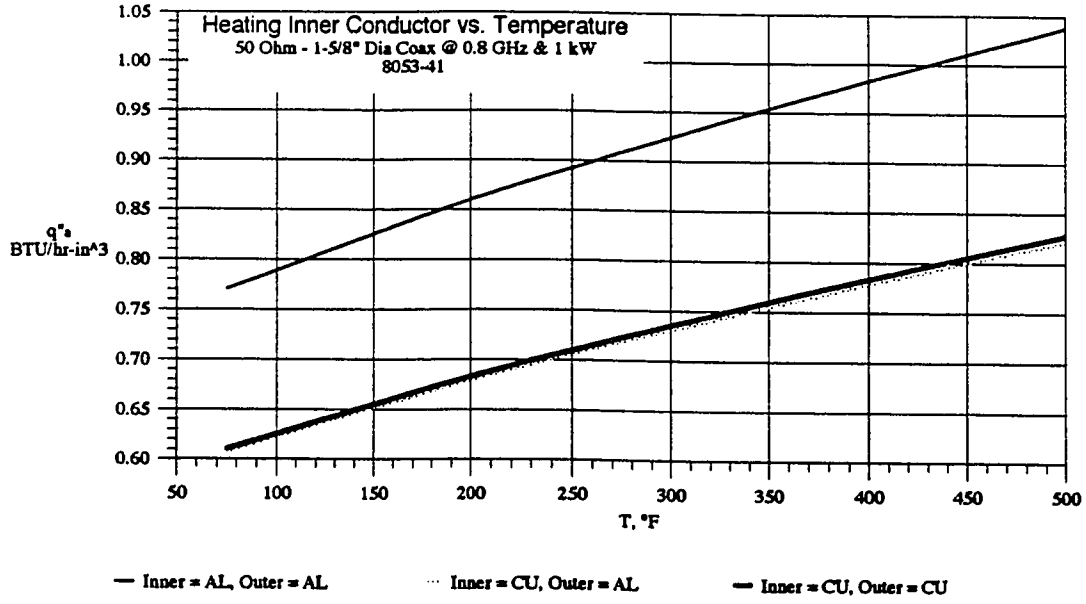
Heating Inner Conductor vs. Temperature
50 Ohm - 1-5/8" Dia Coax @ 0.8 GHz & 1 kW
8053-41
q'a
BTU/hr-in^3
1.05
1.00
0.95
0.90
0.85
0.80
0.75
0.70
0.65
0.60
50
100
150
200
250
300
350
400
450
500
T, °F
Inner = AL, Outer = AL
Inner = CU, Outer = AL
Inner = CU, Outer = CU

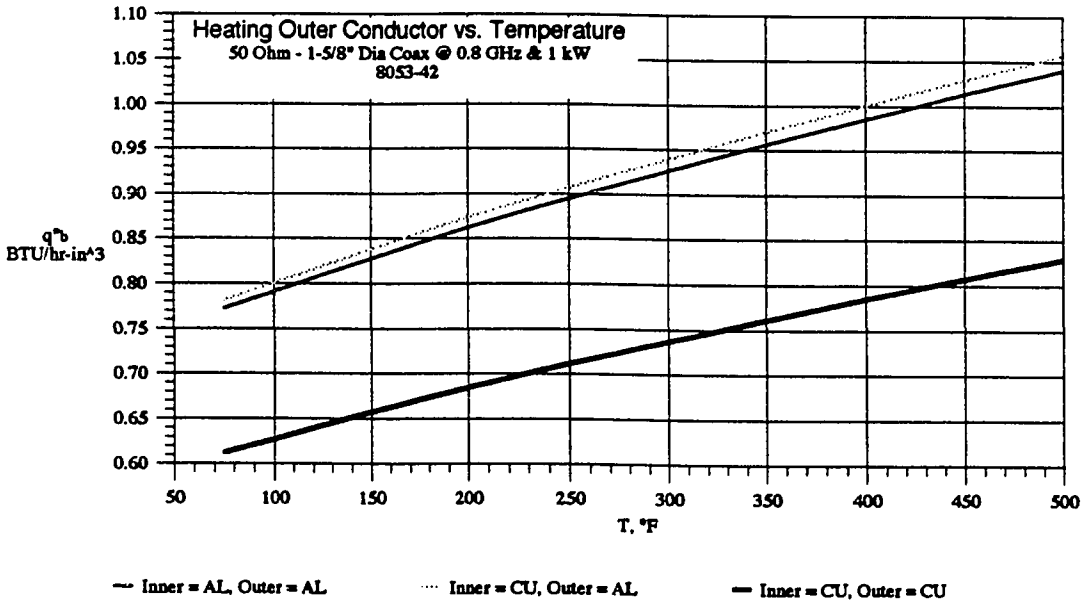
Heating Outer Conductor vs. Temperature
50 Ohm - 1-5/8" Dia Coax @ 0.8 GHz & 1 kW
8053-42
q'b
BTU/hr-in^3
1.10
1.05
1.00
0.95
0.90
0.85
0.80
0.75
0.70
0.65
0.60
50
100
150
200
250
300
350
400
450
500
T, °F
Inner = AL, Outer = AL
Inner = CU, Outer = AL
Inner = CU, Outer = CU

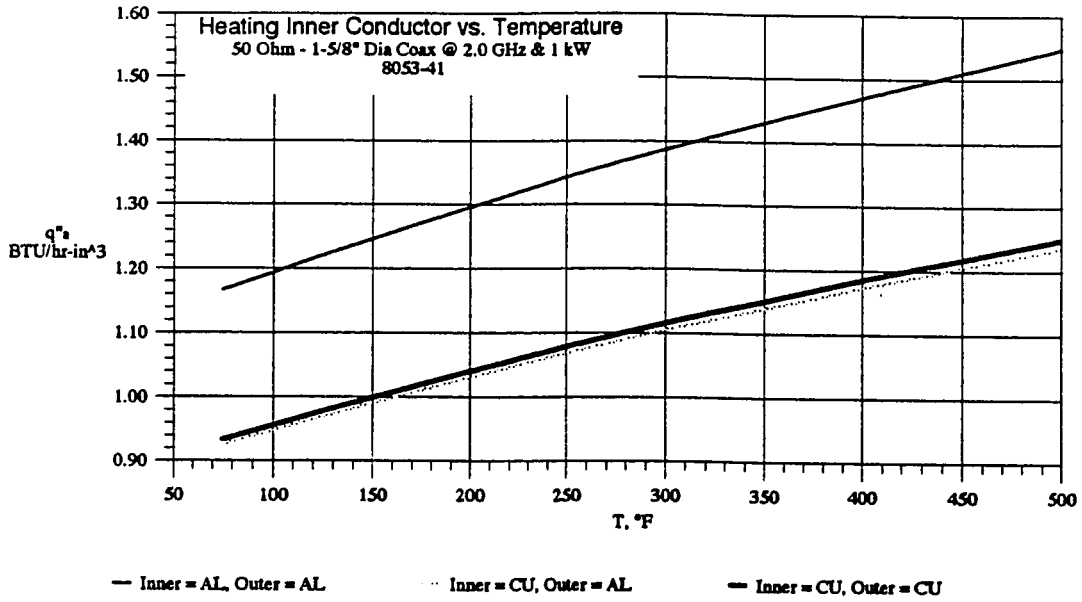
Heating Inner Conductor vs. Temperature
50 Ohm - 1-5/8" Dia Coax @ 2.0 GHz & 1 kW
8053-41
q"a
BTU/hr-in^3
1.60
1.50
1.40
1.30
1.20
1.10
1.00
0.90
50
100
150
200
250
300
350
400
450
500
T, °F
Inner = AL, Outer = AL
Inner = CU, Outer = AL
Inner = CU, Outer = CU

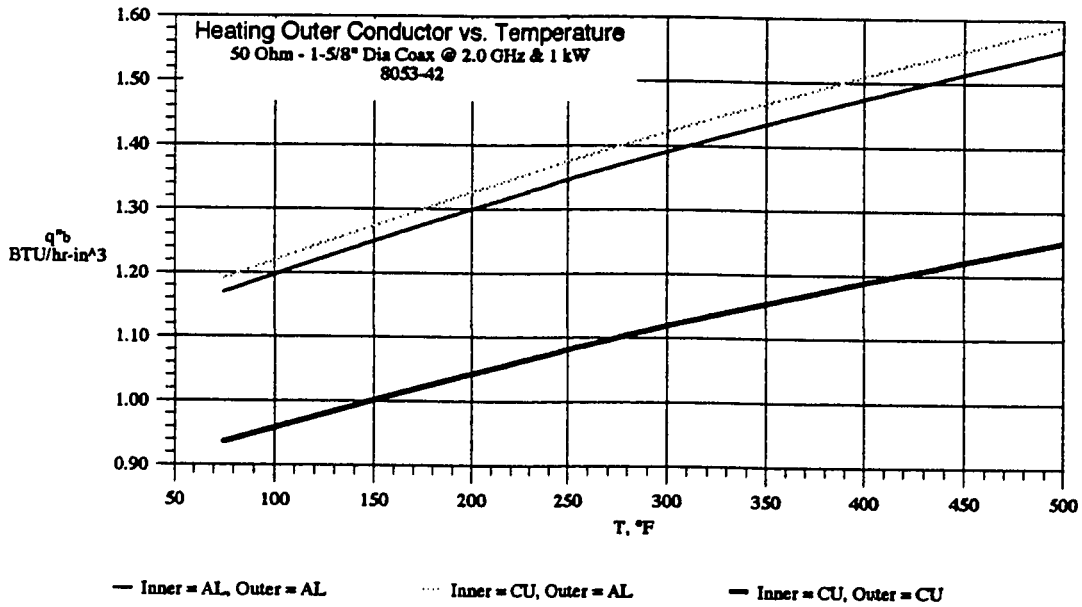
Heating Outer Conductor vs. Temperature
50 Ohm - 1-5/8" Dia Coax @ 2.0 GHz & 1 kW
8053-42
q"b
BTU/hr-in^3
1.60
1.50
1.40
1.30
1.20
1.10
1.00
0.90
50
100
150
200
250
300
350
400
450
500
T, °F
Inner = AL, Outer = AL
Inner = CU, Outer = AL
Inner = CU, Outer = CU